Manipulating Brain Manganese and Behavior in Huntington's Disease

By

Jordyn Michelle Wilcox

Dissertation

Submitted to the Faculty of the

Graduate School of Vanderbilt University

in partial fulfillment of the requirements

for the degree of

DOCTOR OF PHILOSOPHY

in

Neuroscience

May 31, 2021

Nashville, Tennessee

Approved:

Aaron B. Bowman, Ph.D. (co-mentor)

Fiona E. Harrison, Ph.D. (co-mentor)

Kevin C. Ess, M.D., Ph.D. (chair)

Matthew S. Schrag, M.D., Ph.D.

Daniel O. Claassen, M.D., M.S.

To my best friend, my husband, Matt. You are the best I know. Thank you for loving me, understanding me, and always believing in me.

—

To my son, Theo, who made me a mom, giving me the only title I have ever wanted more than 'Dr.' I love you more than you could know.

—

And to my parents. My dad, who from day one saw something special about me and inspires me to be the best version of myself. And in loving memory of my mom, who always encouraged me to reach for the stars.

—

I love you all endlessly.

ACKNOWLEDGMENTS

The work presented in this thesis was supported by funding from the National Institute of Health (NIH)/National Institute of Environmental Health Sciences (NIEHS): R01 ES016931 awarded to Aaron B. Bowman (ABB), R01 ES010563 awarded to ABB and Michael Aschner, and R01 ES031401 awarded to ABB and Fiona E. Harrison. Funding from the NIH/NIEHS Training Program in Environmental Toxicology (T32 ES007028) and the Vanderbilt Interdisciplinary Graduate Program (IGP) supported Jordyn M. Wilcox. All behavioral experiments were conducted in the Vanderbilt Mouse Neurobehavioral laboratory which receives support from the Vanderbilt Kennedy Center (P50 HD103537). The Vanderbilt University Medical Center (VUMC) Translational Pathology Shared Resource (TPSR) is supported by NCI/NIH Cancer Center Support Grant 5P30 CA68485-19 and the Shared Instrumentation Grant S10 OD023475-01A1 for the Leica Bond RX. The Vanderbilt Brain Institute (VBI) Neurochemistry Core receives support from the VBI.

I have so much to be thankful for during my five years at Vanderbilt University. I am lucky to have been co-mentored by two fantastic scientists, Dr. Aaron Bowman and Dr. Fiona Harrison. Thank you, Dr. Bowman, for your incredible enthusiasm and endless creative ideas. I am grateful for our discussions that push me to think critically about my data. Dr. Harrison, thank you for your phenomenal support with experimental design and encouraging me to believe in myself and my abilities. You are an amazing role model and have guided me to become the scientist I am. Thank you to my committee members, Dr. Kevin Ess, Dr. Matthew Schrag, and Dr. Daniel Claassen for scientific discussion, constructive feedback, and support.

There are many people who have contributed to my work directly and indirectly. I would like to highlight a few without whom this work truly would not have been possible. First, thank you Dr. Anna Pfalzer, a lab mate and friend, with whom I performed much of this work. There's nobody else I'd rather inject 120 mice with on Thanksgiving and Christmas mornings two years in a row because science doesn't pause for holidays. Thank you to each of the Bowman lab members, past and present, including Dr. Miles Bryan, Dr. Kyle Horning, Dr. Piyush Joshi, (*almost* Dr.) Rachana Nitin, Dr. Diana Neely, and the many amazing undergraduates who have worked in the lab. Thank you to Brittany Parker in the Ess Lab for all of your help with the many mouse perfusions and having the best lab space that you graciously shared with Anna and I. Thank you to the entire Harrison lab, including honorary members. Specifically, thank you to Dr. Shilpy Dixit, whose eloquence I always admired and mentorship I am grateful for. Thank you, David Consoli, Adriana Tienda, Krista Paffenroth, and Ines Debbiche for your direct contributions to my work. Thank you, Dr. Gabriella DiCarlo, Amanda Marino, Rebecca Buchanan, Dr. Brittany Spitznagel, and all past and present Harrison lab undergraduate and rotation students. I appreciate the scientific conversations and am so thankful for the day-to-day comradery and our Wellness Room chats. Thank you, Dr. Erin Calipari and lab, for assistance with fast scan cyclic voltammetry studies. And thank you,

Dr. John Allison in the Vanderbilt Mouse Neurobehavioral Core, for your never-ending help with all things mouse behavior.

Finally, thank you to all of my family and friends – you know who you are. I am surrounded with people who love and support me, and that makes all of this possible. Earning a PhD is hard. Finishing a PhD during a global pandemic *and* with a new baby is even harder. I cannot thank my friends and family, especially my husband, Matt, enough for everything they do and the constant support they provide. Thank you to my precious pup, Gracie, for all of the snuggles and to my son, Theo, who brings me boundless joy. You all keep me sane and made this feat possible.

TABLE OF CONTENTS

Page

LIST OF TABLES

LIST OF FIGURES

Chapter 1

Introduction

1.1 Manganese is an Essential Micronutrient

Micronutrients are vitamins and minerals that are required in small amounts for development and maintenance of health. Manganese (Mn) is one of five essential trace minerals required by all living organisms and is critical for brain function (Sandstead, 1986). Mn does not exist naturally as a free metal, but instead as oxides, carbonates and silicates. Natural erosion of crustal rock leads to sufficient presence of Mn in soil and groundwater, and Mn is therefore reliably found in vegetable and animal food sources (ATSDR, 2012). Foods that are particularly rich in Mn include whole grains, rice, nuts, legumes, and leafy green vegetables. A recommended dietary allowance (RDA) has not been established but the U.S. Food and Drug Administration's (FDA) Food and Nutrition Board has outlined adequate intake (AI) as 1.8 mg/day for adult females, 2.2 mg/day for adult males, and 2.6 mg/day for lactating females (Trumbo, Yates, Schlicker, & Poos, 2001). Females absorb Mn more efficiently than males (Finley, Johnson, & Johnson, 1994), and younger individuals accumulate Mn more easily due to both increased demand and underdeveloped regulatory systems (P. Chen, Bornhorst, & Aschner, 2018). Tolerable upper intake levels have been set at 9-11 mg/day for adults and only 2-6 mg/day for children (Trumbo et al., 2001). When ingested, only 1-5% of Mn is absorbed in the gastrointestinal (GI) tract and through tightly regulated absorption and excretion, relatively stable levels of Mn from dietary sources are maintained in the blood and bodily tissues although exact mechanisms governing this regulation are unclear (J. L. Aschner & Aschner, 2005). Given the diverse food sources rich in Mn, dietary deficiency is rare, though poor cognition and impaired growth can result as a consequence (Bhang et al., 2013; Henn et al., 2011; Zidenberg-Cherr, Keen, Casey, & Hurley, 1985).

Mn overexposure from food sources under non-experimental conditions is unlikely because of efficient hepatobiliary excretion. However, excess Mn ingestion from contaminated drinking water can lead to detrimental effects (Frisbie, Ortega, Maynard, & Sarkar, 2002). More commonly, overexposure occurs via routes that bypass the GI tract and liver metabolism such as inhalation, dermal absorption, or even intravenous injection. Ambient air contains Mn from air erosion of dust or soil. Additionally, Mn is a common component in steel and used for production of dry-cell batteries, leather, textiles, cosmetics, fireworks, and as a gasoline additive. Industrial waste and mining activities contribute to air polluted with Mn, and outside of specific occupational exposure, is the primary source of Mn overexposure by inhalation in the U.S. (ATSDR, 2012). Dermal exposures can occur for those working in the manufacturing industries in contact with the products mentioned previously but is not a main

route of overexposure. Intravenous exposure can take place from injection of the illicit, self-prepared drug methcathinone (pseudoephedrine oxidized by potassium permanganate) (De Bie, Gladstone, Strafella, Ko, & Lang, 2007; Sikk, Haldre, Aquilonius, & Taba, 2011) or through the medical administration of total parenteral nutrition (TPN) (Khan, Hingre, & Dhamoon, 2020). Excess Mn exposure by neonatal TPN is especially concerning, given the concurrence of an immature hepatic regulatory system and a critical neural developmental period (Keith M. Erikson, Thompson, Aschner, & Aschner, 2007). Neurotoxicological outcomes of Mn overexposure are discussed in further detail below (p. 5).

1.2 Manganese in the Healthy Brain

Mn absorption and distribution throughout the body depends on exposure route and chemical speciation. For example, soluble manganese chloride ($MnCl_2$) and manganese sulfate ($MnSO_4$) are more readily absorbed and distributed than insoluble forms such as manganese dioxide (MnO_2) even when administered by the same route (Dobson, Erikson, & Aschner, 2014; H. Roels et al., 1997). As previously mentioned, 1-5% of ingested Mn is absorbed via the GI tract. Precisely how this Mn is transported from the GI tract to the bloodstream is not well known, but from the blood Mn is then quickly distributed throughout the body (P. Chen et al., 2018; Horning, Caito, Tipps, Bowman, & Aschner, 2015). Mn exists in several oxidation states, but Mn^{2+} and Mn^{3+} are most common species in biological systems. Given its unstable nature, elemental Mn is not freely dissolved in the bloodstream, but instead bound to small molecules such as citrate or albumin in its +2 state or transferrin (Tf) in its +3 state (Reaney, Kwik-uribe, & Smith, 2002). Mitochondrial-rich (i.e., high energy demand) tissues require high concentrations of Mn, and these tissues appropriately retain more Mn than other tissues (Dobson et al., 2014). In descending order, the organs that contain the highest Mn concentrations are liver, pancreas, bone, kidney, and brain (P. Chen et al., 2018).

Exactly how Mn crosses the blood-brain barrier (BBB) is still under investigation. It is thought that Mn enters the central nervous system (CNS) by different routes, either the capillary endothelium or the choroid plexus, depending on normal or high plasma concentrations respectively (M. Aschner, 1999). Mn can also bypass the BBB by entering directly via the olfactory epithelium (Henriksson & Tjälve, 2000). From the plasma, Mn bound to Tf or bound in a citrate complex can cross the BBB via carrier-mediated transport (Crossgrove, Allen, Bukaveckas, Rhineheimer, & Yokel, 2003; Malecki, Devenyi, Beard, & Connor, 1999). Divalent metal transporter 1 (DMT1) has high affinity for Mn and is one proposed entry method for Mn into the CNS, but there are inconsistent reports regarding its importance as a BBB transporter for Mn (Fitsanakis, Piccola, Dos Santos, Aschner, & Aschner, 2007; Yokel, 2009). Other methods of entry into the brain include zinc-interacting proteins,

ZIP8 and ZIP14, and calcium channels (Nyarko-Danquah et al., 2020). Exact transport mechanisms may be poorly understood, but it is certain Mn enters the CNS one way or another to fulfill its crucial roles.

Within the brain, Mn accumulates in a regionally specific manner. The highest concentrations of Mn are found in basal ganglia structures (globus pallidus, caudate and putamen) and hypothalamus in the normal human brain (Duflou, Maenhaut, & De Reuck, 1989; Ramos et al., 2014). Following exposure, olfactory bulb, pre-frontal cortex and the parahippocampal gyrus are also areas susceptible to high Mn accumulation (Yamada et al., 1986). Regional expression of Mn transporters may explain the relative distribution throughout the brain, however, other trace metals that share many of the same transporters are concentrated in other areas (e.g., zinc in the hippocampus) (Kasarskis, 1984; Ramos et al., 2014). The anatomical regions enriched with Mn may have a greater requirement for the trace element to function optimally, though this has not yet been shown. Interestingly, Mn accumulates in structures sensitive to neurodegeneration in Huntington's Disease, discussed in further detail to follow (p. 9).

Mn is found in several cell types where it serves its essential role regulating physiological processes including amino acid and neurotransmitter recycling, urea metabolism, antioxidant defense, and energy metabolism (Horning et al., 2015). Each of these processes involve at least one enzyme that requires Mn as a co-factor.

Amino acid neurotransmitter recycling. Under physiological concentrations (i.e., not in excess), Mn contributes to protection against excitotoxicity by maintaining glutamate-glutamine homeostasis. The astrocytic protein glutamine synthetase (GS) carries out a condensation reaction of glutamate and ammonia to form glutamine. Mn^{2+} coordinates adenosine triphosphate (ATP) into the GS active site and rate of this reaction is directly dependent on co-factor availability (magnesium can fulfill this role, however GS has a 300-1000x higher affinity for Mn) (Eisenberg, Gill, Pfluegl, & Rotstein, 2000; Suárez, Bodega, & Fernández, 2002; Frederick C. Wedler, Denman, & Roby, 1982; Zou et al., 2010). Approximately 80% of total brain Mn is bound to GS, helping to maintain appropriate extracellular glutamate concentration and protect neurons against excitotoxicity (M. Aschner, 1999; F C Wedler & Denman, 1984).

Urea metabolism. The urea cycle is an important physiological process for removing toxic nitrogenous waste that is generated from amino acid catabolism. Two ureahydrolases found in the brain are Mn-dependent enzymes: arginase (ARG) and agmatinase (AGM). ARG hydrolyzes arginine to ornithine and urea with a specific catalytic requirement for Mn. There are two isoforms, ARG1 and ARG2, which are cytosolic and mitochondrial respectively. ARG2 activity in neurons is critical for regulating arginine and ornithine concentrations for biosynthetic reactions including nitric oxide (NO) synthesis (Kanyo, Scolnick, Ash, & Christianson, 1996; Morris, 2002; Morris, Bhamidipati, & Kepka-Lenhart, 1997; Spector, Jenkinson, Grigor, Kern, & Cederbaum,

1994). AGM converts agmatine, a putative neurotransmitter with anti-convulsant and anti-depressant effects, to putrescine and urea (Nguyen et al., 2003; Reyes et al., 2020; Romero et al., 2017).

Redox status. Maintaining redox homeostasis, or the balance between oxidants and antioxidants, is crucial to the health of a cell. Antioxidant molecules and enzymes contribute to this protection. Mn can itself be a prooxidant molecule and induce oxidative damage (Milatovic, Zaja-Milatovic, Gupta, Yu, & Aschner, 2009) but can also protect against oxidative stress. Mitochondrial super oxide dismutase (SOD), also known as MnSOD or SOD2, is a Mn-dependent enzyme that detoxifies superoxide anions into hydrogen peroxide which is further reduced by catalase (Holley, Bakthavatchalu, Velez-Roman, & St. Clair, 2011). Under Mn-deficient conditions, MnSOD can switch from an antioxidant protein to a primarily prooxidant protein (Ganini, Santos, Bonini, & Mason, 2018).

Energy metabolism. Pyruvate carboxylase is a Mn-dependent mitochondrial enzyme that forms oxaloacetate by carboxylation of pyruvate. This is an important step for entrance into the Krebs cycle and subsequent energy production (Scrutton, Utter, & Mildvan, 1966). The insulin-like growth factor (IGF-1)/Akt pathway is also Mn-responsive. Mn exposure upregulates IGF-1 expression and increases Akt signaling (Cordova et al., 2012; Hiney, Srivastava, & Dees, 2011). Mn itself has an insulin mimetic effect and protects against diet-induced diabetes (S. H. Lee et al., 2013; Subasinghe, Greenbaum, & McLean, 1985).

While Mn import to the brain is essential for proper functioning of the previously mentioned biological pathways, efficient efflux mechanisms are necessary to avoid neurotoxicity. Ferroportin, sodium-calcium exchanger, and SLC30A10 are identified Mn exporters (P. Chen et al., 2018). SLC30A10 (also known as ZnT10) is the only currently known selective Mn efflux transporter and it is highly expressed in brain and liver (P. Chen, Bowman, Mukhopadhyay, & Aschner, 2015). SLC30A10 was originally characterized as a zinc-transporting protein, hence its assigned name, but it was later determined to be an exclusive Mn-efflux protein (Bosomworth, Thornton, Coneyworth, Ford, & Valentine, 2012; Leyva-Illades et al., 2014). Localized to the cell surface, SLC30A10 exports Mn via a currently unknown mechanism to protect against cellular accumulation and toxicity (Balachandran et al., 2020; Taylor et al., 2019). In the liver, SLC30A10 exports Mn into the bile for excretion via the feces (Mercadante et al., 2019). SLC30A10 mutations lead to hypermanganesemia in body and brain, even without additional exposures, resulting in cirrhosis, polycythemia, and dystonia (Mukhopadhyay, 2018). Recent research on this transporter has contributed to our knowledge of Mn homeostasis and the ability to treat certain forms of Mn toxicity.

1.3 Manganese as a Neurotoxicant

Mn toxicity occurs following an excess exposure or as the result of inherited mutations in Mn transporters. Respiratory, reproductive and developmental effects are prominent with Mn toxicity, but the neurological effects that cause a Parkinsonian-like condition known as Manganism are most devastating (ATSDR, 2012). Historically, occupational exposures were the focus of Mn toxicity research. Welders, smelters and miners are exposed to high levels of Mn (Kendzia et al., 2017; O'Neal & Zheng, 2015). A 2020 study examined a cohort of South African miners and identified strong positive correlations between estimated cumulative Mn exposure and Parkinsonian-like signs, and inverse correlations between Mn exposure and quality of life measures (Dlamini, Nelson, Nielsen, & Racette, 2020). Outside of an occupational setting, excess Mn exposure results from drinking contaminated water or breathing in polluted air nearby industrial factories (Bhang et al., 2013; Gerke, Little, & Barry Maynard, 2016; Schullehner et al., 2020). There is also a growing body of research connecting Mn exposures and high brain Mn concentrations to the progression of neurodegenerative diseases such as Alzheimer's Disease (Bowman, Kwakye, Herrero Hernández, & Aschner, 2011; Martins Jr. et al., 2019).

Manganese preferentially accumulates in basal ganglia structures, pre-frontal cortex, and hippocampus following exposure (Ramos et al., 2014). Not surprisingly, the main behavioral effects observed from Mn neurotoxicity are motor impairments and abnormal cognition, working memory, and attention (Balachandran et al., 2020; Chang et al., 2010; Schneider, Williams, Ault, & Guilarte, 2015). It is unknown exactly how Mn exerts these effects at a cellular level, but increased oxidative stress and mitochondrial dysfunction are likely candidates (Dobson et al., 2014; O'Neal & Zheng, 2015). Mn also impacts several neurotransmitter systems, including the glutamatergic, cholinergic, GABA-ergic, and dopaminergic systems (Balachandran et al., 2020). Better understanding the factors that influence individual susceptibility to Mn toxicity will help elucidate mechanistically how Mn exerts its toxic effects.

1.4 Factors Influencing Manganese Homeostasis

These factors are summarized in **Figure 1.1.**

Exposure route. Mn absorption and distribution depends on whether it is inhaled, ingested, or injected. When inhaled, soluble forms such as $MnCl_2$ are more readily distributed throughout the body than insoluble forms such as MnO_2 (Dobson et al., 2014). Ingested Mn is the primary source of sufficient levels for heathy functioning, and liver and enterocyte SLC30A10 transporters protect against toxic levels to an extent (Taylor et al., 2019). However, as previously mentioned, detrimental effects can occur when contaminated drinking water is consumed (Gerke et al., 2016). Brain Mn is easily increased by excess dietary Mn under experimental conditions as well

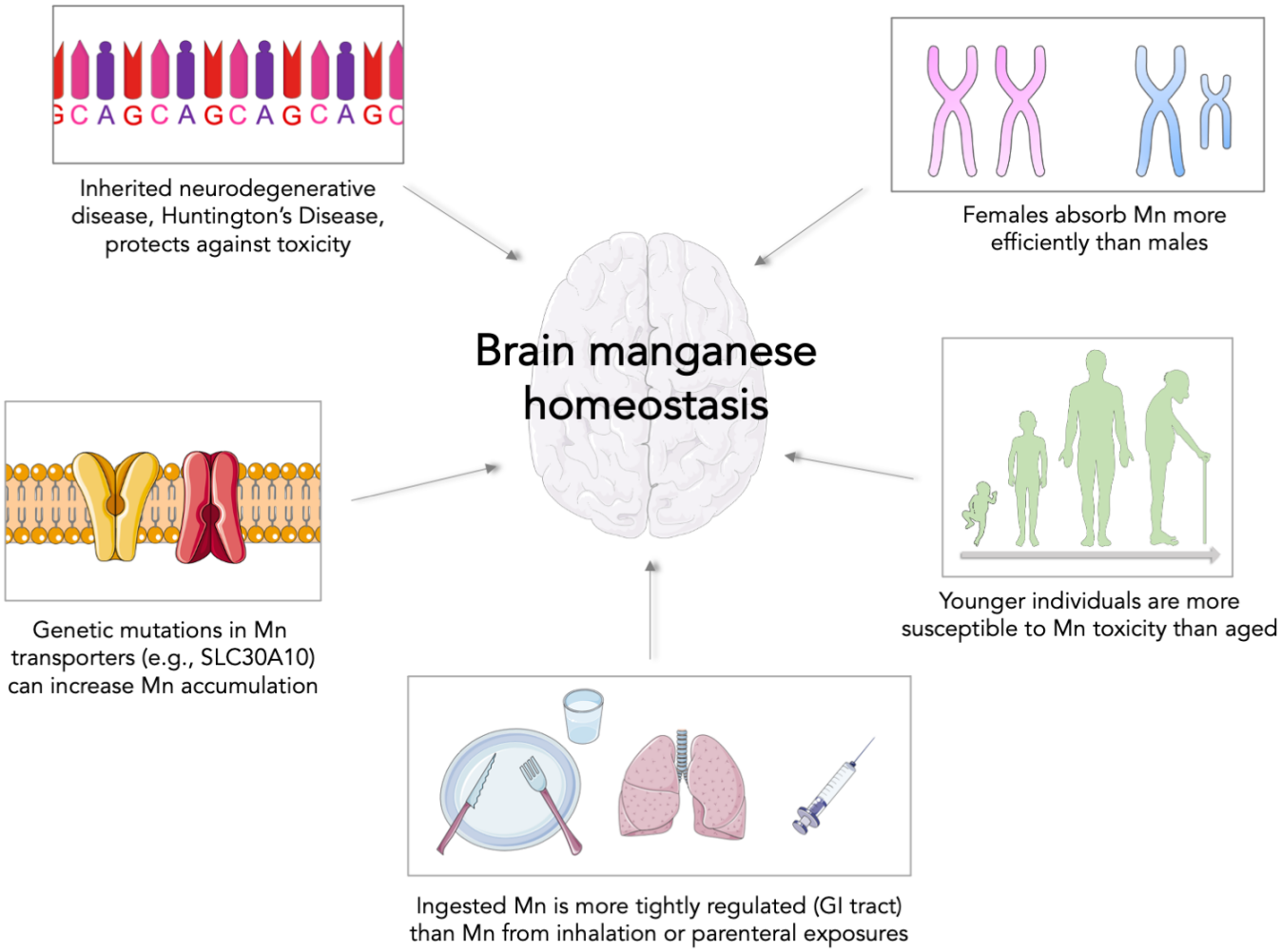

Figure 1.1 Summary of factors influencing Mn homeostasis as described in Section 1.4 (pp. 5-9).

(Garcia, Gellein, Syversen, & Aschner, 2006; Tran, Chowanadisai, Crinella, Chicz-DeMet, & Lönnerdal, 2002). The presence of other metals in the diet can influence how much Mn is absorbed and one study identified differential effects by Mn when in the presence of natural sediment in drinking water (Freeman, O'Neal, Zhang, Bouwer, & Wang, 2020; O'Neal & Zheng, 2015). One research group hypothesized that rats on a Mn-deficient diet would be more susceptible to Mn accumulation when exposed via inhalation, but their studies did not support this. They concluded dietary Mn status did not affect accumulation by a secondary route (D C Dorman et al., 2001; David C Dorman, Struve, & Wong, 2002). Mn exposure by injection occurs in real-world settings when individuals abuse the self-prepared drug methcathinone (De Bie et al., 2007). Injection exposures are more common in experimental settings, including the experiments described in chapters to follow. Intraperitoneal (IP) and subcutaneous (SC) injections of $MnCl_2$ bypass the gut and first pass hepatic metabolism, to an extent (Turner, Brabb, Pekow, & Vasbinder, 2011), and can therefore easily increase brain Mn while reducing other confounding factors that influence Mn homeostasis.

Sex. Females absorb dietary Mn more efficiently than males, and therefore unless pregnant or lactating, females have a slightly lower (1.8 mg/day) adequate intake (AI) level compared to males (2.2 mg/day) (Finley et al., 1994; Trumbo et al., 2001). Females of childbearing age were found to have the highest blood Mn concentrations in a cohort of 7,720 U.S. participants ranging from 1 to 80 years of age (Oulhote, Mergler, & Bouchard, 2014). It is postulated that this is due to higher demand for iron in this group of individuals and upregulation in DMT1 (Chua & Morgan, 1996). Under presumably the same toxic Mn exposure level, female smelters experienced more detrimental cardiotoxic effects than their male co-workers suggesting increased accumulation of or sensitivity to Mn (Jiang & Zheng, 2005). However, sex differences in Mn metabolism are more complicated than a simple difference in iron demand and increased Mn uptake as some pregnant women with similar blood Mn concentrations as pathologically-affected adult men have experienced no adverse effects (Kim, 2018). In rats IP injected with Mn, males and females exhibited similar tissue distribution of Mn but differential toxic effects on mitochondrial complexes I and II (Richter Schmitz et al., 2019). Mice on a high Mn diet experienced increased SLC30A10 expression in liver and intestine, but the effect was only observed in male mice (Felber, Wu, & Zhao, 2019). We are far from understanding mechanistically the difference between male and female Mn metabolism, but it is clear that biological sex impacts Mn homeostasis.

Age. Mn requirements during development exceed those in adulthood (ATSDR, 2012; Trumbo et al., 2001). Nutrient deficiency during the critical developmental period known as the "brain growth spurt" can have profound consequences on behavioral outcomes later in life (Bhang et al., 2013; Henn et al., 2011; Smart & Dobbing, 1971). Severe in utero Mn deficiency can lead to ataxia following birth. However, this incoordination is primarily associated with an improperly developed otolith and vestibular system dysfunction rather than a direct

impact on the brain (Sandstead, 1986). In addition to the increased requirement for Mn, younger individuals are also more susceptible to toxicity due to underdeveloped regulatory systems and a preferential accumulation in the striatum compared to aged individuals (Keith M. Erikson et al., 2007; Kern, Stanwood, & Smith, 2011). This can be especially concerning when exposed to TPN as a neonate, or for babies drinking soy (200-300 ug/L Mn) or cow's milk formula (~100 ug/L Mn) compared to breast milk (<10 ug/L Mn) (Keith M. Erikson et al., 2007). Appropriate intake is especially important at younger ages to meet the critical demand without ensuing toxicity.

Disease. Mn homeostasis is affected by liver disease and specific genetic mutations in known metal transporters. Individuals with hepatic cirrhosis experience Mn overload in brain and blood (Rose et al., 1999; Spahr et al., 1996). High exposure to Mn can itself induce cirrhosis, exacerbating Mn toxicity, but initial impairments in liver function can cause Mn overload. Evidence from rat studies shows that a portacaval shunt resulted in Mn accumulation in frontal cortex, globus pallidus, and striatum (caudate and putamen) (Rose et al., 1999). Additionally, abnormally high blood manganese concentration secondary to biliary atresia (blocked bile duct in infancy) was normalized within months following liver transplantation in two case reports (Ikeda et al., 2000). Several mutations in metal transporters that directly impair Mn homeostasis have been identified. Mutations in *SLC39A14* (*ZIP14*) lead to Mn overload. SLC39A14 transports Zn, Mn, Fe and Cd and is highly expressed in liver, intestine and brain (Aydemir et al., 2020; Tuschl et al., 2016; Winslow, Limesand, & Zhao, 2020). *SLC30A10* (*ZnT10*), coding the previously mentioned Mn exporter, also causes hypermanganesemia when mutated (Carmona et al., 2019; Mukhopadhyay, 2018; Taylor et al., 2019). Mutations in the gene coding another metal transporter, SLC39A8 (ZIP8), cause Mn deficiency (Winslow et al., 2020) and the consequential decreased activity of the Mn-dependent enzymes ARG and β-1,4-galactosyltransferase (W. Lin et al., 2017; Sunuwar et al., 2020). In 2010, our lab reported a novel disease-toxicant interaction between Huntington's Disease and Mn that paved the way for over a decade of subsequent research in the Bowman laboratory (Williams, Li, et al., 2010).

1.5 Discovery of a Huntington's Disease-Mn Interaction

Data from the Bowman laboratory highlighted striking similarities between the neurotoxicology of certain metals and the pathophysiology of Huntington's Disease (HD) that prompted a disease-neurotoxicant screen. Specifically, the sensitivity of striatal neurons to the mitochondrial complex II inhibitor 3-nitroproprionic acid (3NPA) sparked an interest in examining what other toxicants produced similar HD-like phenotypes. The original hypothesis was that any disease-toxicant interactions revealed would identify shared targets or mechanisms of pathology. Using wild-type (WT; $STHdh^{Q7/Q7}$) and mutant *Huntingtin* (HD; $STHdh^{Q111/Q111}$) striatal cell lines and a variety of metals, the screen revealed that HD cells were more sensitive to cadmium (Cd) but less sensitive to Mn based on cell survival. Further probing of the HD-Mn interaction showed that HD cells had decreased Akt

activation compared to WT and less accumulation following exposure. These findings were specific to Mn and not identified for any other metal assessed (Fe, and divalent metals Cu, Pb, Co, Zn, Ni, Cd, and Mn). Decreased sensitivity to Mn was directly caused by expression of mutant *Htt.* In this same study, the YAC128 mouse model of HD was examined and decreased Mn accumulation following exposure was reported for the first time. This novel HD-Mn interaction laid the foundation for following research supporting a bioavailable Mn deficit in HD (Williams, Kwakye, et al., 2010; Williams, Li, et al., 2010).

1.6 Huntington's Disease

Huntington's Disease (HD) is an autosomal dominant neurodegenerative disease resulting from an expanded cytosine-adenine-guanine (CAG) repeat in the Huntingtin (HTT) gene. The disease is fully penetrant when ≥40 CAG repeats are present in at least one allele of the HTT gene, which translates to an expanded poly-glutamine (polyQ) tract near the N-terminus of the mutant Huntingtin protein (mHTT) (Finkbeiner, 2011; Potter, Spector, & Prior, 2004). Changes in mood, cognitive decline, and chorea are hallmark symptoms that typically manifest mid-life (< 50 years of age) with a median survival of 18 years following symptom onset. There is no cure and current treatment, such as tetrabenazine, focuses on alleviating symptoms with no effect on progression of the disease (Bates et al., 2015; Frank, 2014). HTT is ubiquitously expressed throughout all tissues and life stages, but expression of mutant HTT (mHTT) primarily causes dysfunction and atrophy of GABAergic medium spiny neurons (MSN) of the striatum through currently unknown mechanisms (Aronin et al., 1995; Arrasate & Finkbeiner, 2012; Rikani et al., 2014).

The precise function of wild-type (WT) huntingtin protein (HTT) is uncertain. It is essential for development, demonstrated by embryonic lethality observed in mice homozygous null for Htt (Zeitlin, Liu, Chapman, Papaioannou, & Efstratiadis, 1995), and broadly necessary for neural maintenance (Bano, Zanetti, Mende, & Nicotera, 2011; Clabough, 2013). Its large size (348 kDa) and the presence of several HEAT (Huntingtin, Elongation factor 3, protein phosphatase 2A, and TOR1) repeats have deemed it a general scaffolding protein and a "protein-protein interaction hub" (Cattaneo, Zuccato, & Tartari, 2005; Clabough, 2013; Guo et al., 2018; Schulte & Littleton, 2011). Through its interactions with nearly 200 proteins (Saudou & Humbert, 2016), HTT plays a role in vesicle trafficking and axonal transport (Colin et al., 2008; Gauthier et al., 2004; Trushina et al., 2004), transcriptional regulation (Luthi-Carter & Cha, 2003; C. Zuccato et al., 2007; Chiara Zuccato et al., 2001, 2003), autophagy (Gelman, Rawet-Slobodkin, & Elazar, 2015; Wong & Holzbaur, 2014; Zheng et al., 2010), and cell survival (Rigamonti et al., 2000; Zeitlin et al., 1995; Chiara Zuccato et al., 2001). Many of these functions and protein-protein interactions, particularly those related to transcription regulation and cell signaling, depend on the non-expanded polyQ tract (< 35 repeats) present in WT HTT (Bates et al., 2015; Schaefer, Wanker,

& Andrade-Navarro, 2012; Totzeck, Andrade-Navarro, & Mier, 2017). When mutated, the elongated polyQ tract not only interferes with normal HTT function but also leads to the formation of toxic cytosolic and nuclear protein aggregates (Bao et al., 1996; Benn et al., 2008; Schaffar et al., 2004).

Though somewhat controversial, there is evidence to suggest that HD pathology is caused by the combined loss of WT HTT function and toxic gain of function exerted by mHTT aggregates (Arteaga-Bracho et al., 2016; Cisbani & Cicchetti, 2012; Finkbeiner, 2011). This could, in part, explain why HD manifests as a neurodegenerative disease with mid-life onset despite continuous HTT expression throughout development. Reduced WT HTT function results in abnormal neuron development and could subsequently render these cells more vulnerable to mHTT aggregate toxicity; neurodevelopment and neurodegeneration are not mutually exclusive (Nopoulos, 2016). For example, striatal MSNs rely on brain-derived neurotrophic factor (BDNF) produced by cortical neurons to be delivered via axonal transport, a process impaired by mHTT (Gauthier et al., 2004). Throughout the aging process, mHTT aggregates accumulate in all cell types but particularly vulnerable striatal cells atrophy, contributing to signs and symptoms of the disease (Koyuncu, Fatima, Gutierrez-Garcia, & Vilchez, 2017; Nopoulos, 2016; Rikani et al., 2014).

The clinical symptoms of HD include cognitive, psychiatric, and motor impairments. Cognitive deficits present as executive dysfunction, difficulty multi-tasking, memory loss, and difficulty learning. Psychiatric disturbances include depression, apathy, suicidal ideation, anxiety, irritability, and agitation. Motor impairments present differently depending on the stage of the disease. Early on, chorea is typical, while in late-stage HD rigidity, dystonia, and dyskinesia are prevalent. Cognitive and psychiatric symptoms often precede motor symptoms, though this is often identified in hindsight. Manifest HD is defined by the point in time when characteristic motor symptoms develop (Novak & Tabrizi, 2011).

Age at disease onset is largely determined by the length of HTT CAG repeats, such that a longer repeat length is associated with younger disease manifestation (Andrew et al., 1993; Duyao et al., 1993; J. Lee, Ramos, & Lee, 2012; Snell et al., 1993). Interestingly, CAG repeat length is also negatively correlated with age of onset in other polyQ diseases, including the spinocerebellar ataxias (Du Montcel et al., 2014). Innate toxicity of expanded polyQ proteins has been demonstrated by the development of neurodegenerative phenotypes from the insertion of a large CAG repeat into an arbitrary mouse gene (Ordway et al., 1997). However, CAG repeat length only accounts for 70% of the total variance in HD age of onset (Arning & Epplen, 2012). In patients with repeat lengths in the 40-50 range, disease manifestation can vary by several decades between two individuals with the same number of CAG repeats. This remarkable variability and the anatomical selectivity of neuronal dysfunction despite ubiquitous HTT expression suggest a pivotal role for environmental and genetic modifiers in the manifestation and progression of HD (Gusella & Macdonald, 2009; Van Dellen & Hannan, 2004; Walker, 2007).

After accounting for expanded CAG repeat length, the remaining variance in age of onset is attributable to other genes (~40%) and environmental factors (~60%) (Wexler, 2004). Variants of genes coding for proteins involved in glutamatergic neurotransmission, energy metabolism, and autophagy have been shown to delay or accelerate HD pathology (Arning & Epplen, 2012; Arning et al., 2005; Metzger et al., 2010; Weydt et al., 2009). Interestingly, CAG repeat length of the non-expanded allele has no influence on disease onset (Arning & Epplen, 2012; Snell et al., 1993). Environmental factors have the ability to influence disease onset as well. For example, high caffeine intake has been associated with earlier progression of disease (Simonin et al., 2013) but cognitive and sensorimotor stimulation, physical exercise, and caloric restriction have been identified as positive modulators that may delay onset (Duan et al., 2003; Mo, Hannan, & Renoir, 2015; Stefanko, Shah, Yamasaki, Petzinger, & Jakowec, 2017; Van Dellen, Blakemore, Deacon, York, & Hannan, 2000).

Environmental exposures to transition metals also influence disease progression and possibly age of onset. In mouse models of HD, neonatal (but not adult) iron supplementation potentiates HD phenotypes (Berggren et al., 2015; Berggren, Lu, Fox, Dudenhoeffer, & Agrawal, 2016). Dysregulation of iron homeostasis in HD is well-documented although not well-understood (Muller & Leavitt, 2014). In addition to increased iron, elevated copper and zinc have been detected in post-mortem HD brains, but it is unknown if these exposures influence age of onset or disease progression (Rosas et al., 2012). As previously discussed (p. 8), our lab discovered an interaction between HD and Mn revealing a specific neuroprotective effect of *mHTT* against Mn toxicity. Following this discovery, evidence from *in vitro* and *in vivo* HD models as well as patient studies has accumulated in support of a bioavailable Mn deficiency in HD.

1.7 Mn-Dependent and Mn-Responsive Processes are Disrupted in HD

Mn is a necessary cofactor for many of the cellular processes impaired in HD, such as regulation and recycling of glutamate, urea cycle homeostasis, redox status, and energy metabolism. The role of Mn in each of these processes in a healthy brain was previously outlined (pp. 2-4). At least one specific Mn-dependent metalloprotein from each of these cellular functions is altered in HD, which will be discussed below. Glutamine synthetase (GS) and arginase (ARG) activities are significantly altered in HD while reported changes in Mn superoxide dismutase (SOD) or pyruvate carboxylase are varied.

Amino acid (glutamate) neurotransmitter regulation. Astrocytic GS, which preferentially requires Mn, plays a major role in protecting against excitotoxicity by maintaining glutamate-glutamine homeostasis (F C Wedler & Denman, 1984; Zou et al., 2010). GS activity is significantly reduced in the caudate, putamen, frontal and temporal cortices, and cerebellum of postmortem HD brains compared to control brains (Butterworth, 1986; Carter, 1982, 1983). GS activity has not yet been investigated in animal models of HD, but there are substantial

disruptions in the glutamate-glutamine cycle with an increase in glutamate toxicity in R6/2 HD model mice (expressing exon 1 of human mHTT with 150 CAG repeats) (Behrens, Franz, Woodman, Lindenberg, & Landwehrmeyer, 2002; Liévens et al., 2001). The direct effect of Mn exposure on GS expression and activity in WT or HD models has not been elucidated, but a preferential affinity (300-1000x) for Mn implies a bioavailable Mn deficit could lower overall GS activity contributing to glutamate toxicity phenotypes observed in HD.

Astrocytic glutamate transporter 1 (GLT-1; excitatory amino acid transporter 2, EAAT2) also plays a major role in glutamate recycling by clearing glutamate from the synapse. GLT-1 is not Mn dependent, but is Mn-responsive. Glutamate uptake by both GLT-1 and glutamate aspartate transporter (GLAST) is inhibited by high concentrations of Mn (Hanker & Onnewald, 2005). The proposed mechanism for this effect is through a yin-yang repressor 1 (YY1) mediated decrease in GLT-1 mRNA and protein (Karki, Smith, Johnson, Aschner, & Lee, 2015). Mn therefore exhibits contradictory roles on glutamate regulation and recycling, as it is required for GS function but itself can induce neurotoxicity from decreased GLT-1 and the ability to clear excess extracellular glutamate (Keith M. Erikson & Aschner, 2003; Normandin & Hazell, 2002). Interestingly, reduced GLT-1 mRNA and protein have been reported in both HD models and postmortem brain tissue, likely contributing to decreased glutamate buffering and excitotoxicity (Khakh et al., 2017). Decreased GLT-1 expression is the opposite of the expected phenotype based on the proposed role of Mn deficiency in HD, as high Mn levels lead to downregulation of GLT-1. However, the precise interactions between Mn and GLT-1 in an HD model have yet to be studied. Further, while GLT-1 is primarily astrocytic, approximately 10% is neuronal. One study demonstrated that a neuronal GLT-1 knockout independent of the Htt mutation produced a pattern of transcriptional dysregulation in mice similar to that seen in HD (Laprairie et al., 2018), suggesting that the mechanism of neuronal dysfunction in HD is closely linked with glutamate regulation and Mn may produce differential responses in the disease state.

Urea metabolism. Disturbances in the urea cycle have been observed in HD animal models and HD human brains. Our lab has shown enzymatic activity of ARG2 is decreased with concomitant elevation of select urea cycle metabolites (citrulline, arginine and ornithine) in the striatum of prodromal YAC128 mice (Bichell et al., 2017). Total striatal ARG2 protein levels were reportedly lower in aged YAC128 mice, but only female mice were examined at the time. Urea cycle perturbations have also been documented in postmortem human brain tissue and a prodromal HD sheep model (OVT73), presumably due to changes in ARG2 activity but this has not been directly addressed in these studies (Chiang et al., 2007; Handley et al., 2017; Patassini et al., 2015, 2016; Skene et al., 2017).

Redox status. Increased oxidative stress has been implicated in HD, although it is not clear if this is a causative factor in the disease or the consequence of other dysfunctional processes (Gil-Mohapel, 2016; A. Kumar & Ratan, 2016). Cells are protected from oxidative damage in part by MnSOD, which reduces superoxide anions to hydrogen peroxide. Decreased activity of this protective enzyme could increase levels of oxidative stress,

evidenced by MnSOD knockdown (+/-) mice that exhibit increased oxidative stress (Brown, Didion, Andresen, & Faraci, 2007). In mouse models of HD, MnSOD activity is elevated in young mice compared to WT and significantly decreased in older mice (Santamaría et al., 2001). Dietary Mn exposure can increase MnSOD activity (S. H. Lee et al., 2013). However, the effect of Mn exposure on MnSOD activity in the context of an HD model has not been explored.

Energy metabolism. There is substantial evidence for overall perturbations in energy and glucose metabolism in HD. Specific reports of alterations in pyruvate carboxylase activity in HD are inconsistent (Butterworth, 1986). However, in 1985, before the *HTT* gene had even been identified, it was known that there is a greater prevalence of diabetes mellitus (type II) in HD patients than age-matched controls (Farrer, 1985). Reduced glucose metabolism was subsequently reported in the caudate of pre-symptomatic individuals at risk for HD in 1987 (Mazziota et al., 1987). Mouse models of HD also develop type II diabetes at higher rates than WT counterparts (Lüesse et al., 2001). HD models also exhibit differential expression of genes related to glycolysis, the Krebs cycle, and glucose transport (Chaves et al., 2017). Even if a diagnosis for diabetes was not met, a defect in insulin secretion was found in one group of HD patients compared to controls (NM et al., 2008). Impairment in insulin production goes beyond simple glucose metabolism, as alterations in the insulin-like growth factor 1 (IGF-1)/Akt pathway have been identified in both HD animal models and HD patients (Colin et al., 2005). The net result is a decrease in activated Akt in HD, which normally serves a neuroprotective role via phosphorylation of HTT itself to inhibit HTT-induced cell death (Humbert et al., 2002). These alternations are disease-relevant as treatment with insulin or IGF-1 attenuate disease phenotypes in both cell and animal models of HD by rescuing the neuroprotective effects of the Akt pathway and restoring regular energy metabolism (Lopes et al., 2014; Naia et al., 2014, 2016).

Dietary Mn deficiency mirrors certain HD phenotypes. Although rare under non-experimental conditions, Mn deficiency can result in outcomes that recapitulate some HD phenotypes. Many of the Mn-dependent and Mn-responsive pathways altered in HD discussed above are also affected by a Mn-deficient diet. Glutamate recycling and clearance has not been directly investigated in a Mn-deficient state, but low blood Mn levels have been detected in individuals with epilepsy compared to healthy controls, suggesting an association between dysregulation of the glutamatergic system and low Mn concentrations (Carl et al., 1986). Rats placed on a Mn-deficient diet showed decreased liver ARG activity, although elevations in arginine were not detected and the effect on the neuronal urea cycle was not examined in this study (Brock, Chapman, & Ãœlman, 1994). Impaired antioxidant defenses have also been reported in Mn-deficient conditions (Keen et al., 1999). A Mn-deficient diet also impairs insulin production and decreases IGF-1 signaling in rats (Clegg et al., 1998). Cholesterol metabolism, which is perturbed in HD, is also impacted by Mn-deficiency (Keen et al., 1999; Leoni & Caccia, 2015). Finally, Mn deficiency in rats beginning in utero and continuing through adulthood produced changes in liver

mitochondria structure at 9 months of age (Zidenberg-Cherr, Keen, & Hurley, 1985); mitochondrial dynamics are altered in HD and contribute to the pathophysiology of the disease (Reddy, 2014; Reddy, Mao, & Manczak, 2009). Despite the overlap between HD phenotypes and those of Mn-deficiency, additional consequences arise from inadequate Mn that are not observed phenotypes in HD. For example, skeletal bone growth abnormalities, osteoporosis, decreased fertility and irregular estrous cycles can occur without sufficient Mn (McDowell, 2017). However, the overall consistency between Mn deficiency and molecular HD phenotypes strongly supports a role for perturbed Mn homeostasis in the pathogenesis of HD (**Fig. 1.2**).

1.8 Manganese Exposure Attenuates Select HD Phenotypes

Since the original discovery of an HD-Mn interaction, our lab has sought to determine which Mn-related HD phenotypes could be rescued via Mn exposure. Defects in the urea cycle, glucose metabolism, and autophagy have been corrected by Mn.

Urea cycle pathology was directly linked to bioavailable Mn deficiency in YAC128 mice by work performed in our lab. Further, an acute Mn exposure (adapted from (Dodd, Ward, & Klein, 2005) and employed in subsequent chapters) decreased the elevated levels of citrulline, arginine, and ornithine in 12-week-old YAC128 mice to match levels of WT vehicle-treated mice. This Mn supplementation paradigm also attenuated the reduction in striatal ARG2 activity levels in HD mice with no negative impact observed in WT mice (Bichell et al., 2017). As previously mentioned, there are disruptions in energy metabolism observed in HD and Mn has been shown to attenuate these phenotypes. In HD cells, impaired IGF signaling and glucose uptake were connected to Mn biology and co-treatment with IGF and Mn rescued these disease phenotypes (Bryan et al., 2020). In HD cells (mouse striatal and human-derived neuroprogenitors), the defective autophagy phenotype was corrected by Mn exposure (Bryan et al., 2019). However, not all HD phenotypes investigated have been corrected by Mn exposure. For example, defects in cholesterol synthesis and metabolism noted in HD were unaffected by Mn exposure (Pfalzer, Wages, Porter, & Bowman, 2019).

1.9 Manganese as a Modifier of Huntington's Disease versus Huntington's Disease as a Modifier of Manganese Toxicity

The ability for Mn exposure to rescue *any* HD phenotype is remarkable. Normalized urea cycle perturbations in HD mice and corrections in both glucose metabolism and autophagic cargo load in HD cells are inspiring and promising discoveries. But what does this mean? An individual with HD is not so concerned about elevated urea cycle metabolites or defective autophagosome cargo loading. An individual with HD is bothered by

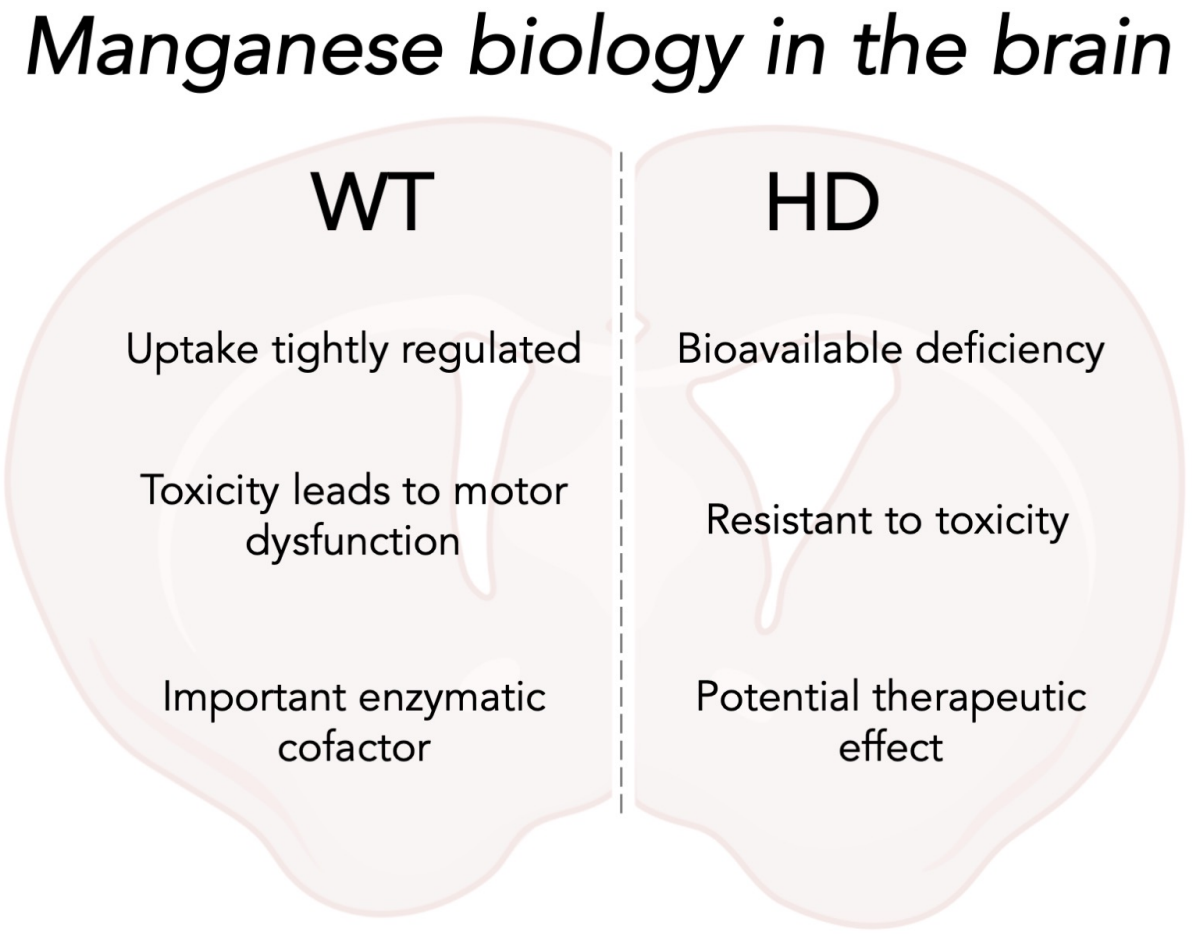

Figure 1.2 Manganese biology in wild-type (WT) compared to Huntington's Disease (HD).

their impaired cognition and devastating motor symptoms and hopes for the potential to live a "normal" healthy life. Thus, when I joined the Bowman lab, I was most interested in investigating the impact of Mn exposure on behavioral phenotypes in HD. I sought to determine if Mn has the ability to attenuate or delay the awful symptoms experienced by those suffering with HD. The following chapters describe the research I performed to examine this possibility using the YAC128 mouse model of HD.

In **Chapter 2**, we examined how several Mn exposure paradigms differentially affected the global response to Mn in WT compared to HD mice. This was assessed using both acute and chronic Mn injections, in young and aged mice, across two genetic backgrounds. We repeatedly found suppressed changes by Mn in the transcriptome, striatal metabolome and in the expression of specific proteins in HD mice. This led us to evaluate the behavior of WT and HD mice in response to chronic Mn injections of various doses over time, which comprises the work represented in **Chapter 3**. I hypothesized that a chronic Mn exposure may attenuate HD behavioral phenotypes depending on when treatment began. We had previously focused on administering Mn beginning at a specific age (12 weeks) and via a specific route (subcutaneous injection), but in **Chapter 4** I explored the behavioral changes induced by excess dietary Mn at both a younger age (beginning at weaning) and well into the manifestation of disease (12 months old). Finally, to begin to understand molecular changes caused by Mn in HD versus WT, I explored alterations in dopaminergic dynamics following an acute Mn injection exposure using fast scan cyclic voltammetry in **Chapter 5**.

Throughout my research, I found subtle pieces of evidence that supported my hypothesis that Mn could treat HD behavioral deficits. However, I more often found outstanding evidence that HD alters the normal or expected response following Mn exposure. Mn can certainly rescue a handful of molecular HD phenotypes but the studies I performed did not result in rescue of behavioral phenotypes. However, the substantial work outlined in the following chapters supports a differential response to Mn between HD and WT following both subcutaneous and dietary Mn exposures. Continuing research on this disease-toxicant interaction will further elucidate both mechanisms of HD pathology and regulation of Mn homeostasis.

Chapter 2

Huntington's Disease Genotype Suppresses Global Manganese-Responsive Processes in Pre-Manifest and Manifest YAC128 Mice

2.1 Publication Acknowledgement

This chapter is published in *Metallomics* and has been reproduced with the permission of the publisher and my co-authors (A. C. Pfalzer & A. B. Bowman). *ACP and JMW contributed equally. Supplemental material available online.

Pfalzer, A. C.*, **Wilcox, J. M.*,** Codreanu, S. G., Totten, M., Bichell, T. J. V., Halbesma, T., Umashanker, P., Yang, K. L., Parmalee, N. L., Sherrod, S. D., Erikson, K. M., Harrison, F. E., McLean, J. A., Aschner, M., & Bowman, A. B. (2020). Huntington's disease genotype suppresses global manganese-responsive processes in pre-manifest and manifest YAC128 mice. *Metallomics*, *12*(7), 1118- 1130. DOI: 10.1039/d0mt00081g

2.2 Abstract

Manganese (Mn) is an essential micronutrient required for the proper function of several enzymes. Accumulating evidence demonstrates a selective decrease of bioavailable Mn in vulnerable cell types of Huntington's Disease (HD), an inherited progressive neurodegenerative disorder with no cure. Amelioration of underlying pathophysiology, such as alterations in Mn-dependent biology, may be therapeutic. We therefore sought to investigate global Mn-dependent and Mn-responsive biology following various Mn exposures in a mouse model of HD. YAC128 and wildtype (WT) littermate control mice received one of three different Mn exposure paradigms by subcutaneous injection of 50 mg/kg $MnCl_2 \bullet 4(H_2O)$ across two distinct HD disease stages. "Pre-manifest" (12-week-old mice) mice received either a single (1 injection) or week-long (3 injections) exposure of Mn or vehicle (H_2O) and were sacrificed at the pre-manifest stage. "Manifest" (32-week-old) mice were sacrificed following either a week-long Mn or vehicle exposure during the manifest stage, or a 20-week-long chronic (2x weekly injections) exposure that began in the pre-manifest stage. Tissue Mn, mRNA, protein, and metabolites were measured in the striatum, the brain region most sensitive to neurodegeneration in HD. Across all Mn exposure paradigms, pre-manifest YAC128 mice exhibited a suppressed response to transcriptional and protein changes and manifest YAC128 mice showed a suppressed metabolic response, despite equivalent elevations in whole striatal Mn. We conclude that YAC128 mice respond differentially to Mn compared to WT as measured by global transcriptional, translational, and metabolomic changes, suggesting an impairment in Mn homeostasis across two different disease stages in YAC128 mice.

2.3 Introduction

Manganese (Mn) is an essential metal required for several biological processes regulating human health. Mn functions as a co-factor for several enzymes, including glutamine synthetase (GS), superoxide dismutase 2 (MnSOD), pyruvate carboxylase (PC), and arginase 2 (ARG2) (Horning et al., 2015). In addition, there are several canonical signaling pathways which are Mn-responsive, such as ATM (Tidball et al., 2014), p53, PI3K, insulin and IGF-1 (Bryan & Bowman, 2017; Bryan et al., 2018). Attention has been paid to the toxicological properties of Mn as it is a potent neurotoxicant with overexposure resulting in Manganism, which manifests with parkinsonian features (Cersosimo & Koller, 2006). Despite potential toxicity, it is clear that maintaining adequate levels of Mn is crucial for proper neurological function (Horning et al., 2015) and therapeutic Mn exposures may ameliorate select neurodegenerative disorders in which Mn-dependent or Mn-responsive processes are suppressed or insufficient (Pfalzer & Bowman, 2017). Mn deficiency is rare as the average human diet provides sufficient amounts of Mn (Horning et al., 2015). There is, however, a consistent link between divalent metal homeostasis and neurodegenerative disorders (Cicero et al., 2017) – suggesting that neuronal metal biology may be impaired under these conditions.

HD is an autosomal dominant neurodegenerative disorder which develops as a result of a trinucleotide repeat expansion in the Huntingtin gene (*HTT*). The mutation results in selective degeneration of the medium spiny neurons within the striatum (caudate and putamen), as well as select other neurons, and often presents clinically with chorea, mood disorders, psychiatric symptoms and cognitive impairment. Symptom onset is largely dictated by length of CAG-repeat with longer expansions associated with earlier onset (J. Lee et al., 2012; Walker, 2007); however, there is a great amount of variability (Andrew et al., 1993) which has been attributed to other genetic and environmental modifiers. There is clear evidence for a link between Mn and HD. Williams *et al* found reduced Mn-dependent neurotoxicity in HD mouse striatal cells compared to control striatal cells (Williams, Li, et al., 2010). This neuroprotective effect of the HD genotype against Mn neurotoxicity has been replicated, with evidence for this phenomena occurring through an ATM-p53 mediated molecular pathway in the same mouse HD striatal cell model as well as human neuroprogenitors (Tidball et al., 2014).

We have also investigated the impact of Mn exposure on a well-established HD mouse model that replicates key features of HD pathobiology: the YAC128. The YAC128 line contains a mutant copy of the human *Huntingtin* gene and is described in greater detail below (Slow et al., 2003). YAC128 mice mirror the selective striatal and cortical degeneration observed in humans and furthermore, recapitulate several cognitive and motor symptoms observed in humans (Slow et al., 2003). Specifically, YAC128 mice exhibit impairments in aspects of executive function (motor learning) as early as 2 months of age that progressively worsen (J. M. Van Raamsdonk, 2005). At this early age, there are no consistently observed motor phenotypes – which is also commonly observed in prodromal HD patients. Starting around 4-6 months of age, YAC128 mice demonstrate more overt deficits in

executive function (memory) and motor coordination and these also worsen with age (J. M. Van Raamsdonk, 2005). This particular model is well suited for evaluating behavioral or pharmacokinetic interventions as disease progression is modest: 2-month old YAC128 mice resemble pre-manifest disease and 12-month old mice exhibit more severe manifest motor symptoms (J. M. Van Raamsdonk, 2005). We have previously demonstrated that several HD phenotypes are attenuated following Mn exposure. For example, elevations of striatal urea cycle metabolites in a pre-manifest HD mouse model can be corrected with a 1-week Mn exposure (Bichell et al., 2017). Additionally, acute Mn treatment attenuates the "cargo-recognition failure" in autophagy and partially rescues the reduced glucose uptake phenotypes observed in HD cell lines (Bryan et al., 2020, 2019). It is worth noting that not all HD phenotypes examined are corrected by Mn exposure. For example, altered striatal sterols in HD model mice are not changed by acute Mn exposure (Pfalzer et al., 2019). Given the evidence for reduced bioavailable Mn in HD and that specific HD phenotypes can be ameliorated by Mn exposure, we further investigated the global striatal response to Mn in pre-manifest and manifest HD mice and WT controls using various lengths of Mn exposure.

The molecular mechanisms by which HD impairs Mn biology are uncertain; we demonstrate here that the gene-environment interaction between HD and Mn are consistent across several stages of disease and diverse biological processes. We demonstrate that single, 1-week-long, and 20-week-long Mn exposures in pre-manifest and manifest HD model mice suppress multiple Mn-dependent and Mn-responsive biological processes at the gene expression (mRNA), protein and metabolic levels in the mouse brain. Further examination on the impact of these Mn exposures on HD phenotypes, including the behavioral manifestations observed in this HD mouse model are warranted in future studies.

2.4 Materials and Methods

2.4.1 Materials

Unless otherwise noted, all chemicals were purchased from Sigma-Aldrich (St. Louis, MO). Optima grade LC-MS solvents for the mass spectrometry analysis were obtained from Thermo Fisher Scientific (Fair Lawn, NJ). All sterol standards, natural and isotopically labeled, used in this study are available from Kerafast, Inc. (Boston, MA).

2.4.2 Animals

All animal use was approved by the Vanderbilt University Medical Center Institutional Animal Care and Use Committee. Animal husbandry and genotyping information has been previously described (Bichell et al., 2017). Briefly, male and female FVB-Tg(YAC128)53Hay/J mice (Jackson Laboratory, Bar Harbor, ME; stock number: 027432) were weaned at 21 days and co-housed in groups of 2-5. These mice, which will be referred to as YAC128, contain two WT copies of the mouse Huntingtin *(Htt)* gene and are hemizygous mutant with one full-length copy of the human *HTT* gene (Slow et al., 2003). Thus, our mutant YAC128 mice contain 3 copies of the Huntingtin gene compared to our wild-type (WT) littermates with 2 copies of mouse *Htt*. An additional mouse line of C57-YAC128 was generated by crossing the FVB-YAC128 mouse with the C57BL/6J mouse and backcrossed for at least 10 generations. These mice will be referred to as C57-YAC128. At weaning, mice were genotyped using Transnetyx qPCR-based genotyping as previously described (Bichell et al., 2017). Hemizygous mutant animals and wild-type (WT) littermates were used for experiments. Pre-manifest male C57-YAC128 and C57-WT mice are exclusively used for the single injection exposure experiment. Male and female YAC128 and WT mice at 12-weeks and 32-weeks of age were included in the 1-week and 20-week long Mn exposure studies. Data presented are the result of several independent experiments. Specifically, data presented in pre-manifest mice with 1-week Mn exposure are from three independent experiments (*experiment 1*: striatal Mn, Arginase 2 protein; *experiment 2*: BDNF, SLC30A10 mRNA, GLT-1 protein; *experiment 3*: RNAseq, qRT-PCR). Data presented in manifest mice receiving either 1-week or 20-week Mn exposure are from a fourth experiment. See **Table 2.1**.

2.4.3 Manganese exposure paradigms

This study utilized three Mn exposure paradigms: 1) a single subcutaneous exposure of either a 1% solution of $MnCl_2 \bullet 4(H_2O)$ in filtered MilliQ water at 50 mg/kg body weight or vehicle (filtered water), 2) a 1-week, and 3) 20-week chronic exposure. The 1-week exposure is a previously published week-long exposure protocol (intermittent injections given on days 0, 3 and 6, with sacrifice on day 7) known to elevate brain Mn levels (Dodd et al., 2005). The 20-week exposure is a twice weekly injection (Mondays and Thursdays) based on the estimated half-life of 3.5 days for Mn administered via this route and pilot work suggesting the absence of observable toxicity with this exposure paradigm (including no weight loss or physical signs of distress).

Age	Mn Exposure	Outcome measures	Associated figures
13-weeks	1-week-long	striatal Mn, ARG2 protein, RNAseq	2.1 A-E
13-weeks	single exposure	*Bdnf* and *Slc30a10* mRNA, ARG2 and GLT1 protein	2.2 A-D
32-weeks	1-week-long	striatal Mn, ARG2 protein, metabolomics	2.3 A-E
32-weeks	20-week-long	striatal Mn, ARG2 protein, metabolomics	2.4 A-E

Table 2.1 Summary of Mn exposures and age of mice for each outcome measure.

2.4.4 Tissue collection

For the single injection exposure, mice were sacrificed either 0, 1, 4, 12 or 24 hours after the injection to examine acute changes to Mn. For 1-week and 20-week Mn exposures, mice were sacrificed 24 hours after the final injection. For all studies, mice were sacrificed by cervical dislocation without anesthesia. Mice were decapitated with sharp scissors and the brain removed. The striatum was dissected out under a dissecting microscope, flash-frozen in liquid nitrogen and stored at -80°C until later analysis.

2.4.5 Striatal Mn levels

Striatal Mn concentrations were measured with graphite furnace atomic absorption spectrometry (GFAAS, Varian AA240, Varian, Inc., Palo Alto, CA). Protein lysates were prepared as described below (Western Blotting). These striatal protein lysates were further digested in ultrapure nitric acid (1:10 wt/vol dilution) for 48–72 h in a sand bath (60 °C); 100 µL of digested tissue was brought to 1 mL of total volume with 2% nitric acid and analyzed for Mn. This dilution ensured that all samples were analyzed in the middle of the standard curve of 0 mg Mn/L, 2.25 mg Mn/L, 4.5 mg Mn/L, and 9 mg Mn/L. The detection limit on the GFAAS for Mn is 5 ng/L. A bovine liver (NBS Standard Reference Material, USDC, Washington, DC) (10 µg Mn/g) was digested in ultra-pure nitric acid and used as an internal standard for analysis (final concentration 5 µg Mn/L).

2.4.6 RNA processing for RNA sequencing and qRT-PCR

RNA was extracted from frozen striatal tissue using Trizol (Invitrogen, cat # 15596026) following the standard protocol. Tissues were homogenized with plastic tissue grinders. RNA was quantified with a NanoDrop spectrophotometer, then converted to cDNA with the SuperScript III Reverse Transcriptase kit (Invitrogen 18080044) following manufacturer's protocol.

2.4.7 Library preparation

Library preparation was performed as previously described in Parmalee et al. (2015). Briefly, an Illumina RNASeq compatible library was prepared by ligating TruSeq adaptors to the cDNA and treating with UNG prior to amplification. RNA sequencing was performed at the Albert Einstein College of Medicine Center for Epigenomics / Computational Genomics Core. It was performed on an Illumina Hiseq2500 machine with 100bp single-end reads. All sample libraries were multiplexed with TruSeq indexed adaptors and ran on one lane. The

output of the Illumina machine was raw FASTQ files. Quality control of raw FASTQ data files from the Illumina sequencing machine was done with FASTQC (Version 0.11.5; https://www.bioinformatics.babraham.ac.uk/projects/fastqc/). Trimming of low-quality base calls was done with cutadapt (Version 1.16), setting the quality cutoff to 20 and minimum read length to 20 (Martin, 2011). STAR (Version 2.5.3a) was used for alignment of 100bp reads to the mm10 reference genome, FVB/NJ genome (ftp://ftp.ensembl.org/pub/), and human *HTT* gene, all downloaded from ENSEMBL (Dobin & Gingeras, 2015). The corresponding gtf annotation files from ENSEMBL were used. The human *HTT* gene was manually changed to have 128 CAG repeats in exon 1, and the start and stop positions in its annotation file were modified according to the added bases. Alignment files were in BAM format sorted by coordinate. FeatureCounts from the subRead package (Version 1.6.1) was used to assign reads to genes, generating count tables (Liao, Smyth, & Shi, 2014). Count tables were uploaded to R for differential expression analysis with DESeq2 (Love, Huber, & Anders, 2014). The mouse ENSEMBL IDs (ENSMUSG) returned by DESeq2 were matched to their respective common gene names using the R package biomaRt.

2.4.8 Western blotting

Striatal tissue lysates were prepared by homogenizing frozen tissue in 180µL Pierce RIPA lysis buffer (Thermo Scientific, Cat# 89900) with protein and phosphatase inhibitors (Sigma Aldrich, cat #P0044, #P2850, #P5726, and #P2714). Protein concentration was measured using a standard quantification protocol (Pierce BCA Protein Assay Kit, Thermo Scientific). Samples were prepared with denaturing sample buffer (Bio-Rad Cat# 0610747) and either 10 µg of protein (GLT1) or 40 µg of protein (ARG2) were loaded onto Mini-Protean TGX Pre-cast gels (Bio-Rad Cat# 4561094) and gel transfer was done using the iBlot™ system. Membranes were blocked with Odyssey blocking buffer (Odyssey Cat # 927-40000) for 1 hour prior to incubation with primary antibodies using Arginase 2 (ARG2) at 1:1,000 (Santa Cruz, sc-20151) and Glutamate Transporter 1 (GLT1) at 1:4,000 (Millipore Sigma, AB1783). Secondary antibodies were anti-rabbit or anti-guinea pig (Licor IRDye 700 or 800CW) diluted at 1:10,000 in Odyssey blocking buffer. Protein was detected using the Odyssey infrared system and analyzed with ImageStudio (www.licor.com) and normalized to total protein quantified from Coomassie stained gel signal.

2.4.9 Metabolomics

Previously frozen striatal tissue was lysed in 400µL ice-cold lysing buffer (1:1:2, ACN:MeOH:Ammonium Bicarbonate (0.1M, pH 8.0) (LC-MS grade). Individual samples were sonicated using

a probe tip sonicator, 10 pulses, at 30% power and cooled down on ice between samples. A BCA protein assay was used to determine the protein concentration for each individual sample and adjusted to a total amount of protein of 200µg in 200 µL of lysis buffer. Isotopically labeled standards, Creatinine-D3 and Lysine-D4, were added to each sample to assess sample processing steps (metabolite extraction and reconstitution). Following lysis and standard addition, protein precipitation was performed by adding 800µL of ice-cold methanol (4x by volume). Samples were incubated at -80°C overnight. Following incubation, samples were centrifuged at 10,000 rpm for 10 min to eliminate proteins. The supernatants containing metabolites were dried via speed-vacuum.

Dried metabolite extracts were stored frozen at -80°C until ready to use. Prior to mass spectrometry analysis, extracts were reconstituted in 100 µl of acetonitrile/ water (80:20, v/v) and centrifuged for 5 min at 15K rpm to remove insoluble material. Quality control samples were prepared by pooling equal volumes of each sample. Isotopically labeled standards, Valine-D8 and Inosine-4N15, were added to each sample to determine MS instrument reproducibility.

Global, untargeted mass spectrometry analyses was performed on a high resolution Q-Exactive HF hybrid quadrupole-Orbitrap mass spectrometer (Thermo Fisher Scientific, Bremen, Germany) equipped with a Vanquish UHPLC binary system (Thermo Fisher Scientific, Bremen, Germany) using an optimized parallel reaction monitoring (PRM) method. This method permits monitoring and detection of all metabolites as well as specific molecules (precursor ions) added to an inclusion list. In the same run (injection), associated fragment ions (MS2 scan) of individual ions are also detected. Particular to this study, parameters consisted of an MS1 (precursor ion) scan at 60,000 resolution with an automatic gain control (AGC) value of 1e6, max injection time (IT) of 100 ms, and scan range from *m/z* 70–1050 recorded as profile data. Following the MS1 scan, the method allows for up to six targeted MS2 scans at a resolution of 15,000 and with an AGC value of 1e5, a max injection time of 50 ms, a 1.3 *m/z* isolation window, with stepped collision energy of 20 and 40, and was performed and recorded as profile data. Lastly, the method was set with the following PRM parameters: a timed inclusion list containing the target precursor *m/z* value, charge, and a 2 min retention time window. These values were determined from prior analyses of synthetic standards.

After reconstitution, metabolite extracts (5uL injection volume) were separated on a SeQuant ZIC-HILIC 3.5-µm, 2.1 mm × 100 mm column (Millipore Corporation, Darmstadt, Germany) held at 40°C. Liquid chromatography was performed at a 200 µl min^{-1} using solvent A (5mM Ammonium formate in 90% water, 10% acetonitrile) and solvent B (5mM Ammonium formate in 90% acetonitrile, 10% water) with the following gradient: 90% B for 2 min, 90-40% B over 16 min, 40% B held 2 min, and 40-90% B over 10 min, 90% B held 10 min (gradient length 40 min).

2.4.9.1 Data processing

Ultra-performance liquid chromatography - tandem mass spectrometry (UPLC-MS/MS) raw data were imported, processed, normalized and reviewed using Progenesis QI v.2.1 (Non-linear Dynamics, Newcastle, UK). Sample runs were aligned against a quality control pool reference run, and peak picking was performed on individual aligned runs to create an aggregate data set. Unique ions (retention time and m/z pairs) were grouped (a sum of the abundancies of unique ions) using both adduct and isotope deconvolutions to generate unique compounds (retention time and m/z pairs) representative of unannotated metabolites. Data were normalized to all compounds using Progenesis QI and normalized data was utilized for relative quantitation. Significance was assessed using p-values and fold changes calculated from normalized compound abundance data. Tentative and putative annotations were determined by using accurate mass measurements (< 5 ppm error), isotope distribution similarity, and fragmentation spectrum matching (when applicable) by searching the Human Metabolome Database (HMDB), METLIN, NIST, and an internal curated library (A. Jablonski, F. Salvat, C. J. Powell, 2016; Smith et al., 2005; Wishart et al., 2013).

Metaboanalyst 4.0 (www.metaboanalyst.ca/) was used to perform pathway and metabolite enrichment analyses from annotated compounds with statistical significance ($p<0.05$) after Mn exposure in each genotype. Briefly, MetaboAnalyst assigns a pathway impact factor which reflects the location of an enriched compound within that particular biologic pathway and its impact on the downstream targets. Negative log p-values were calculated based upon the number of enriched compounds detected by UPLC-MS/MS within a particular metabolic pathway compared to the total number of compounds known to be present in that pathway. All metabolic pathways found to be significantly enriched after Mn exposure are annotated and circle color (yellow -> red) and circle size (small -> large) reflect increasing pathway impact and -log(p-value), respectfully. Each pathway network (**Figs. 2.3E** and **2.4E**) is scaled to a particular pathway impact and -log(p-value) in response to Mn; thus, pathway figures are not meant for direct visual comparisons between WT and YAC128.

The metabolomics data is available at the NIH Common Fund's National Metabolomics Data Repository (NMDR) Web site, the Metabolomics Workbench, https://www.metabolomicsworkbench.org where it has been assigned Project ID (PR001333).

2.4.10 Statistics

The statistical analyses for striatal Mn, body weights, mRNAs, ARG2 and GLT1 protein were conducted using a 2-way ANOVA with post hoc comparisons after determining either a main effect of either genotype or Mn exposure or a statistically significant ($p<0.05$) interaction between genotype and Mn exposure (GraphPad

Prism 6.0). ARG2 and GLT1 protein levels were quantified by normalizing all samples to the mean of all WT-0 (WT-vehicle) samples within the same protein membrane. Data are represented as the mean ± standard error of the mean (sem).

2.5 Results

2.5.1 Pre-manifest YAC128 mice exhibit reduced striatal Mn uptake and transcriptional responses despite similar fold-changes in ARG2 protein levels after 1-week Mn exposure

Our initial experiments in pre-manifest mice utilized a 1-week Mn exposure first published by (Dodd et al., 2005) to elevate levels of brain Mn. This nearly 5-fold elevation in striatal Mn levels has been previously confirmed in our lab (Williams, Li, et al., 2010). For reference, environmental exposures in young children living near oil refineries found approximately 50% higher levels of blood Mn compared to children living further away (Röllin, Mathee, Levin, Theodorou, & Wewers, 2005). We found no difference in basal striatal Mn levels between WT and YAC128 mice at the pre-manifest age; however, after exposure, YAC128 animals had significantly less striatal Mn than compared to exposed WT animals (**Fig. 2.1 A**). A 1-week Mn exposure did not show any overt signs of toxicity or sickness indicated by the absence of weight loss in Mn-exposed animals in both genotypes (**Fig. 2.1 B**). As expected, YAC128 mice were heavier compared to WT (Carroll et al., 2015), with no significant effect of Mn exposure. Additionally, the obligate Mn-dependent enzyme, arginase 2 (ARG2), was elevated nearly 3-fold after Mn exposure in both WT and YAC128 in weeklong exposed pre-manifest mice (**Fig. 2.1 C**) with no basal difference between genotypes. Similar fold changes in ARG2 in response to Mn in YAC128 have been previously reported (Bichell et al., 2017).

We next sought to determine the extent to which Mn-dependent effects were suppressed by the HD genotype across several biological processes. Therefore, we next examined the effects of a 1-week Mn exposure in pre-manifest mice on the global transcriptome to capture differences in steady-state levels of mRNAs. RNA sequencing (RNAseq) of striatal tissue collected from YAC128 mice demonstrated a global reduction in the sensitivity to Mn-induced transcriptional changes compared to WT mice. Using two statistical thresholds of $q<0.05$ and $q<0.10$, the number of genes differentially expressed after Mn were significantly greater in WT at both cut-offs (with 191 and 239 differentially expressed genes, respectively) compared to YAC128 (n= 31, n=40). The volcano plots in **Figure 2.1 D** demonstrate that although the range in mRNA fold changes after Mn exposure are similar for WT and YAC128, a chi-square test confirms that a greater proportion of genes are altered in WT after exposure compared to YAC128 ($p<0.0001$). Pathway analysis of differentially expressed mRNAs identified from RNAseq indicates that the top biological pathway enriched in WT mice after Mn exposure was centered around brain derived neurotrophic factor (*Bdnf*) and related to "Neurological Disease, Organismal Injury and

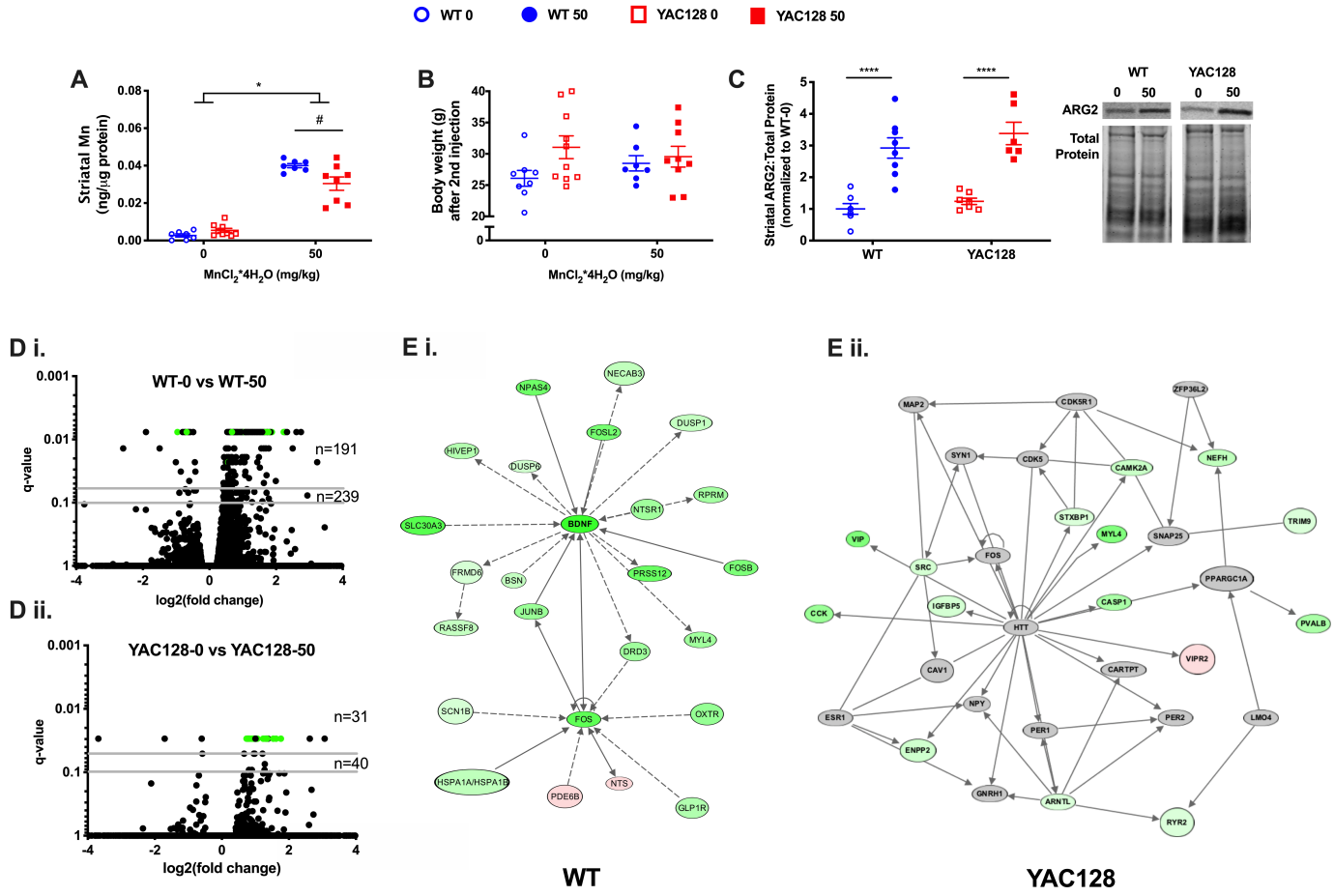

Figure 2.1 Striatal Mn **(A)**, body weights **(B)**, striatal Arginase 2 protein **(C)**, volcano plots representing striatal RNAseq **(D)** and pathway analysis of differentially expressed (DE) genes **(E)** in pre-manifest WT and YAC128 male and female mice after 1-week subcutaneous Mn exposure. Weights collected after second subcutaneous injections of 0 or 50mg/kg $MnCl_2$•$4H_2O$ and demonstrate a main effect of genotype ($p=0.04$). Data presented in A, B, and C are shown as mean ± sem and **** indicates significance level at $p<0.001$; n=6-8. Data presented in D and E are from a second independent experiment with the same Mn exposure and animal age. Volcano plots **(D)** indicate fold change in mRNA expression, black dots indicate a single mRNA and horizontal grey lines mark q-values of 0.10 and 0.05. n=191 and n=239 indicate the number of significantly altered genes at q-value <0.05 and q-value 0.10, respectively. The number of DE genes by Mn exposure is greater in WT than YAC128 by chi-square, $\chi^2=66.3$, df=1, $p<0.0001$. Green dots represent significantly altered genes in both WT and YAC128 (n=20). Top biological networks **(E)** enriched after Mn exposure in WT (E-i left) and YAC128 (E-ii right) mice. Genes in green (upregulated) or red (downregulated) backgrounds indicate those that were significantly DE after Mn exposure while genes in grey were not DE but function as genetic hubs through which DE genes may signal or impact. The intensity of the color indicates the degree of fold change. Solid grey lines indicate a direct relationship and dotted lines indicate an indirect relationship. Arrows indicate the direction of the relationship. Data represents gene changes in n=3 in each genotype and exposure.

Abnormalities" (**Fig. 2.1 E**; Qiagen, Ingenuity Pathway Analysis). Interestingly, in YAC128 mice exposed to Mn, the top biological network altered after Mn exposure was focused upon the *Htt* gene and related to "Molecular Transport, Cellular Development, Cellular Growth and Proliferation". Not surprisingly, there were a greater number of differentially expressed genes included in the WT network compared to the YAC128 top network (**Figure 2.1 E**). We sought to validate 9 genes of interest (10 comparisons) differentially expressed in our RNAseq analysis (Supplemental Table 1). These genes were selected due to their role in Mn-biology, HD pathology or degree of fold-change predicted by RNAseq. Only BDNF and IRS2 of the 10 comparisons identified from RNAseq were validated ($q<0.05$) by qRT-PCR in an independent set of samples. Although unexpected, this is likely the result of a small sample size (n=3 per group) and the difference in sensitivity between RNAseq and qRT-PCR methodology. However, both insulin receptor substrate 2 (*Irs2*) and *Bdnf* showed significant differences in expression by Mn in WT, but not in YAC128 mice (Supplemental Figure 1), despite RNAseq analysis identifying decreased *Bdnf* in YAC128 after Mn exposure (Supplemental Table 1).

2.5.2 Pre-manifest YAC128 mice exhibit a blunted transcriptional and protein response after a single Mn exposure

The 1-week exposure paradigm is likely to identify gene expression changes that are both directly tied to changes in brain Mn levels, as well as those that are indirectly responsive to direct effects of Mn on brain gene expression. Therefore, we sought to determine under more acute conditions, in which Mn-dependent changes are more likely to be directly related to changes in cell Mn levels, if HD suppression of Mn-dependent effects could be observed. Transcriptional and post-transcriptional consequences of a single subcutaneous Mn exposure were thus investigated to better understand how quickly Mn administration can impact Mn-dependent and Mn-responsive biology in the striatum. We report that as early as 1 hour after a single Mn injection, striatal mRNA levels of known Mn-responsive genes Solute Carrier 30 Family member 10 (*Slc30a10)* and *Bdnf* are significantly elevated in WT animals while there is no response at any time point in HD mice (**Figs. 2.2 A and 2.2 B**). Consistent with previous literature on BDNF in HD (Massaro et al., 2018; Stansfield, Bichell, Bowman, & Guilarte, 2014; Yu et al., 2018), we have also found that BDNF mRNA levels are significantly lower in the YAC128 striatum compared to WT (**Fig. 2.2 A**). The same single-injection paradigm had no impact on ARG2 protein expression up to 24 hours after Mn exposure (**Fig. 2.2 C**) with only notable changes in protein level after the 1-week exposure (data not included). Similarly, Glutamate Transporter 1 (GLT1) levels were not significantly altered after a single Mn exposure in YAC128 mice; however, WT levels show a small, predicted reduction compared to YAC128 animals at 24 hours after Mn exposure in GLT1 (**Fig. 2.2 D**).

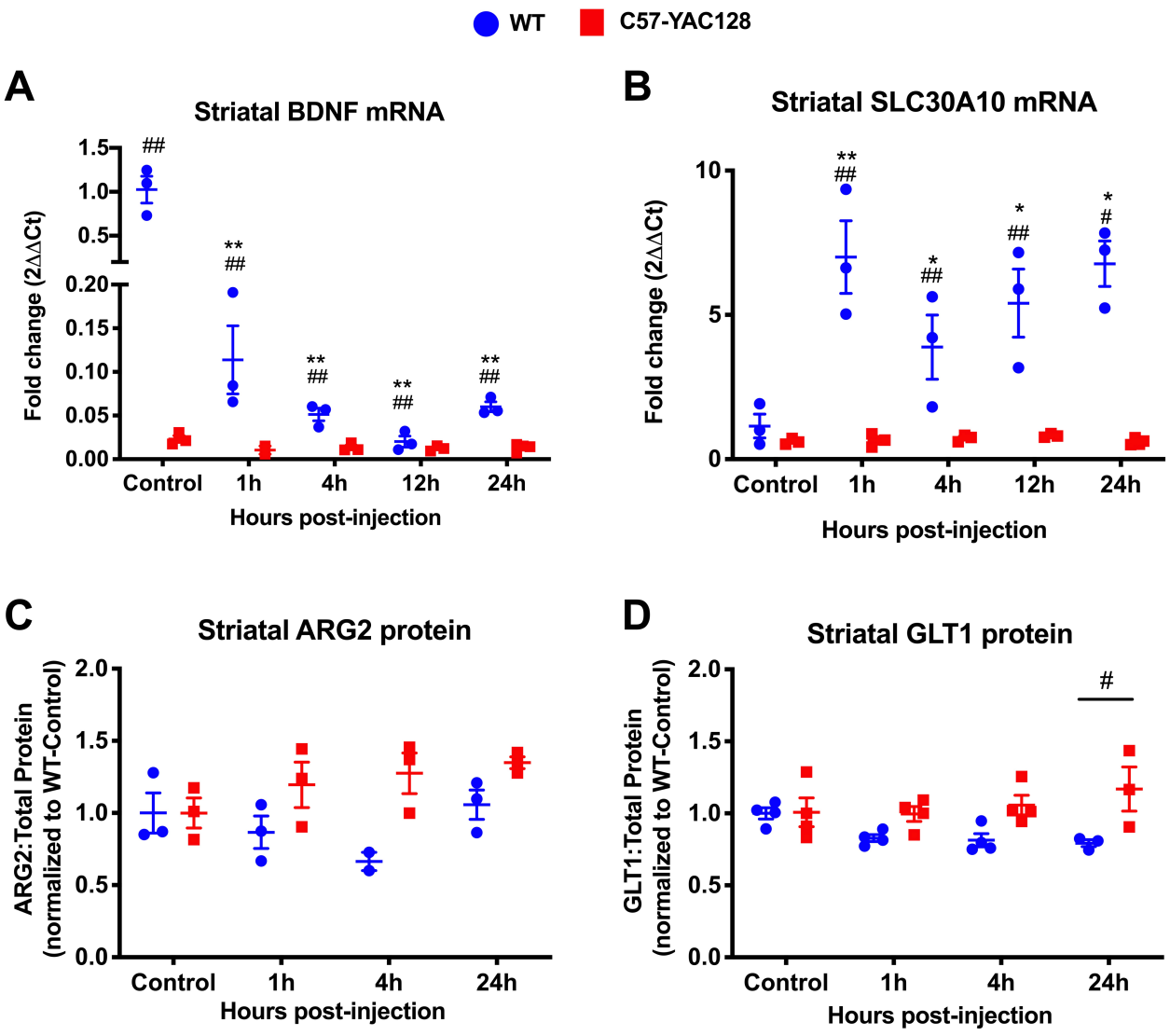

Figure 2.2 Striatal mRNA and protein changes in pre-manifest mice after a single subcutaneous Mn exposure. An 'h' represents hour post-injection. Data presented as mean ± sem and * indicates significant Mn effect at $p<0.05$ and ** $p<0.01$ compared to control, # indicates significant genotype effect at $p<0.05$ and ## $p<0.01$; n=3-4. **(A)** Brain-derived neurotrophic factor (BDNF) mRNA, **(B)** Solute Carrier Family 30 Member 10 (SLC30A10) mRNA, **(C)** Arginase 2 (ARG2) protein, **(D)** Glutamate transporter 1 (GLT1) protein.

2.5.3 Manifest YAC128 mice exhibit reduced basal levels of striatal Mn and fewer changes in striatal metabolites following a 1-week Mn exposure

Previous studies of HD-Mn interaction have focused on this 12- to 13-week old YAC128 pre-manifest HD model. To determine if HD-Mn interaction effects persisted as disease processes progress, we investigated specific phenotypes at later disease manifest stages. To address this question, we exposed 32-week old manifest YAC128 mice to the same 1-week Mn exposure and examined the striatal metabolic and post-transcriptional consequences. In manifest mice, basal striatal Mn levels were lower in YAC128 mice compared to WT providing the first evidence in this HD model for a Mn deficiency phenotype without exogenous Mn exposure. These reduced HD striatal Mn levels were mitigated following a 1-week Mn exposure (**Fig. 2.3 A**). This novel finding may implicate that the impairment in Mn homeostasis in HD changes with disease state; namely that as the HD animals age, the uptake impairment observed in younger animals (**Fig. 2.1 A**) leads to a basal deficiency later in life. Mn administration in these manifest mice does not impact body weight – suggesting no general indication of toxicity (**Fig. 2.3 B**) similar to pre-manifest mice (**Fig. 2.1 B**). Mn-dependent ARG2 protein levels were elevated approximately 3-fold in WT and 2-fold in YAC128 (**Fig. 2.3 C**) with no differences in basal ARG2 levels.

To determine if the HD genotype suppression of global biological processes extends beyond the transcriptome, we performed a metabolomic analysis of HD and WT striatum at manifest stage (32-week old animals). This global analysis of the striatal metabolomic profile is highly similar to the HD-suppressed Mn-induced transcriptional changes in pre-manifest animals; far fewer metabolites are altered in YAC128 (**Fig. 2.3 D ii**) with Mn exposure compared to WT mice (**Fig. 2.3 D i**). Volcano plots indicate that the fold-change in metabolite abundance after Mn exposure were similar for WT and YAC128 mice although in WT mice, 103 and 210 metabolites were significantly dysregulated after Mn exposure at $q<0.05$ and $q<0.10$, respectively. In contrast, YAC128 mice exposed to 1-week Mn had only 41 and 99 metabolites significantly different detected at $q<0.05$ and $q<0.10$, respectively. A chi-square test further confirms that the proportion of significantly different striatal metabolites detected is indeed greater in WT mice (Fig. 2.3 E; $\chi= 14.00$, z-statistic= 3.74) and that there are 15 metabolites altered by Mn in both WT (**Fig. 2.3 E i**) and YAC128 mice (**Fig. 2.3 E ii**). Pathway analysis of striatal metabolites significantly ($q<0.05$) altered with Mn indicates that histidine metabolism and β-alanine metabolism are enriched in both WT and YAC128 mice (**Fig. 2.3 E**) although a larger number of metabolites related to these pathways were observed in WT (4 and 3 metabolites, respectively) animals compared to YAC128 (3 and 2 metabolites, respectfully) in these pathways.

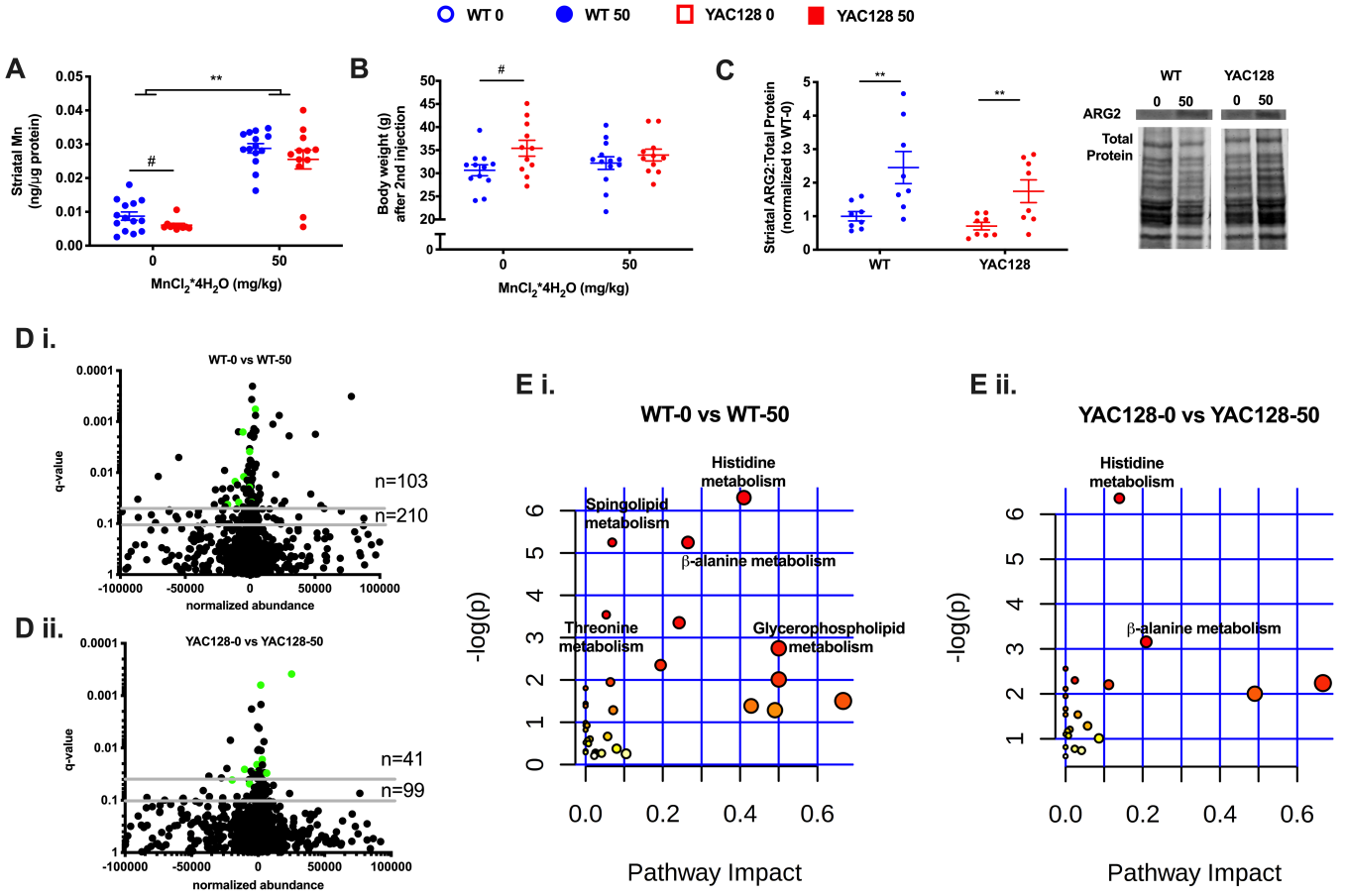

Figure 2.3 The effect of 1-week long Mn exposure in aged mice on striatal Mn **(A)**, body weight **(B)**, Arginase 2 protein levels **(C)**, striatal metabolome **(D)**, and metabolic pathways **(E)** enriched in the striatum. Data represented in A, B, and C as the mean ± sem and n=10-14 and an asterisk (*) indicates a Mn effect and a hashtag (#) indicates a genotype effect at significance level of $p<0.05$. Changes in the striatal metabolome (D) depicted in volcano plots indicate metabolites altered at q-value<0.05 and q-value<0.10 with horizontal grey lines. n=103 and n=210 indicate the number of significantly altered metabolites in WT at q-value <0.05 and q-value 0.10, respectively. n=41 and n=99 indicate the number of significantly altered metabolites in HD at q-value <0.05 and q-value 0.10, respectively. The number of significantly altered metabolites is greater in WT than HD, $\chi^2=14.0$, df=1, $p<0.001$. Green dots indicate those significantly altered metabolites in both WT and HD (15 metabolites). Pathway analysis of striatal metabolites indicates similar metabolic pathways. Colored dots ranging from yellow to red indicate increasing significance by -log(p-value); Biological pathways significantly enriched ($p<0.05$) are annotated. Pathway impact relates to the ability of enriched metabolites to impact additional compounds within that pathway. Circle color (yellow -> red) and circle size (small -> large) reflect an increasing pathway impact and –log (p-value), respectfully. Metabolomic data represent feature changes in n=10-14 for each genotype and exposure.

2.5.4 Manifest YAC128 mice exhibit similar increases in striatal Mn yet fewer changes in striatal metabolites following 20-week Mn exposure

Finally, we sought to determine if chronic elevations in systemic Mn would reveal HD-Mn interaction effects. Thus, another cohort of manifest mice were examined following chronic exposure to the same 50 mg/kg Mn dose for approximately 20-weeks (beginning at 12 weeks and sacrificed at 32 weeks of age). In this particular cohort of mice, striatal Mn levels were similarly elevated approximately 3-fold in both WT and YAC128 mice (**Fig. 2.4 A**). Since there is no difference in basal striatal Mn levels between WT and YAC128 manifest mice chronically exposed to vehicle, it was unexpected that chronic vehicle exposure would alter striatal Mn relative to the acute Mn exposure (**Fig. 2.3 A** vs **2.4 A**). As seen with acute Mn exposures, chronic Mn exposure did not result in a change in body weight for either WT or YAC128 mice (**Fig. 2.4 B**). In fact, Mn exposure slightly accentuated the genotype difference in body weight between WT and YAC128 animals. Striatal ARG2 levels were similarly elevated nearly 4-fold after Mn exposure in both WT and YAC128 mice versus vehicle exposure (**Fig. 2.4 C**). A second interrogation of the global striatal metabolomic profile was performed for mice after a 20-week Mn exposure. Similar to the 1-week exposure data in animals of the same age (**Figs. 2.3 D-E**), we observed that chronic Mn exposure also resulted in a greater number of differentially dysregulated metabolites in WT (n=139, n=246) compared to YAC128 (n=93, n=154) at two different significant levels, $q<0.05$ and $q<0.10$ (**Fig. 2.4 D**). Among the significantly changing metabolites in response to Mn in either genotype, the changes are greater in magnitude in WT compared to YAC128 mice for almost every metabolite (Supplemental Table 2). Among the metabolites altered by Mn at $q<0.05$, there were 30 significantly altered in both WT and YAC128 (**Fig. 2.4 D**). A chi-square test confirms these findings, in particular the proportion of differentially abundant striatal metabolites is greater in WT mice ($\chi= 4.60$, z-statistic= 2.15). Pathway analysis of these animals indicates that both WT and YAC128 have similar metabolite enrichment profiles as arginine metabolism appears in both analyses (**Fig. 2.4 E**).

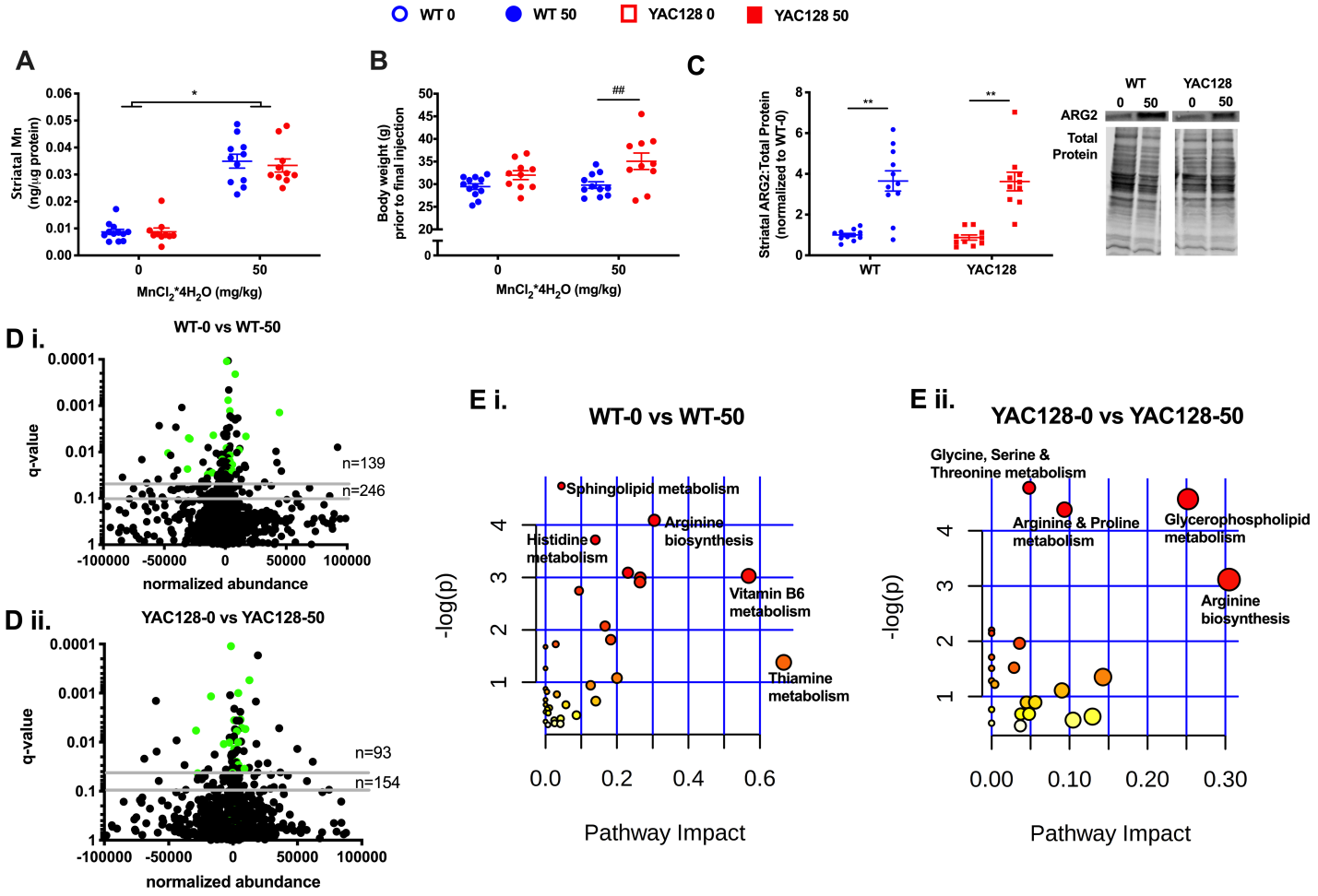

Figure 2.4 The effect of chronic (20-week long) Mn exposure in aged WT and HD mice on striatal Mn **(A)**, body weights **(B)**, striatal Arginase 2 protein levels **(C)**, striatal metabolome **(D)**, and metabolic pathways **(E).** Data for A, B, and C are represented as mean ± sem and n=10-12; an asterisk (*) indicates a significant Mn effect and a hashtag (#) indicates a significant genotype effect at a significance level of $p<0.05$ (*, #) or $p<0.01$ (**, ##) . Volcano plots **(D)** indicate metabolites altered at q-value<0.05 and q-value<0.10 with horizontal grey lines. n=139 and n=246 indicate the number of significantly altered metabolites in WT at q-value <0.05 and q-value 0.10, respectively. n=93 and n=154 indicate the number of significantly altered metabolites in HD at q-value <0.05 and q-value 0.10, respectively. More metabolites were altered by Mn in WT than in HD, $X^2=4.6$, df=1, $p<0.05$. Green dots indicate metabolites significantly altered with Mn in both WT and HD (30 metabolites) at $p<0.05$. Biological pathways **(E)** significantly enriched ($p<0.05$) are annotated. Pathway impact relates to the ability of enriched metabolites to impact additional compounds within that pathway. Circle color (yellow -> red) and circle size (small -> large) reflect an increasing pathway impact and –log (p-value), respectfully. Metabolomic data represent feature changes in n=10-12 for each genotype and exposure.

2.6 Discussion

As an essential co-factor for several enzymes regulating neuronal health, impairments in Mn handling and utilization may play a part in the pathophysiology of neurodegenerative diseases. Others have investigated the impact of Mn exposure on a wild-type transcriptome (Fernandes et al., 2019; Tian et al., 2018) and metabolome in rats (Neth et al., 2015) or cells. Differentially expressed genes following a single injection of a Mn dose that was half the one used here (25 vs 50 mg/kg $MnCl_2 \bullet 4(H_2O)$) have been reported. Many of the genes altered by Mn related to the dopaminergic system and oxidative stress pathways. In addition, the transcriptome is differentially altered by toxic compared to physiological Mn exposures (Fernandes et al., 2019). Given the difference detected in striatal Mn uptake (and hypothesized differences in intracellular compartmentalization) between WT and YAC128 mice following our 1-week Mn exposure, this may explain why only a small subset of the same genes were differentially altered by Mn in both genotypes (**Fig. 2.1 D**). Metabolite changes by Mn detected in our studies are similar to others. Specifically, amino acid metabolism was altered by a single intravenous injection of Mn in rats (Neth et al., 2015) and SH-SY5Y cells exposed to both physiological and toxic concentrations of Mn (Fernandes et al., 2018). While others have determined transcriptomic and metabolomic changes by Mn exposure, the current study is unique in that we investigated how the HD genotype alters the global responses to Mn exposure across different disease stages and Mn exposure paradigms. These experiments sought to further elucidate the mechanisms of the gene-environment interaction between HD and Mn. However, they also reveal the nature of striatal metabolomic and transcriptomic changes to Mn exposure under new and differing conditions.

Mn levels within the brain are most concentrated in the basal ganglia (Larsen, Pakkenberg, Damsgaard, & Heydorn, 1979), which include the specific region that degenerates in HD – the striatum. In HD mouse models, the tissue distribution of Mn is not consistent, so it appears to be dependent upon the different mouse model used and Mn exposure paradigm. It is noteworthy to mention that the effect size of Mn exposure on transcriptional, translational and metabolic markers is largely dependent on the mechanism of exposure. For instance, we utilize a subcutaneous Mn exposure, although dietary and genetic manipulations to alter brain Mn content have also been utilized (Hutchens et al., 2017; Taylor et al., 2019). Models utilizing dietary or subcutaneous administration exhibit 2-4 fold increases in brain Mn (Bichell et al., 2017; Hutchens et al., 2017; Taylor et al., 2019) whereas mice with mutations SLC30A10 exhibit approximately 10-fold increases in brain Mn (Hutchens et al., 2017). Despite the exposure mechanism, a compelling argument for the role of Mn in HD pathology comes from the observed reductions in the level of or activity of many manganoproteins in HD (Butterworth, 1986; Carter, 1982). Our data presented here further support a link between Mn biology and disease pathology at the systemic level of the transcriptome and metabolome by examining the impact of Mn exposure at both pre-manifest and manifest stages of disease. In addition to different disease stages, we also investigated the impact of different exposure

paradigms on the interaction between Mn and HD pathophysiology. Our data demonstrate suppression of global Mn-responsive biology in the YAC128 mouse model of HD. Specifically, we observed differences in Mn-responsiveness across different molecular processes governing transcription, protein translation and metabolic function.

In pre-manifest mice exposed to Mn for 1-week, we observed a reduction in the uptake of striatal Mn in YAC128 mice compared to WT animals (**Fig. 2.1 A**), corroborating previous findings by our lab (Williams, Li, et al., 2010). There was no basal difference in striatal Mn between WT and pre-manifest age YAC128 mice suggesting that at this stage in disease and under this exposure paradigm, there is an impairment in Mn homeostasis only following Mn exposure, although the exact mechanism is unknown. Furthermore, at this younger age and under this sub-chronic exposure paradigm, Mn elevated the protein expression of the Mn-dependent enzyme Arginase 2 (ARG2) nearly 3-fold in both WT and YAC128 mice. We did not see a reduction in ARG2 levels at baseline in YAC128; however, this might be expected given that Mn predominantly regulates ARG2 activity, not expression (Bichell et al., 2017). Additionally, we see no genotype difference in ARG2 levels after exposure, despite a reduction in Mn uptake. This discrepancy may be due to a difference in cellular composition (i.e. increase in astrocytes in HD compared to control) (Gray, 2019). Prior work found that the same Mn exposure paradigm rescued elevated levels of striatal arginine, citrulline and ornithine (Bichell et al., 2017) suggesting that there are potentially pathogenic metabolic alterations in pre-manifest HD which can be corrected with Mn. In our RNAseq transcriptome analysis, we found that fewer genes were altered by Mn exposure in the striatum of YAC128 (**Fig. 2.1 D ii**.) compared to WT (**Fig. 2.1 D i**.) mice at both q-values of <0.10 and <0.05. Furthermore, the transcriptional effect of Mn on YAC128 appears unique as only 20 mRNAs are differentially expressed in both YAC128 and WT mice (at $q<0.05$). It is noteworthy to acknowledge that our attempt to validate select transcripts of interest using qRT-PCR was minimally successful—with only 27% of genes replicating our RNAseq results. While this finding is uncommon, we suspect it is largely due to relatively high biological variability between animals, and the relatively small sample size (n=3 for each study arm). However, this study was designed to discover global effects rather than be powered to identify specific single gene changes. Furthermore, although the effect size as it relates to fold-change in our RNAseq data is relatively modest, a previous study examining the impact of Cadmium exposure in mice on mRNA profile reports similar fold-changes (Go et al., 2015). It is also important to note that even modest changes in these biological pathways can have robust functional consequences. Interestingly, one of the genes that we did validate was brain derived neurotrophic factor (*Bdnf*) which has been previously shown to be lower in HD (Gauthier et al., 2004) and reduced after Mn administration (Liang et al., 2015). Pathway analysis of genes differentially expressed after Mn exposure revealed that *Bdnf* was a central target for mRNAs in WT and related to "Neurological disorders" while *Htt* was the central target in the top pathway for YAC128 and was most related to "Cellular development and

proliferation". Our pathway analysis provides additional evidence of a global transcriptional response difference to Mn exposure in WT versus YAC128. Specifically, it suggests that Mn significantly impacts BDNF signaling in healthy animals and this, coupled with our qRT-PCR validation of *Bdnf* mRNA levels indicates that Mn may be a potential modifier of BDNF levels (an established pathological mechanism in HD (Chiara Zuccato et al., 2001)). We found that basal levels of *Bdnf* were lower in the YAC128 striatum compared to WT, as previously reported by us and others, and interestingly that Mn increased *Bdnf* in WT yet reduced it in YAC128 animals. The interaction between HD and Mn on *Bdnf* provides additional evidence for the role of Mn homeostasis in HD pathology and has clinically meaningful implications as BDNF protein is reduced in HD patient postmortem striatal tissue (Gauthier et al., 2004). Given that BDNF is synthesized in the cerebral cortex and transported into the striatum, future studies need to examine the impact of Mn on BDNF in the cortex of these animals. BDNF overexpression has been shown to prevent striatal atrophy in the YAC128 mouse model (Xie, Hayden, & Xu, 2010). The ability of a naturally occurring supplement, such as Mn, to increase BDNF expression and potentially ameliorate an HD molecular phenotype is worthy of additional investigation.

The 1-week Mn exposure paradigm has been previously shown to elevate brain Mn levels; however, it is unknown how quickly Mn can alter relevant biologic pathways within the striatum. Thus, we investigated the transcriptional impact after a single Mn exposure and observed differences in Mn-responsive genes in the striatum as early as 1-hour post subcutaneous injection in WT animals whereas there were no differences in mRNA levels of two well-known Mn-responsive genes: *Bdnf* and Solute Carrier Family 30 member 10 (*Slc30a10*) (**Fig. 2.2 A**). Consistent with previous literature, we confirmed that BDNF levels are significantly lower in the striatum of YAC128 animals compared to WT (Stansfield et al., 2014). We found that BDNF levels were decreased in WT after Mn exposure up to 12 hours after exposure whereas there was no detectable change in YAC128 mice (**Fig. 2.2 A**). Our observed decrease in BDNF after Mn exposure in WT animals is consistent with previous reports as Guilarte *et al* demonstrate a reduction in BDNF levels after Mn exposure in primates (Stansfield et al., 2014). *Slc30a10* mRNA increased and remained elevated in WT mice for 24 hours post-exposure while YAC128 had no change within 24 hours (**Fig. 2.2 B**). *Slc30a10* is a known systemic Mn efflux transporter (P. Chen et al., 2015; Hutchens et al., 2017; Mercadante et al., 2019; Taylor et al., 2019) and has been shown to be elevated after various Mn exposures. The change in expression of both *Bdnf* and *Slc30a10* in WT animals only following Mn exposure further supports the notion that YAC128 mice exhibit a suppressed sensitivity to Mn compared to WT with clearly established protein markers of cellular Mn status. We also investigated the impact of a single Mn exposure on Mn-responsive protein levels in YAC128 mice compared to WT. At the time of these experiments, there was no direct assay to measure SLC30A10 protein in mice and BDNF is notoriously difficult to quantify with standard protein quantification techniques. As previously shown in Figure 1, ARG2 has a robust response to Mn in addition to Glutamate transporter 1 (GLT1), documented previously in cultured astrocytes (Karki et al., 2014) and mouse

striatum (Pajarillo et al., 2018). However, in this experiment, ARG2 remained unchanged 24 hours after a single exposure providing greater insight into the time course and Mn exposure required to achieve the protein changes observed after 3-injections. We observed a reduction in GLT1 levels in WT striatum whereas this trend was suppressed in YAC128 mice (**Fig. 2.2 D**). The molecular mechanism for this phenomenon remains unclear, but Aschner *et al.* suggest that GLT1 levels are mediated through an interaction with select forms of Protein Kinase C (Sidoryk-Wegrzynowicz, Lee, & Aschner, 2012). This reduction in GLT1 levels may be detrimental to neurons because of excitotoxicity in response to impaired synaptic glutamate clearance and as such, we may in future investigate GLT1 levels after lower Mn exposures to evaluate harmful or toxic effects; however, the primary focus of our current work is to demonstrate that Mn biology or at least Mn responsiveness is suppressed in HD.

Finally, we investigated whether the suppression of Mn biology was specific for pre-manifest HD by utilizing manifest mice which consistently exhibit impairments in motor function (Lopes et al., 2014; C. L. Moreno, Ehrlich, & Mobbs, 2016; J. M. Van Raamsdonk, 2005). After a 1-week exposure in manifest mice, we observed a similar increase in striatal Mn after exposure in both WT and YAC128; however, we also detected a difference in basal Mn levels at this age (**Fig. 2.3 A**). Differences in basal levels of striatal Mn has never been documented in HD rodent models and might reflect a change in Mn handling over the course of HD pathology. It may also reflect the change in cellular composition within the striatum with a reduction in neurons and rise in astrogliosis with the progression of HD (Gray, 2019). Although Mn is preferentially accumulated within astrocytes and one might anticipate a corresponding rise in Mn, there is also considerable cell death within the striatum which might prevent notable rises in cellular Mn. It should be noted that Mn administration did not appear overtly toxic to either WT or YAC128 mice as indicated by stable body weights (**Fig. 2.3 B**), however specific cell death or morphological changes were not examined in the present study. After Mn exposure, there remains a significant increase in ARG2 expression; however, the fold change appears diminished in the YAC128 mice (**Fig. 2.3 C**) compared to the Mn response in pre-manifest YAC128 mice (**Fig. 2.1 C**). The suppression of Mn-responsive biology in YAC128 animals is also apparent in the global metabolomic signature. For instance, **Figure 2.3 E** shows that an untargeted metabolomic profile identified significantly more metabolites altered in WT mice compared to YAC128 after Mn exposure at both q-values of <0.10 and <0.05. It is worthwhile to note that the effect size of our Mn exposure on metabolite profile resembles that of mice in previous studies being exposed to Cadmium (Go et al., 2015) or Lead (Gao et al., 2017) in drinking water. Interestingly, YAC128 mice exposed to a chronic Mn paradigm no longer exhibit uptake deficiencies (Figure 4A) or differences in ARG2 fold-change (**Fig. 2.4 C**). Despite the chronic exposure to Mn, mice maintained their body weight and interestingly, the genotype effect on body weight no longer exists in vehicle-treated manifest mice (**Fig 2.4 B**). The untargeted metabolomic profile depicted in **Figure 2.4 E** suggests that chronic exposure in YAC128 (**E ii**.) results in a suppressed response to Mn compared to WT mice (**E i.**). The metabolites altered by chronic Mn in

YAC128 are largely different from those altered in WT – as there is only a small overlap (20% of WT metabolites; **Fig. 2.4 E**). In addition, of the 139 metabolites altered in WT (at $q<0.05$), all but 3 of them had a greater fold change in WT than HD (Supplemental Table 2). These findings are further indicative of both a unique and shared metabolic response to Mn in YAC128 mice is suppressed and provides additional evidence to support the role of Mn biology in HD pathology at multiple stages of disease.

Summary – Our work provides evidence of a global interaction between Mn biology and Huntington's disease pathobiology, versus the pathway selective effects previously reported. We demonstrate a Mn by HD genotype interaction under multiple Mn exposure paradigms in both pre-manifest and manifest disease models. Although there are currently *in vivo* and *in vitro* data to support a Mn and HD interaction in the literature, this study provides additional evidence in support of global molecular change of Mn biology in HD. Specifically, subcutaneous administration of Mn impacts both transcription and translation of Mn-dependent and Mn-responsive biology as quickly as one hour post-exposure in WT mice. Additionally, Mn has a more substantial impact on the metabolomic profile in WT compared to HD animals. These immediate molecular consequences are not observed in HD mice suggesting a resistance to or a suppression of normal Mn-responsive or homeostatic mechanisms (**Fig. 2.5**). Although the exact molecular mechanisms linking Mn biology to HD pathology remain unknown, this study provides evidence that targeting a Mn-BDNF interaction may provide valuable insight into the pathophysiology of HD.

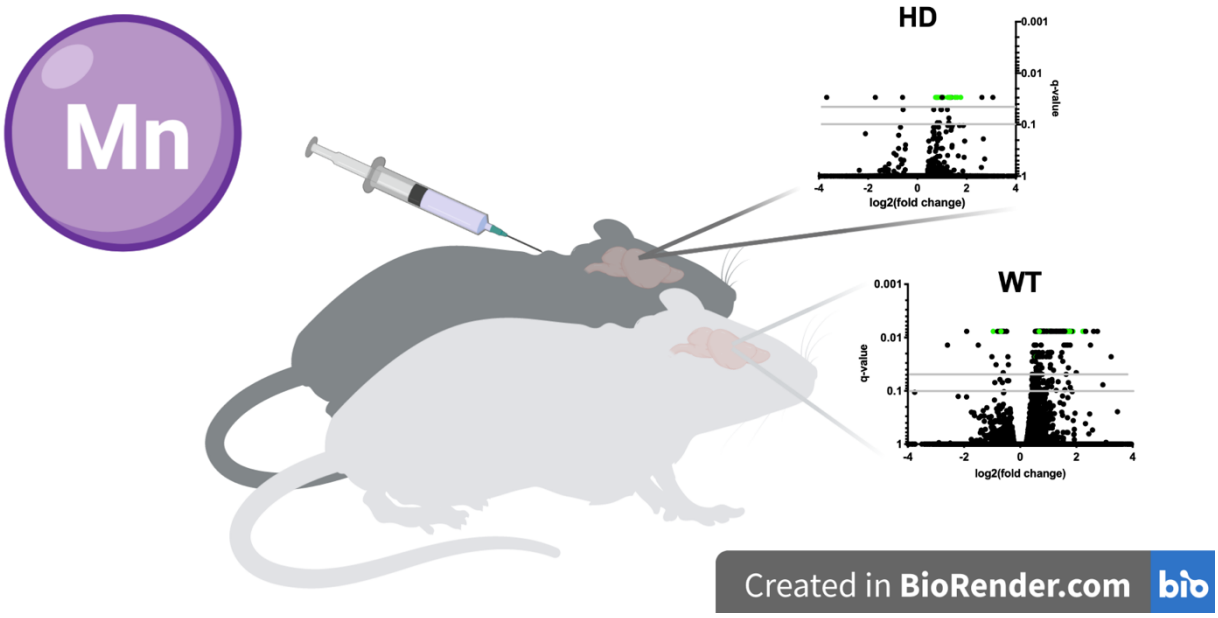

Figure 2.5 Global manganese-responsive processes are suppressed in the YAC128 mouse model of Huntington's Disease (HD) compared to wild-type (WT). Image was originally published as the table of contents entry in our *Metallomics* publication (Pfalzer et al., 2020).

Chapter 3

YAC128 Mouse Model of Huntington's Disease is Protected Against Chronic Manganese-Induced Behavioral Changes

3.1 Abstract

Manganese (Mn) is an essential micronutrient but excessive levels induce neurotoxic effects. Increasing evidence suggests a deficit of bioavailable Mn in Huntington's Disease (HD), an inherited neurodegenerative disease characterized by motor and cognitive disturbances. Previous studies have shown rescue of some molecular HD phenotypes by acute Mn exposure. This study simultaneously examined the potential for chronic Mn exposure to attenuate HD behavioral phenotypes, and for the HD genotype to offer protection against detrimental effects of chronic Mn exposure. In two independent studies a chronic Mn exposure paradigm was implemented in the YAC128 mouse model of HD and behavior was assessed at several timepoints. Study 1 exposed WT and YAC128 mice to twice weekly subcutaneous injections of 0, 5, 15, or 50 mg/kg $MnCl_2 \cdot 4(H_2O)$ from 12-32 weeks of age. A promising protective effect against motor coordination decline in 5 mg/kg $MnCl_2 \cdot 4(H_2O)$-treated YAC128 mice was detected. Study 2 thus exposed WT and YAC128 mice to either 0 or 5 mg/kg $MnCl_2 \cdot 4(H_2O)$ from 12-52 weeks of age (with a partial randomized treatment crossover at 31 weeks). The same protective effect was not observed under these conditions. We report subtle changes in exploratory behavior and total activity induced by chronic (40 weeks) Mn exposure in WT mice only, despite similar total increases in brain Mn in WT and YAC128 mice. Chronic Mn treatment resulted in a 10-12% decrease in striatal NeuN positive cells in WT mice but not YAC128 mice, despite vehicle already being reduced compared to WT mice as expected for the HD genotype. We conclude that these chronic Mn exposures do not significantly rescue behavioral HD phenotypes, but YAC2128 mice are protected against the Mn-induced behavioral changes and striatal cell loss observed in WT mice.

3.2 Introduction

Maintaining appropriate manganese (Mn) homeostasis is crucial because excessive accumulation of this essential micronutrient is toxic (Horning et al., 2015; Pfalzer & Bowman, 2017). Mn is required as an enzymatic cofactor in biological processes such as amino acid synthesis, antioxidant defense, and cellular metabolism. Adequate Mn is acquired through dietary sources and deficiency is rare (J. L. Aschner & Aschner, 2005; M. Aschner, 1999; Balachandran et al., 2020). Overexposure and Mn-induced toxicity are more commonly studied

given the detrimental impact this has on brain health (O'Neal & Zheng, 2015). Mn and other heavy metal imbalances have been implicated in several neurological diseases including Huntington's Disease (HD) and Alzheimer's Disease (AD) (Bowman et al., 2011; Mezzaroba, Alfieri, Colado Simão, & Vissoci Reiche, 2019).

Mn transport and regulation are complex biological processes that are not completely understood. Exposure route, age, sex, and certain genetic mutations influence Mn accumulation (P. Chen, Parmalee, & Aschner, 2014; K M Erikson, Dorman, Lash, Dobson, & Aschner, 2004; J. A. Moreno et al., 2009; O'Neal & Zheng, 2015). For example, mutations in *SLC30A10* decrease Mn efflux and thus result in hypermanganesemia and neurologic abnormalities (P. Chen et al., 2015; Mukhopadhyay, 2018). A disease-toxicant interaction was first identified between Huntington's Disease (HD) and Mn in an HD mouse striatal cell line, in which HD cells were less sensitive to Mn-induced toxicity compared to control cells (Williams, Li, et al., 2010). This resistance to Mn toxicity was replicated in the same striatal HD cells and human neuroprogenitors (Tidball et al., 2014). We have previously reported decreased responsiveness to global Mn-induced changes across several Mn exposure paradigms in HD mouse models during both pre-manifest and manifest disease stages (Pfalzer et al., 2020). These studies strongly suggest that HD can impact Mn homeostasis.

HD is a neurodegenerative disorder caused by an autosomal dominant mutation in the *Huntingtin (HTT)* gene. Clinical presentation includes psychiatric and cognitive impairments, but the most notable symptoms are chorea and associated motor deficits. Progressive cell death of the medium spiny neurons (MSNs) in the striatum (caudate and putamen) constitutes the hallmark neuropathology observed in HD (Bates et al., 2015; Finkbeiner, 2011). Brain areas that accumulate the highest concentrations of Mn include HD phenotype-relevant areas such as basal ganglia (globus pallidus and substantia nigra) (Yamada et al., 1986) and one outcome of excess Mn exposure is a Parkinsonian-like motor condition known as Manganism (Dobson et al., 2014; Hine & Pasi, 1975). Decreased bioavailable Mn has been reported in cell and animal models of HD prior to disease onset (Bichell et al., 2017). Activity of Mn-dependent enzymes arginase 2 (ARG2), Mn-superoxide dismutase (MnSOD), and glutamine synthetase are also decreased in HD models and postmortem HD patient brains (Butterworth, 1986; Carter, 1982; Santamaría et al., 2001). There are functional consequences to this decreased bioavailable Mn and lower enzymatic activity, evidenced by abnormalities in the urea cycle (Handley et al., 2017; Patassini et al., 2015). We have previously shown rescue of several HD phenotypes following Mn treatment. Impairments in the urea cycle, autophagic cargo load, and glucose uptake were attenuated by acute Mn exposure (Bichell et al., 2017; Bryan et al., 2020, 2019). Not all HD phenotypes examined have been positively affected by Mn. HD-related differences in cholesterol metabolism were unaffected by Mn treatment (Pfalzer et al., 2019). Despite generally showing decreased responsiveness, the YAC128 mouse model of HD was shown to more sensitive to neurite damage by acute Mn exposure than controls when examining decreased dendritic complexity by Mn exposure in striatal MSNs (Madison, Wegrzynowicz, Aschner, & Bowman, 2012).

In the present study we studied for the first time the HD-Mn interaction with a chronic Mn exposure paradigm in the YAC128 mouse model of HD. The YAC128 model is a full-length transgenic line that recapitulates key features of HD such as progressive motor impairments and selective striatal atrophy. Early deficits in motor learning have been reported at 2 months of age in these mice with impairments progressively worsening at 4-6 months and older (Slow et al., 2003; J. M. Van Raamsdonk, 2005; Jeremy M. Van Raamsdonk, Warby, & Hayden, 2007). In the current study, Mn treatment began at 12 weeks of age (3 months), prior to substantial behavioral deficits and striatal cell loss presenting in YAC128 mice. Mice were chronically exposed to $MnCl_2 \bullet 4(H_2O)$ via twice weekly subcutaneous injections for 20 – 40 weeks and underwent behavioral testing prior to measuring tissue Mn levels and Mn-induced protein changes in the striatum. We hypothesized that behavioral HD phenotypes would be ameliorated or prevented by chronic Mn exposure and HD mice would be protected against toxic effects experienced by wild-type (WT) mice from this long-term chronic Mn exposure.

3.3 Methods

3.3.1 Animals

FVB-Tg(YAC128)53Hay/J mice (Jackson Laboratory, Bar Harbor, ME; stock number: 027432) were originally obtained from Jackson Laboratories and used to found the mouse colony for these studies. These mice carry 3 copies of the *Huntingtin* gene – both wild-type (WT) copies of mouse *Huntingtin (Htt)* and one full-length copy of human mutant *Huntingtin* (*HTT)* – and will be referred to as YAC128. Hemizygous YAC128 males/females were bred with opposite sex WT mice from the same colony to maintain the line. Mice were weaned at 3 weeks old and housed in groups of 2-5; on occasion, mice were singly housed if cagemates became aggressive or died mid-study. Genotyping was performed at 3 weeks old using Transnetyx, as previously described (Bichell et al., 2017). YAC128 mice model HD by exhibiting behavioral impairments by 4-6 months which progressively worsen and that correlate to selective striatal neurodegeneration by 12 months old (Slow et al., 2003; J. M. Van Raamsdonk, 2005). Approximately equal numbers of male and female mice were used in each genotype-treatment group. Mice had *ad libitum* access to standard lab chow (LabDiet 5L0D, TX) and water in a temperature- and humidity-controlled housing room on a 12:12 light:dark cycle. All protocols were approved by the Vanderbilt University Institutional Animal Care and Use Committee under protocol number M1600073. All experiments were conducted in accordance with the NIH Guide for the Care and Use of Laboratory Animals.

3.3.2 Manganese exposures

Manganese chloride tetrahydrate ($MnCl_2 \cdot 4(H_2O)$, Fisher Scientific) was made up in DI water as a 1% stock solution, filtered through a 0.2 μm membrane, and administered as 50 mg/kg body weight. The 1% stock solution was further diluted with filtered DI water to 0.1-0.4% for the 5 – 20 mg/kg body weight doses; filtered DI water was used as vehicle. All doses were administered at a volume of 5 mL/kg injected subcutaneously in the left or right (alternating) inguinal area using an insulin syringe (27 G, ½ inch). A 50 mg/kg $MnCl_2 \cdot 4(H_2O)$ corresponds to a dose of 13.8 mg/kg Mn^{2+}.

The acute exposure (**Fig. 3.1 A**) is a previously adapted exposure paradigm (Dodd et al., 2005). Mice were injected on days 1, 4, and 7 prior to sacrifice and dissection on day 8 (24 hours after the final injection).

3.3.2.1 Study 1. Mice were injected twice weekly (Mondays and Thursdays) with one of four Mn doses [0, 5, 15, and 50 mg/kg $MnCl_2 \cdot 4(H_2O)$] starting at 12 weeks of age until 32 weeks of age, with sacrifice and dissection approximately 24 hours after the final injection (**Fig. 3.2 A**). Mn treatment was randomly assigned prior to behavioral testing. Molecular outcome measurements (striatal Mn and ARG2 protein) for 0 and 50 mg/kg $MnCl_2 \cdot 4(H_2O)$ treated mice only were previously reported as a subset of additional measurements not included in the present study (striatal metabolomics) (Pfalzer et al., 2020). Only molecular measurements from mice that completed the entirety of behavioral testing are included here.

3.3.2.2 Study 2. Mice were injected twice weekly (Mondays and Thursdays) with either vehicle (0) or 5 mg/kg $MnCl_2 \cdot 4(H_2O)$ starting at 12 weeks of age. Assignment to either vehicle or Mn was pseudo-random. We re-assigned exposure group so that the rotarod performance at 11 weeks was equivalent between assigned exposure groups within a genotype. At 31 weeks of age, half of the mice crossed over to the other treatment group; this was randomly pre-determined. The abbreviation "0_5" indicates the group that received vehicle and then Mn, and "5_0" is the group that were changed from Mn to vehicle at 31 weeks. Injections continued until 52 weeks and mice were sacrificed and dissected approximately 24 hours after the final injection (**Fig. 3.4 A**). During the behavioral battery, injections were administered after completion of a behavioral task to avoid assessing acute effects in both Studies 1 and 2.

3.3.3 Behavioral testing

3.3.3.1 Elevated zero maze (EZM). A standard black elevated zero maze (EZM; San Diego Instruments, CA) was used to assess anxiety and exploratory behavior. A mouse was placed in an open zone and freely explored

for 5 minutes. The task was recorded by a camera suspended from the ceiling above the maze and time spent in each zone was analyzed using AnyMaze (Stoelting Co., IL). An experimenter monitored the recording of the task live in an adjacent room.

3.3.3.2 Inverted screen. A wire mesh screen (approximately 30 x 7.5 cm) was mounted horizontally on a metal rod and plexiglass dividers created four 7.5 x 7.5 cm compartments. A single mouse was placed in each of the four chambers. The rod was slowly rotated 90° and returned to its original position three times to ensure mice gripped the mesh screen with all four paws before rotating the rod a full 180° to an inverted position. The screen was 40 cm above the padded apparatus floor. Latency to fall during three trials was recorded and averaged, with a maximum trial length of 60 s and a 5-10 min inter-trial interval.

3.3.3.3 Wire hang. Mice were individually placed by their front paws on a thin circular wire suspended 30 cm above a padded table. The latency to achieve a stable position (all four paws, or three paws and a tail) was recorded (60 s max per trial). If a mouse fell, a maximum latency of 60 s was assigned. Mice performed two trials with a 5–10 min inter-trial interval.

3.3.3.4 Grip strength. Grip strength was measured using a force meter (San Diego Instruments, San Diego, CA). Mice were allowed to grab a square wire grid with the two front paws while being held by the tail. When the mouse had a firm grip on the grid, the experimenter gently pulled the mouse back in a horizontal plane until the grip was broken, and maximum force (N) was measured automatically by the apparatus. Each mouse was given three trials and average force per mouse was used for analysis.

3.3.3.5 Locomotor activity. Spontaneous locomotor activity was measured automatically via the breaking of infrared beams over 30 minutes in the open field using standard sound-attenuating, light- and air-controlled locomotor activity chambers (27 x 27 x 20.5 cm, ENV-510; MED Associates, VT).

3.3.3.6 Balance beam. Motor coordination was assessed by the ability to traverse a circular horizontal beam (2.5 cm diameter, 80 cm long, suspended 51.5 cm above a table) between two platforms. The beam connected a small (5 cm x 10 cm) uncovered starting platform and a covered ending platform (18 cm x 18 cm) containing home cage bedding to encourage retreat into the area. Mice were placed on the starting platform and a timer started when they stepped on to the beam with all four paws. The time to cross the beam (max 30 s) and the number of hind paw slips were recorded. If a mouse fell, it was placed back on the starting platform. Two trials were completed and the average time to cross the beam was reported and the total accumulated number of hind paw slips was used for analysis.

3.3.3.7 Rotarod. Motor coordination was measured using a standard rotarod apparatus (Ugo Basile). The rod was 3 cm in diameter, suspended approximately 25 cm above a plastic lever on to which mice fell. There were five equal compartments (6 cm length of rod) divided by beige plexiglass. An accelerating protocol was used in which the rod began rotating at 4 rpm and ramped up to a max speed of 40 rpm by 5 min. The rod was rotating at 4 rpm when mice were placed on the apparatus and a timer was started, recording the latency to fall from the rod. Mice completed three trials per day, max 5 min per trial, with inter-trial intervals of 15 - 30 minutes. The daily average time to fall for each mouse was used in analysis of data.

3.3.3.8 Test order. For Study 1, baseline behavior was completed at 11 weeks of age and final behavior at 30 weeks of age. A mid-study behavioral battery was completed at 22 weeks of age to confirm that the HD phenotype had not progressed so far as to reach a floor effect in any time at this age. Data were analyzed and group differences did not differ from baseline/final behavior and this is not reported for brevity of results. Testing order was Day 1: EZM and inverted screen, Day 2: locomotor activity and wire hang, Days 3-5: accelerating rotarod. In Study 2, baseline behavior was completed at 11 weeks of age. Mid-way study behavior was completed at 30 weeks of age and final behavior at 50 weeks of age. Behavioral batteries were also completed at 20 and 40 weeks to confirm HD-phenotypes had not progressed to a floor effect at these ages (not reported). Testing order was Day 1: EZM and inverted screen, Day 2: balance beam, Day 3: locomotor activity, Days 4-6: accelerating rotarod (only a single day of rotarod was completed for behavior after baseline testing). All behavioral testing was completed between 9am-1pm and each apparatus was cleaned with 10% ethanol between animals.

3.3.4 Tissue collection

3.3.4.1 Study 1 and acute Mn exposure. Mice were sacrificed by cervical dislocation without anesthesia approximately 24 hours after the final injection. Mice were decapitated with sharp scissors and the brain removed from the skull. The brain was micro-dissected on ice under a dissecting microscope, collecting striatum and olfactory bulb. Liver tissue was also collected by cutting off a piece of the largest hepatic lobe. All tissue was flash frozen in liquid nitrogen and stored at -80° C until used for biochemical analyses.

3.3.4.2 Study 2. Mice were euthanized approximately 24 hours following the final injection. Mice were deeply anesthetized using isoflurane and ~40-65 mL cold PBS (1.3x body weight) was perfused by pump. Mice were decapitated with sharp scissors and the brain removed. The brain (including olfactory bulbs and medulla) was placed on tared parafilm and total brain weight recorded (mg). The brain was bisected with a razor blade and the left hemisphere immersion-fixed in 4% paraformaldehyde (PFA) for 8 days when hemispheres were then

paraffin embedded and stored until all brains were collected and a tissue microarray was assembled. The right hemisphere was micro-dissected under a dissecting microscope on ice, collecting striatum and cortex. Liver was also collected. Fresh tissue was flash frozen in liquid nitrogen and stored at -80° C until later analysis (Mn levels and western blotting).

3.3.5 Mn levels

Mn concentration was measured by graphite furnace atomic absorption spectroscopy (GFAAS, Varian AA240, Varian, Inc., Palo Alto, CA) using a protein lysate as previously reported (Pfalzer et al., 2020).

3.3.6 Western blotting

Protein lysates were prepared by homogenizing frozen tissue by sonication in 100 – 400 uL Pierce RIPA lysis buffer (Thermo Scientific, cat # 89900) with protein and phosphatase inhibitors (Sigma Aldrich, cat # P0044, #P2850, #P5726, and #P2714) at 1:100 dilution. Lysates were spun down at 12,000 g for 10 min and supernatant collected. Protein concentration was measured using a standard bicinchoninic acid (BCA) assay protocol (Pierce BCA Protein Assay Kit, Thermo Scientific). Samples were prepared with 4x Laemmli sample buffer (Bio-Rad cat# 0610747) and 2-mercaptoethanol. For ARG2, samples were boiled for 5 min at 95° C and 40 μg protein was loaded onto 4–20% Criterion™ TGX™ Precast Midi Protein Gel (Bio-Rad cat #5671095). Gels were run at 90 volts for 120 min and transferred to nitrocellulose membranes using the iBlot™ system. Following transfer, gels were rehydrated in DI water overnight and stained with Coomassie (Bio-Rad, cat # 161-0786) for 60 min for use as a loading control. Membranes were blocked for 60 min in Odyssey Blocking Buffer (Odyssey cat # 927-40000) prior to blocking in primary anti-ARG2 at 1:1000 (Santa Cruz, sc-20151) overnight at 4° C. Membranes were washed with TBST prior to incubation for 120 min in anti-rabbit secondary (Licor IRDye 700 or 800CW) diluted 1:10,000 in Odyssey blocking buffer. Protein bands were detected using the Odyssey infrared system and analyzed with ImageStudio Lite (www.licor.com) and normalized to total protein quantified from Coomassie stained gel signal and then the average WT vehicle signal per blot. For GLT-1, samples were not boiled and 10 μg protein was loaded onto Bolt™ 4-12% Bis-Tris Plus gels (Thermo Scientific, cat # NW04120BOX) and run for 30 min at 200 volts prior to transfer on to nitrocellulose membranes (Thermo Scientific, cat # IB23001) using the iBlot2™ system. Gels were rehydrated in DI water overnight and Coomassie stained as described above. Membranes were blocked in 5% nonfat milk in TBST for 1 h prior to incubation overnight with primary anti-GLT-1 at 1:4,000 (Millipore Sigma, AB1783). Membranes were washed with TBST prior to incubation with HRP-conjugated anti-guinea pig secondary at 1:10,000 in 5% nonfat milk in TBST for 2 h. Protein bands were

detected by chemiluminescence (Perkin Elmer, Western Lightning Plus-ECL, cat # NEL104001EA) and analyzed with ImageJ (imagej.nih.gov). For GLT-1, signal intensity was normalized to Coomassie stained gel signal and reported as arbitrary units.

3.3.7 Immunohistochemistry

3.3.7.1 Tissue microarray. To minimize technical variability and maximize the number of mice represented on a histological slide, a tissue microarray (TMA) was constructed by the VUMC Translational Pathology Shared Resource. Paraffin embedded hemispheres were sectioned coronally until visualization of the anterior commissure (+1.1 to +0.5 mm relative to bregma), a 4 μM thick section was H&E stained and used to annotate a 2 mm core encompassing the striatum. Embedded brain blocks were loaded on to the TMA Grandmaster (PerkinElmer) automated arrayer and the machine automatically constructs a TMA by removing cores from donor blocks based on annotations provided by the experimenter. Following construction, an H&E slide was made and evaluated for quality. From the TMA block (~50 cores/mice per block), 20 μM thick sections were cut and mounted for staining. Four TMA slides (200 microns apart) were stained with NeuN (below) for cell counting.

3.3.7.2 NeuN staining. Slides were placed on a Leica Bond Max IHC Stainer. All steps except dehydration, clearing and cover slipping were performed on the Bond Max. Slides were deparaffinized. Heat induced antigen retrieval was performed on the Bond Max using Epitope Retrieval 1 solution for 20 minutes. Slides were incubated with anti-NeuN 1:2,500 (MAB377, Millipore Sigma) for 15 min. The Bond Polymer Refine detection system was used for visualization. Slides were dehydrated, cleared and cover slipped.

3.3.7.3 Striatal cell counts. Each core was visualized at 4x magnification (EVOS Core XL) and evaluated for quality. Tissue cores that were damaged (i.e., folded over on itself or missing tissue) were excluded from analysis. Three non-overlapping 40x magnification images were taken per core, per slide (total 12 images per mouse). Cell counting was performed using ImageJ automated software. In brief, 40x images were converted to 16-bit, threshold was adjusted to highlight cells visualized by NeuN staining, watershed algorithm applied and particles greater than 1200 square-pixels and with 0.35-1.00 circularity counted. These parameters were set based on first two independent experimenters manually counting cells in 10 images and optimizing the automated protocol to match manual counts. From each set of counts per mouse, to reduce the effect of individual outliers the three values that clustered together the most closely were averaged to give a final representative cell count used for comparisons between groups.

3.3.8 Statistics

Data are reported as mean ± S.E.M. unless otherwise noted. Data analyses were completed in SPSS 26.0 or GraphPad Prism 8. All analyses were first run with sex as a fixed variable. There were no meaningful differences according to sex, and thus all data were collapsed and analyzed together except for body weight data. For all dependent variables, two-way univariate ANOVA (2 genotype x 2-4 treatments) was conducted with appropriate post-hoc follow up tests. Repeated measures (RM)-ANOVA was used for rotarod at baseline. Non-parametric tests were used when appropriate and noted in the results section. Outliers were removed if due to experimental error and if outside of 95% confidence interval.

3.4 Results

3.4.1 YAC128 mice were less sensitive to acute Mn exposure

A one-week 50 mg/kg $MnCl_2 \cdot 4(H_2O)$ injection paradigm has previously been reported to increase both Mn concentration (Dodd et al., 2005; Williams, Li, et al., 2010) and arginase 2 (ARG2) protein levels in the striatum (Bichell et al., 2017; Pfalzer et al., 2020). Twelve-week-old mice were injected subcutaneously with vehicle (0), 10, 20 or 50 mg/kg $MnCl_2 \cdot 4(H_2O)$ over one week to determine if lower concentrations would lead to the same ARG2 increase and to estimate an approximate EC50 for Mn-induced changes in ARG2 protein expression (**Fig. 3.1 A**). Mn increased striatal ARG2 in both genotypes (Treatment $F_{3, 51}$=19.07, P<0.0001, Genotype $F_{1, 51}$=2.867, P=0.096). Both 20 and 50 mg/kg $MnCl_2 \cdot 4(H_2O)$ significantly increased ARG2 protein in WT but only the 50 mg/kg $MnCl_2 \cdot 4(H_2O)$ dose increased ARG2 protein in YAC128 mice (**Fig. 3.1 B**). We imputed an approximate EC_{50} of 10 mg/kg for the increase in ARG2 by Mn in WT and >20 mg/kg in YAC128, thus 15 mg/kg was implemented as a dose in our chronic exposure behavioral studies that followed.

3.4.2 Study 1 – Behavior

Acute (1-week) Mn exposure has previously been shown to rescue defects in the urea cycle of YAC128 mice (Bichell et al., 2017). We sought to determine whether a long-term exposure to either 5, 15, or 50 mg/kg $MnCl_2 \cdot 4(H_2O)$ could lessen the severity of disease-relevant behavioral phenotypes (motor coordination) in YAC128 mice and if the reported blunted response to global changes by Mn exposure would offer YAC128 mice protection against Mn-induced behavioral impairments (**Fig. 3.2 A**). Behavior was first evaluated at baseline (**Fig.**

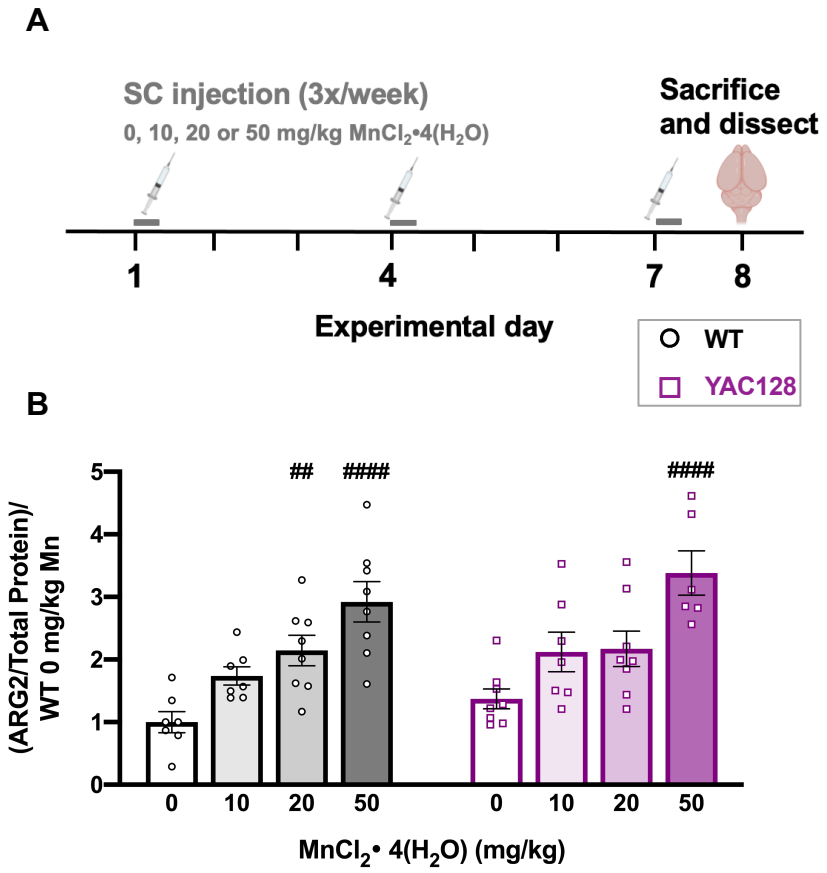

Figure 3.1 **(A)** Experimental timeline. Mice were injected [0, 10, 20, or 50 mg/kg $MnCl_2 \bullet 4(H_2O)$] 3 times over the course of one week (days 1, 4, and 7) and sacrificed 24 hours following the third injection (day 8). in both genotypes, but a larger dose is required **(B)** ARG2 protein expression increased following Mn exposure but a larger dose is required in YAC128 mice compared to WT. Pound symbol indicates significant difference from vehicle within a genotype by post-hoc Dunnett's multiple comparisons. Mean ± SEM plotted. ## $p<0.01$, ####$p<0.0001$

3.2 B-G) and the effect of Mn was determined in each of the 8 genotype-treatment groups at 30 weeks of age (**Fig. 3.2 H-M**), after 18 weeks exposure to Mn.

3.4.2.1 Young YAC128 mice displayed a motor coordination deficit on the rotarod but not wire hang

At 11 weeks of age, both genotypes showed appropriate motor learning during the accelerated rotarod task (**Fig. 3.2 B**), as indicated by increased latency to fall over consecutive training days but YAC128 mice fell from the rod sooner than WT on all three days of the task (Day $F_{2, 66}$ =21.79, P<0.0001, Genotype $F_{1, 66}$=18.90, P<0.0001) suggesting a motor coordination deficit.

Wire hang was performed as an additional assessment of motor coordination (**Fig. 3.2 C**). Mice either achieved a stable position (n=24 WT and n=27 YAC128) or fell (n=8 WT and n=9 YAC128) during the task; a fall was assigned a maximum score of 60 s. There was no significant difference between genotypes on the wire hang task at 11 weeks of age (Mann-Whitney U=529.5, P=0.568).

Several behavioral tasks were performed as controls to support detected deficits on the accelerated rotarod task. There was no significant difference between genotypes for the time (s) spent in the open zone of the elevated zero maze (EZM), suggesting that both genotypes had similar anxiety levels during a novel behavioral task (t_{66}=0.063, P=0.949) (**Fig. 3.2 D**). Locomotor activity as measured by total distance travelled during 30 minutes in an open field chamber was also similar between genotypes (t_{66}=0.707, P=0.482) (**Fig. 3.2 E**). Strength, represented by latency to fall from the inverted screen, was not significantly different between WT and YAC128 mice (Mann-Whitney U=501, P=0.358) (**Fig. 3.2 F**), despite the observed weight difference between genotypes. Males weighed more than females at 12 weeks of age and YAC128 mice weighed more than WT (Sex $F_{1, 64}$=71.768, P<0.0001, Genotype $F_{1, 64}$=5.058, P=0.028) (**Fig. 3.2 G**), which were both expected differences (Pouladi et al., 2010).

The behavioral battery performed at 11 weeks of age established that a motor impairment already existed in the YAC128 mice prior to the start of Mn exposure, which was not due to differences in anxiety, activity levels, or strength. Mn dose was assigned randomly to each mouse prior to any behavioral testing and started following the completion of baseline behavior at 12 weeks of age.

3.4.2.2 Repeated subcutaneous Mn injections were well tolerated

We monitored the weight of all animals to ensure appropriate overall health while administering Mn. Consistent with 12-week measurements, males weighed more than females and as expected YAC128 mice

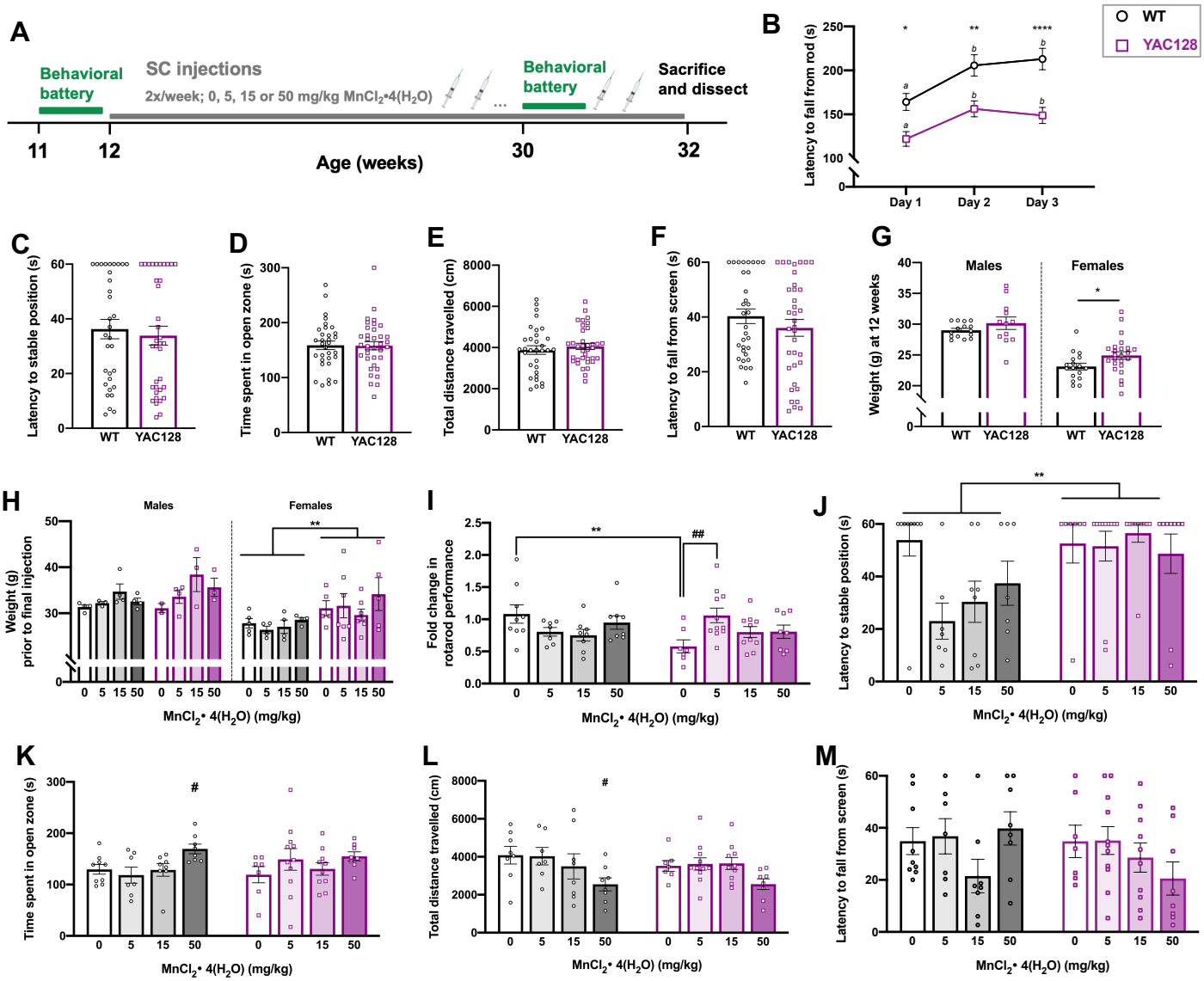
A
Behavioral battery
SC injections
2x/week; 0, 5, 15 or 50 mg/kg MnCl2•4(H2O)
Behavioral battery
Sacrifice and dissect
11
12
Age (weeks)
30
32
B
WT
YAC128
Latency to fall from rod (s)
Day 1
Day 2
Day 3
C
Latency to stable position (s)
D
Time spent in open zone (s)
E
Total distance travelled (cm)
F
Latency to fall from screen (s)
G
Weight (g) at 12 weeks
Males
Females
H
Weight (g) prior to final injection
MnCl2• 4(H2O) (mg/kg)
I
Fold change in rotarod performance
MnCl2• 4(H2O) (mg/kg)
J
Latency to stable position (s)
MnCl2• 4(H2O) (mg/kg)
K
Time spent in open zone (s)
MnCl2• 4(H2O) (mg/kg)
L
Total distance travelled (cm)
MnCl2• 4(H2O) (mg/kg)
M
Latency to fall from screen (s)
MnCl2• 4(H2O) (mg/kg)

Figure 3.2 **(A)** Experimental timeline for study 1 (n=68). Mice underwent a week-long baseline behavioral battery at 11 weeks old (B-G) prior to beginning twice weekly subcutaneous injections (0, 5, 15, or 50 mg/kg $MnCl_2 \cdot 4(H_2O)$) from 12 weeks until 32 weeks of age. The behavioral battery was repeated at 30 weeks of age (I-M) to assess effects of chronic Mn exposure and mice were sacrificed and dissected at 32 weeks of age, 24 hours after the final injection. **(B)** Average latency to fall (3 trials per day; 300 s max per trial) from the rotarod across 3 days. Both genotypes display appropriate motor learning during the task, indicated by increased latency to fall on days 2 and 3 compared to day 1. YAC128 mice fall from the rod sooner than WT on all three days. Asterisks indicate a significant difference between genotypes on that day, and days that do not share a superscript letter are significantly different from each other within a genotype. **(C)** The latency to reach a stable position (all four paws or three paws and a tail) on the wire was measured (max 60 s). A mouse either achieved a stable position (n=24 WT and n=27 YAC128) or fell (n=8 WT and n=9 YAC128) during the task; a fall was assigned as a max score of 60 s. There was no significant difference between genotypes in the time it took to reach a stable position. **(D)** Anxiety during a novel behavioral task was similar between genotypes at 11 weeks of age measured by time (s) spent in the open zone of the elevated zero maze (EZM). **(E)** Total distanced travelled during 30 minutes in an open field chamber was comparable between WT and YAC128 mice. **(F)** Average latency to fall from the inverted screen, indicative of overall limb strength, was not significantly different between WT and YAC128 mice. **(G)** Males weighed more than females and YAC128 mice weighed more than WT at 12 weeks of age. **(H)** There was no effect of Mn treatment on weight. **(I)** Fold change in rotarod performance. Performance at 30 weeks for each individual mouse was divided by 11-week performance and plotted. Post-hoc follow-up tests showed that there was only a genotype difference in the vehicle dose (**), and within a genotype, the only significant Mn effect was between YAC128 vehicle and 5 mg/kg-exposed groups (##). **(J)** YAC128 mice performed more poorly on the wire hang task, but there were no effects of Mn. **(K)** High dose Mn resulted in more time spent in the open zone of the EZM in WT mice. **(L)** WT mice receiving the highest dose of Mn were less active than vehicle-treated WT mice. **(M)** There were no significant differences between genotypes or Mn exposure groups in strength measured by latency to fall from the inverted screen.

For all, mean ± SEM plotted unless otherwise noted. Asterisks * indicate genotype effect, pound # indicates Mn effect within genotype. # $p < 0.05$, ## $p < 0.01$, * $p < 0.05$ **$p < 0.01$, **** $p < 0.0001$

weighed more than WT at 32 weeks of age (Pouladi et al., 2010) (Sex $F_{1, 52}$= 15.279, P<0.001, Genotype $F_{1, 52}$= 8.341, P=0.006) (**Fig. 3.2 H**). There was no effect of the 20-week-long Mn exposure on body weight, indicating lack of overt toxicity or general malaise caused by repeated Mn injections. A small number of animals exhibited mild injection site irritation (hair loss, rigid skin) at all Mn doses, but no gross adverse reactions were noted.

3.4.2.3 Chronic low dose $MnCl_2 \cdot 4(H_2O)$ protected against motor coordination decline on the rotarod in YAC128 mice

Rotarod performance at 30 weeks was analyzed as a fold-change compared to baseline to avoid the expected confound of genotype differences in the degree of age-related decline. WT performance on the rotarod remained relatively stable between 11- and 30-weeks of age (no fold-change) and YAC128 vehicle-treated mice declined to approximately 57% of their 11-week performance (Genotype $F_{1, 60}$= 1.249, P=0.268, Treatment $F_{3, 60}$= 0.788, P=0.505, Interaction $F_{3, 60}$=4.391, P=0.007). However, performance in YAC128 mice exposed to low-dose 5 mg/kg $MnCl_2 \cdot 4(H_2O)$ did not change, suggesting a protective effect against progressive motor coordination decline (**Fig. 3.2 I**). On the wire hang, a mouse either achieved a stable position (n=18 WT and n=9 YAC128) or fell (n=14 WT and n=27 YAC128) during the task. YAC128 mice exhibited a deficit on this task at 30 weeks of age compared to WT, but there were no effects of Mn (Genotype $F_{1, 60}$= 11.70, P=0.001, Treatment $F_{3, 60}$= 1.930, P=0.134) (**Fig. 3.2 J**).

3.4.2.4 Chronic high dose $MnCl_2 \cdot 4(H_2O)$ exposure led to modest behavioral changes in WT mice

WT mice that received the highest dose (50 mg/kg) of $MnCl_2 \cdot 4(H_2O)$ showed subtle changes in behavior during the EZM and open field tasks at 30 weeks of age. There was no significant difference in time spent in the open zone of the EZM between genotypes, but a Mn effect approached significance (Genotype $F_{1, 60}$= 0.035, P=0.852, Treatment $F_{3, 60}$= 2.602, P=0.060). Given that YAC128 mice exhibit blunted responses to Mn, we examined the effect of Mn within WT only to ensure sensitivity to detect Mn-induced changes and found that the WT mice receiving 50 mg/kg $MnCl_2 \cdot 4(H_2O)$ spent significantly more time in the open zone compared to vehicle-treated WT mice (**Fig. 3.2 K**). In the locomotor activity chambers the same group of high-dose Mn-exposed WT mice were significantly less active compared to WT vehicle mice (Genotype $F_{1, 59}$= 0.489, P=0.487, Treatment $F_{3, 59}$= 4.261, P=0.009) (**Fig. 3.2 L**)**.** Overall limb strength, indicated by latency to fall from the inverted screen

was not different between genotypes or Mn exposure groups (Genotype $F_{1, 60}$= 0.6471, P=0.4243, Treatment $F_{3, 60}$= 1.397, P=0.2525) (**Fig. 3.2 M**), even despite a significant weight difference between genotypes.

3.4.3 Study 1 – Molecular biology

3.4.3.1 Mn accumulation occurred at a lower dose in brain than in liver

Mn injections led to significant accumulation in brain (striatum and olfactory bulb) and liver in both genotypes, but not at all doses (**Fig. 3.3 A**). The 15 and 50 mg/kg $MnCl_2 \cdot 4(H_2O)$ doses increased Mn levels in striatum (Genotype $F_{1, 60}$= 0.072, P=0.790, Treatment $F_{3, 60}$= 58.25, P<0.0001) and olfactory bulb (Genotype $F_{1, 60}$=0.629, P=0.431, Treatment $F_{3, 60}$= 36.12, P<0.0001). Mn levels were generally higher in liver compared to brain, but only the 50 mg/kg dose resulted in a significant increase compared to vehicle (Genotype $F_{1, 60}$=0.208, P=0.650, Treatment $F_{3, 60}$= 9.725, P<0.001).

3.4.3.2 Mn increased striatal ARG2 in a dose-dependent manner

Mn increased ARG2 protein levels in the striatum dose-dependently in both genotypes (Genotype $F_{1, 60}$=0.043, P=0.836, Treatment $F_{3, 60}$=21.27, P<0.0001) (**Fig. 3.3 B**). In WT only 50 mg/kg $MnCl_2 \cdot 4(H_2O)$ led to a significant increase but in YAC128 mice both the 15 mg/kg and 50 mg/kg doses increased ARG2 compared to vehicle-treated mice within genotype.

3.4.4 Study 2 – Behavior

We sought to replicate the findings from Study 1 in a longer exposure paradigm in Study 2 (**Fig. 3.4 A**). We selected only the low (5 mg/kg) dose of $MnCl_2 \cdot 4(H_2O)$ for Study 2 because it prevented progressive decline on the rotarod in YAC128 mice and importantly did not lead to statistically significant Mn accumulation in brain, which could exert neurotoxic effects when maintained for the 18-week exposure. Study 2 examined if chronic exposure to low-dose (5 mg/kg) $MnCl_2 \cdot 4(H_2O)$ could prevent motor coordination decline in YAC128 mice at 30-weeks-old (**Fig. 3.4 H-M**) and up to 12 months of age (**Fig. 3.5**). Following the behavioral battery at 30 weeks, half of the mice (randomly predetermined) switched treatment groups. This allowed us to assess the effects

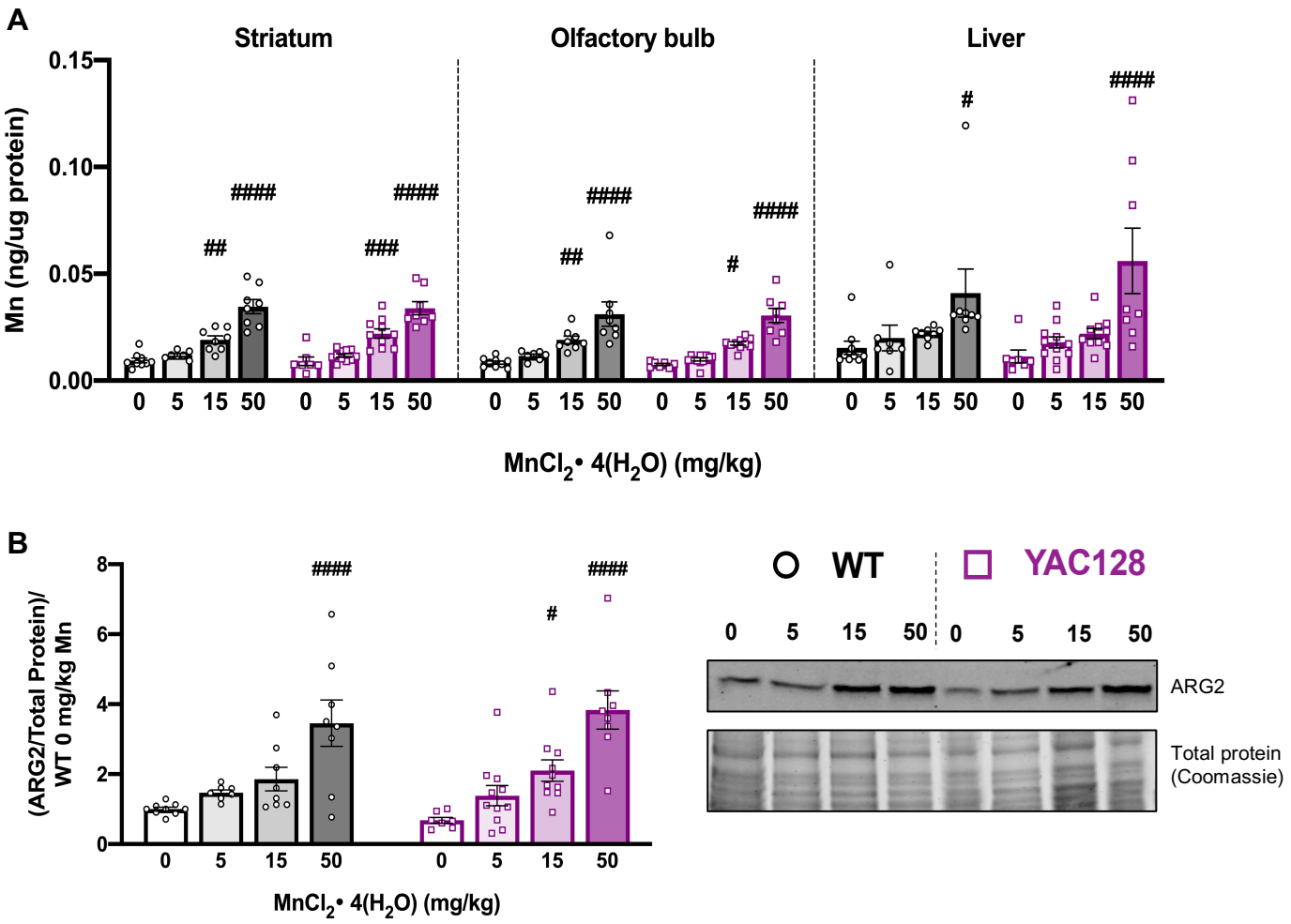

Figure 3.3 (A) Mn levels (ng/ug protein) at 32 weeks of age for striatum (left), olfactory bulb (middle) and liver (right) from mice in Study 1 after 20 weeks of subcutaneous injections. Mn increased in all tissue types following exposure. Only 15 and 50 mg/kg significantly increased brain levels and only 50 mg/kg significantly increased hepatic Mn; # indicates significant differences from vehicle within each genotype by post-hoc Sidak's multiple comparisons. (B) ARG2 protein expression normalized to total protein on gels by Coomassie blue staining for loading control and normalized to average WT 0 for each blot. Mn increased ARG2 expression in both genotypes, which were not different from each other. Within a genotype, only the 50 mg/kg dose was significantly higher than vehicle in WT and both 15 and 50 mg/kg doses led to a significant increase compared to its own genotype vehicle in YAC128, indicated by #. Representative blot and Coomassie stained gel are shown. For all, mean ± SEM plotted unless otherwise noted. # $p < 0.05$, ##, $p < 0.01$, ### $p < 0.001$, #### $p < 0.0001$

of continuous Mn exposure (5 mg/kg all 40 weeks, "5") compared to beginning exposure later in life (vehicle until 31 weeks old, followed by Mn for remainder of study, "0_5"), removing exposure (Mn first, followed by vehicle, "5_0"), or vehicle only (all 40 weeks, "0"). Further, we hypothesized YAC128 mice would be protected from any detrimental behavioral effects of Mn over a chronic (40-week) exposure given blunted response to exposures (Pfalzer et al., 2020).

3.4.4.1 Young YAC128 mice displayed a motor coordination deficit on the rotarod but not balance beam

The same accelerating rotarod protocol was used at 11 weeks in Studies 1 and 2. Replicating the results found in Study 1 (**Fig. 3.2 B**), YAC128 mice in Study 2 fell off the rod sooner and thus exhibited impaired motor coordination as early as 11 weeks of age compared to WT. (**Fig. 3.4 B**). Both genotypes displayed acceptable motor learning, with improved performance across test days (Day $F_{2, 107}$ =85.64, P<0.0001, Genotype $F_{1, 107}$=27.35, P<0.0001, Interaction $F_{2, 107}$=4.909, P=0.008).

As another measure of motor coordination in Study 2, mice performed the balance beam task. The average time to cross the beam (average of two trials; max 30 s) and the total number of hind paw slips (accumulated from both trials) were recorded. At 11 weeks YAC128 mice were not impaired based on the time it took to cross the beam (Mann-Whitney U=1437, P=0.773) (**Fig. 3.4 C**), nor the percentage of mice that displayed hind paw slips during either trial (not shown; WT =14/54 and YAC128= 19/55 animals; χ^2 = 0.959, P=0.327).

3.4.4.2 Young YAC128 mice exhibited normal behavior in baseline control tasks

Similar to Study 1, there were no main effects of or statistical interactions with sex as a variable so for all behavior analyses the sexes were combined in Study 2. During the EZM task, YAC128 mice spent slightly less time (148 s) in the open zone of the maze compared to WT (164 s) at 11 weeks of age (t_{106}=2.602, P=0.011). This genotype effect was driven by a subgroup of 5 YAC128 mice that spent <100 s in the open zone (**Fig. 3.4 D**). Spending approximately 50% time in the open zone is considered normal and does not indicate an anxiety-like phenotype (Eltokhi, Kurpiers, & Pitzer, 2020; Võikar, Kõks, Vasar, & Rauvala, 2001) and thus we do not believe that these data reflect a true anxiety phenotype in the YAC128 mice. During 30 minutes in the open field chamber,

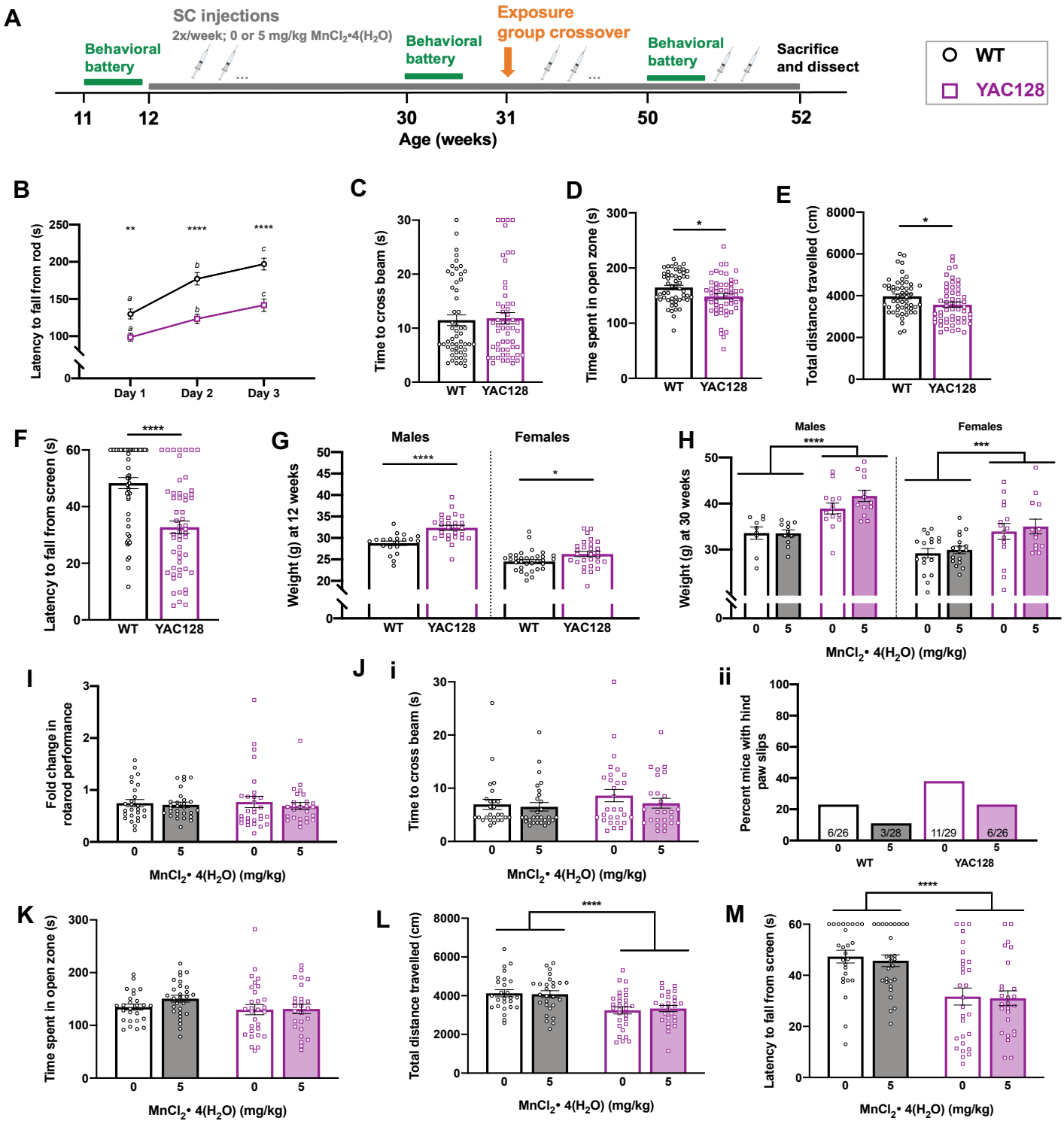
A
SC injections
2x/week; 0 or 5 mg/kg MnCl2•4(H2O)
Behavioral battery
Behavioral battery
Exposure group crossover
Behavioral battery
Sacrifice and dissect
WT
YAC128
11
12
30
31
50
52
Age (weeks)
B
Latency to fall from rod (s)
Day 1
Day 2
Day 3
C
Time to cross beam (s)
D
Time spent in open zone (s)
E
Total distance travelled (cm)
F
Latency to fall from screen (s)
G
Males
Females
Weight (g) at 12 weeks
H
Weight (g) at 30 weeks
MnCl2• 4(H2O) (mg/kg)
I
Fold change in rotarod performance
J
i
ii
Percent mice with hind paw slips
6/26
3/28
11/29
6/26
K
L
M

Figure 3.4 **(A)** Experimental timeline for Study 2. Mice underwent a week-long baseline behavioral battery at 11 weeks old (**B-F**) prior to beginning twice weekly subcutaneous injections [0 or 5 mg/kg $MnCl_2 \bullet 4(H_2O)$] at 12 weeks of age. The behavioral battery was repeated at 30 weeks of age **(I-M),** then half of the mice changed exposure groups at 31 weeks of age and behavioral battery was repeated at 50 weeks of age **(s**ee Fig. 3.5**)** prior to sacrifice and dissection (see Fig. 3.6) at 52 weeks of age. **(B)** Average latency to fall (3 trials per day; 300 s max per trial) from the rotarod across 3 days. Both genotypes displayed appropriate motor learning during the task, indicated by increased latency to fall on days 2 and 3 compared to day 1. YAC128 mice fall from the rod sooner than WT on all three days. Asterisks indicate a significant difference between genotypes on that day, and days that do not share a superscript letter are significantly different from each other within a genotype. **(C)** Average time (across two trials, max 30 s per trial) to cross the balance beam was similar between genotypes. **(D)** YAC128 mice spent less time in the open zone of the EZM compared to WT at 11 weeks of age, however this was driven by the 5 YAC128 mice that spent <100 s in the open zone and does not indicate anxiety in either group. **(E)** YAC128 mice on average covered less distance than WT in 30 minutes of the open field, however the range of distance travelled is similar between genotypes. **(F)** YAC128 mice fell sooner than WT from the inverted screen. **(G)** Males weighed more than females and YAC128 mice weighed more than WT at 12 weeks of age (prior to first injection). **(H)** At 30 weeks, Males weighed more than females, and YAC128 mice weighed more than WT within each sex. There was no effect of Mn. **(I)** Fold change in rotarod performance at baseline (11 weeks) to the 30-week assessment. Performance of each individual mouse at 30 weeks was divided by 11-week performance. On average there was a 25% decrease in performance for WT mice and 31% decrease for YAC128 mice. **(J)** There was no impairment in the average time (between two trials, max 30 s each) it took any group to cross the balance beam at 30 weeks of age (i) nor was there a significant difference in the number of mice with hind paw slips (ii) in any group at this age. In each bar, number of mice with 1-3 paw slips. **(K)** There was no difference between genotypes or treatment groups for time spent in open zone of the EZM at 30 weeks. **(L)** Total distance travelled during 30 minutes in the open field. YAC128 mice travelled less than WT, but there was no effect of Mn after this length of exposure. **(M)** Latency to fall from the inverted screen at 30 weeks. YAC128 mice fell from the screen sooner than WT, but Mn had no impact.

For all, mean ± SEM plotted unless otherwise noted. Asterisks * indicate genotype effect. * $p < 0.05$, **, $p < 0.01$, *** $p < 0.001$, **** $p < 0.0001$

there was an approximately 10% decrease in total distance travelled in YAC128 mice compared to WT mice at 11 weeks (t_{107}=2.371, P=0.020) (**Fig. 3.4 E**). The range of distance travelled was comparable between WT (2237-6000 cm) and YAC128 (2244-5873 cm) and is unlikely to have influenced the outcome on additional behavioral tasks such as the rotarod. On the inverted screen task, YAC128 mice fell sooner than WT (t_{107}=5.262, P<0.0001) (**Fig. 3.4 F**). The significant difference between genotypes on the inverted screen at 11 weeks could suggest a lack of strength in the YAC128 mice, however this difference may be driven by the significantly heavier weight of the YAC128 mice. As expected, males weighed more than females and YAC128 mice were significantly heavier than WT at 12 weeks of age prior to beginning Mn exposure (Sex $F_{1, 105}$=90.24, P<0.0001, Genotype $F_{1, 105}$=23.85, P<0.0001) (**Fig. 3.4 G**).

Baseline behavior at 11 weeks of age in Study 2 replicated the motor coordination deficit on the accelerated rotarod observed in Study 1 at the same age, with no meaningful differences in the other behaviors assessed. Mn dose was assigned such that baseline rotarod performance within a genotype was comparable between treatment groups, but whether a mouse would undergo exposure crossover at 31 weeks was randomly assigned.

3.4.4.3 No significant behavioral effects of 18 weeks low dose $MnCl_2 \cdot 4(H_2O)$ exposure

Again, males weighed more than females and YAC128 mice weighed more than WT but there was no effect of Mn exposure in any group (Sex $F_{1, 101}$=29.138, P<0.0001, Genotype $F_{1, 101}$=41.122, P<0.0001) (**Fig. 3.4 H**).

From 11 weeks to 30 weeks of age, the latency to fall from the accelerating rotarod decreased significantly in all genotype and treatment groups (Genotype $F_{1, 105}$=35.890, P<0.0001, Treatment $F_{1, 105}$= 0.090, P=0.765, Age $F_{1, 105}$= 108.017, P<0.0001, all interaction Ps > 0.05). YAC128 vehicle-treated mice fell from the rod on average after 82.2 ± 34.3 s and Mn-treated YAC128 mice fell after 93.6 ± 43.1 s. Overall YAC128 mice displayed a motor coordination deficit compared to WT, who fell on average after 137.2 ± 54.0 s and 132.2 ± 45.2 s for vehicle and Mn-treated groups, respectively (raw data not shown). The fold-change from 11 to 30 weeks, after 18 weeks exposure to Mn or vehicle, is shown for all groups in **Fig. 3.4 I.** WT mice fell from the rod on average 25% sooner at 30 weeks compared to 11 weeks, and YAC128 mice fell 31% sooner at 30 weeks compared to 11 weeks; the change in performance was not significantly different between genotypes or Mn exposure groups.

YAC128 mice did not display a motor coordination deficit on the balance beam task at 30 weeks of age, based on the average time to cross the balance beam (Genotype $F_{1, 105}$ =1.436, P=0.236, Treatment $F_{1, 105}$=0.905, P=0.347) (**Fig. 3.4 J i**) and the total number of hind paw slips accumulated across both trials (vehicle-treated WT and YAC128 mice χ^2=1.42, P=0.234). Mn also had no impact within WT (χ^2=1.48, P=0.223) or YAC128 (χ^2=1.42, P=0.234) mice on the number of hind paw slips after this length of Mn exposure (**Fig. 3.4 J ii**).

At 30 weeks of age, chronic Mn exposure did not influence time spent in the open zone of the EZM (Genotype $F_{1, 105}$ =2.376, P=0.126, Treatment $F_{1, 105}$=1.777) (**Fig. 3.4 K**). Total distance travelled during 30 minutes in the open field was lower for YAC128 mice than WT, but Mn had no effect after this length of exposure (Genotype $F_{1, 104}$ =20.54, P<0.0001, Treatment $F_{1, 104}$=0.018, P=0.893) (**Fig. 3.4 L**). On the inverted screen, 18-weeks of low-dose Mn had no impact on latency to fall from the screen and YAC128 mice fell sooner than WT mice (Genotype $F_{1, 105}$ =28.95, P<0.0001, Treatment $F_{1, 105}$=0.157, P=0.693) (**Fig. 3.4 M**).

3.4.4.4 Body weight at 50 weeks of age was not changed by Mn exposure

By 50 weeks of age, males continued to weigh more than females and YAC128 mice were significantly heavier than WT, but there was no effect of Mn (Sex $F_{1, 93}$=6.909, P=0.010, Genotype $F_{1, 93}$=52.011, P<0.0001, Treatment $F_{1, 93}$=0.364, P=0.779, all Interactions Ps > 0.05) (**Fig. 3.5 A**).

3.4.4.5 By 50 weeks of age YAC128 mice exhibited motor coordination impairments on rotarod and balance beam

On the rotarod, YAC128 mice fell from the rod sooner than WT and overall, both genotype groups declined significantly with age from 11 weeks (Genotype $F_{1, 101}$ =53.327, P<0.001, Treatment $F_{3, 101}$=0.132, P=0.941, Age $F_{1, 101}$=122.794, P<0.001, all interaction Ps > 0.05). Again, we analyzed the change in performance by plotting the fold-change of 50-week performance compared to 11-week performance **(Fig. 3.5 B**). WT mice declined 6-40% and YAC128 mice declined 43-63% by 50 weeks of age, with no effect of Mn (Genotype $F_{1, 101}$ =11.54, P=0.001, Treatment $F_{3, 101}$=1.178, P=0.322). By this age, YAC128 mice had a detectable motor coordination deficit on the balance beam task. YAC128 mice took significantly longer time (s) to cross the balance beam (Genotype $F_{1, 101}$ =9.329, P=0.003, Treatment $F_{3, 101}$=0.946, P=0.422) (**Fig. 3.5 C i**) and displayed more hind paw slips compared to WT (**Fig. 3.5 C ii**). For hind paw slips, the three Mn exposure groups were combined in a single Mn group and compared to vehicle groups for each individual genotype, and there was no effect of Mn. YAC128 mice had more hind paw slips than WT regardless of Mn exposure (χ^2=4.127, P=0.042).

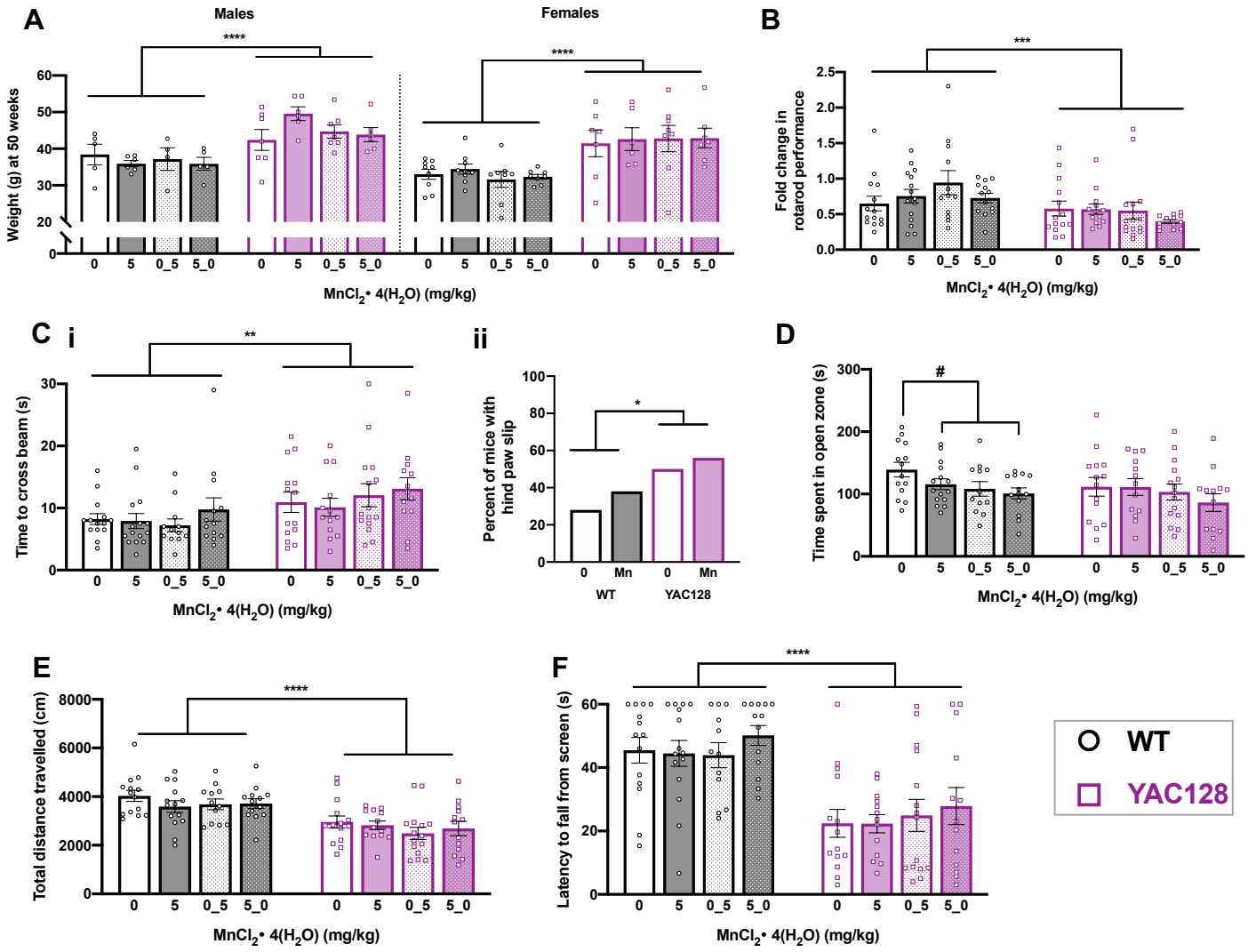
A
Males
Females
****
****
Weight (g) at 50 weeks
60
50
40
30
20
0
0 5 0_5 5_0 0 5 0_5 5_0 0 5 0_5 5_0 0 5 0_5 5_0
MnCl2• 4(H2O) (mg/kg)
B
***
Fold change in rotarod performance
2.5
2.0
1.5
1.0
0.5
0.0
0 5 0_5 5_0 0 5 0_5 5_0
MnCl2• 4(H2O) (mg/kg)
C i
**
Time to cross beam (s)
30
20
10
0
0 5 0_5 5_0 0 5 0_5 5_0
MnCl2• 4(H2O) (mg/kg)
ii
*
Percent of mice with hind paw slip
100
80
60
40
20
0
0 Mn 0 Mn
WT YAC128
D
#
Time spent in open zone (s)
300
200
100
0
0 5 0_5 5_0 0 5 0_5 5_0
MnCl2• 4(H2O) (mg/kg)
E
****
Total distance travelled (cm)
8000
6000
4000
2000
0
0 5 0_5 5_0 0 5 0_5 5_0
MnCl2• 4(H2O) (mg/kg)
F
****
Latency to fall from screen (s)
60
40
20
0
0 5 0_5 5_0 0 5 0_5 5_0
MnCl2• 4(H2O) (mg/kg)
WT
YAC128

Figure 3.5 Body weight and behavior for mice from Study 2, at 50 weeks (experimental timeline shown in Figure 4A). **(A)** Males weighed more than females and YAC218 mice continued to weigh more than WT at 50 weeks of age. There was no difference in body weight between Mn exposure groups. **(B)** Fold change in rotarod performance from 11 to 50 weeks of age. On average, all groups performed worse on the task at 50 weeks compared to 11 weeks. YAC128 mice performance declined to a greater extent than WT. **(C)** YAC128 mice were slower to cross the balance beam than WT at 50 weeks of age (i) and had significantly more hind paw slips (ii), but there was no effect of Mn. For hind paw slips, the three Mn exposure groups were combined for analysis. **(D)** Time spent in open zone of the EZM at 50 weeks. The three WT groups that received any Mn exposure combined were significantly different from vehicle treated WT mice by t-test. **(E)** Total distance travelled during 30 minutes in the open field. YAC128 mice travelled less than WT, with no effects of any length Mn exposure in either genotype. **(F)** YAC128 mice fell from the inverted screen sooner than WT, with no effect of any Mn exposure in either genotype. For all, mean ± SEM plotted unless otherwise noted. Asterisks * indicate genotype effect, pound # indicates Mn effect within genotype. #/* $p < 0.05$, **, $p < 0.01$, *** $p < 0.001$, **** $p < 0.0001$

3.4.4.6 Chronic Mn exposure led to subtle behavioral changes in WT but not YAC128 mice at 50 weeks

At 50 weeks of age, there was no significant difference between genotypes or the four Mn exposure groups on time (s) spent in the open zone of the EZM (Genotype $F_{1, 101}$ =2.235, P=0.138, Treatment $F_{1, 101}$=0.236, P=0.075) (**Fig. 3.5 D**). We also examined effect of *any* Mn exposure (5, 0_5, and 5_0 groups combined) compared to none (vehicle only) in each genotype because a blunted response was expected in YAC128 mice. In WT mice, any Mn exposure led to significantly decreased time spent in the open zone of the EZM compared to WT mice that never received Mn (t_{52}=2.642, P=0.012) but in YAC128 mice there was no effect of any Mn exposure (t_{53}=0.706, P=0.483). Similarly, there was no main effect of Mn for total distance travelled in the open field (Genotype $F_{1, 100}$ =37.15, P<0.001, Treatment $F_{1, 100}$=1.105, P=0.351) (**Fig. 3.5 E**). Despite this, we again compared any Mn exposure against no Mn exposure and found no significant difference in total distance travelled in WT or YAC128 mice based on any Mn exposure (WT t_{51}=1.483, P=0.144; YAC128 t_{53}=1.061, P=0.293). Overall, YAC128 mice covered less distance than WT in the open field.

General limb strength as measured by the latency to fall from the inverted screen was decreased in YAC128 mice compared to WT but not changed by any Mn exposure (Genotype $F_{1, 101}$ =49.93, P<0.0001, Treatment $F_{1, 101}$=0.694, P=0.558, Interaction $F_{1, 101}$=0.087, P=0.967) (**Fig. 3.5 F**). Two paw grip strength was also assessed at 50 weeks as a control measure, and there were no significant differences on this task for genotype or Mn exposure (Genotype $F_{1, 101}$ =0.158, P=0.691, Treatment $F_{3, 101}$=0.065, P=0.978, Interaction $F_{3, 101}$=0.466, P=0.706) (not shown).

3.4.5 Study 2 – Molecular biology

3.4.5.1 Striatal NeuN positive cells were significantly decreased by chronic Mn exposure in WT only

The average brain weight for each of the YAC128 treatment groups was 464 – 469 mg, whereas WT brains weighed more with averages ranging 482 – 486 mg with no effect of Mn (Genotype $F_{1, 100}$ =18.99, P<0.0001, Treatment $F_{3, 100}$=0.124, P=0.946) (**Fig. 3.6 A**). There was a 10% decrease in NeuN positive cells in the striatum of vehicle treated YAC128 mice compared to WT vehicle (P=0.0341) (Genotype $F_{1, 98}$ =0.0644, P=0.8002, Treatment $F_{3, 98}$=0.8446, P=0.4247, Interaction $F_{3, 98}$=3.633, P=0.0156) (**Fig. 3.6 B**), consistent with previous reports (Slow et al., 2003). Notably, the number of NeuN positive cells was significantly decreased (~10-12%) in the WT Mn exposure groups compared to WT vehicle (P=0.052, 0.015, and 0.016 for “5_5”, “0_5”, and

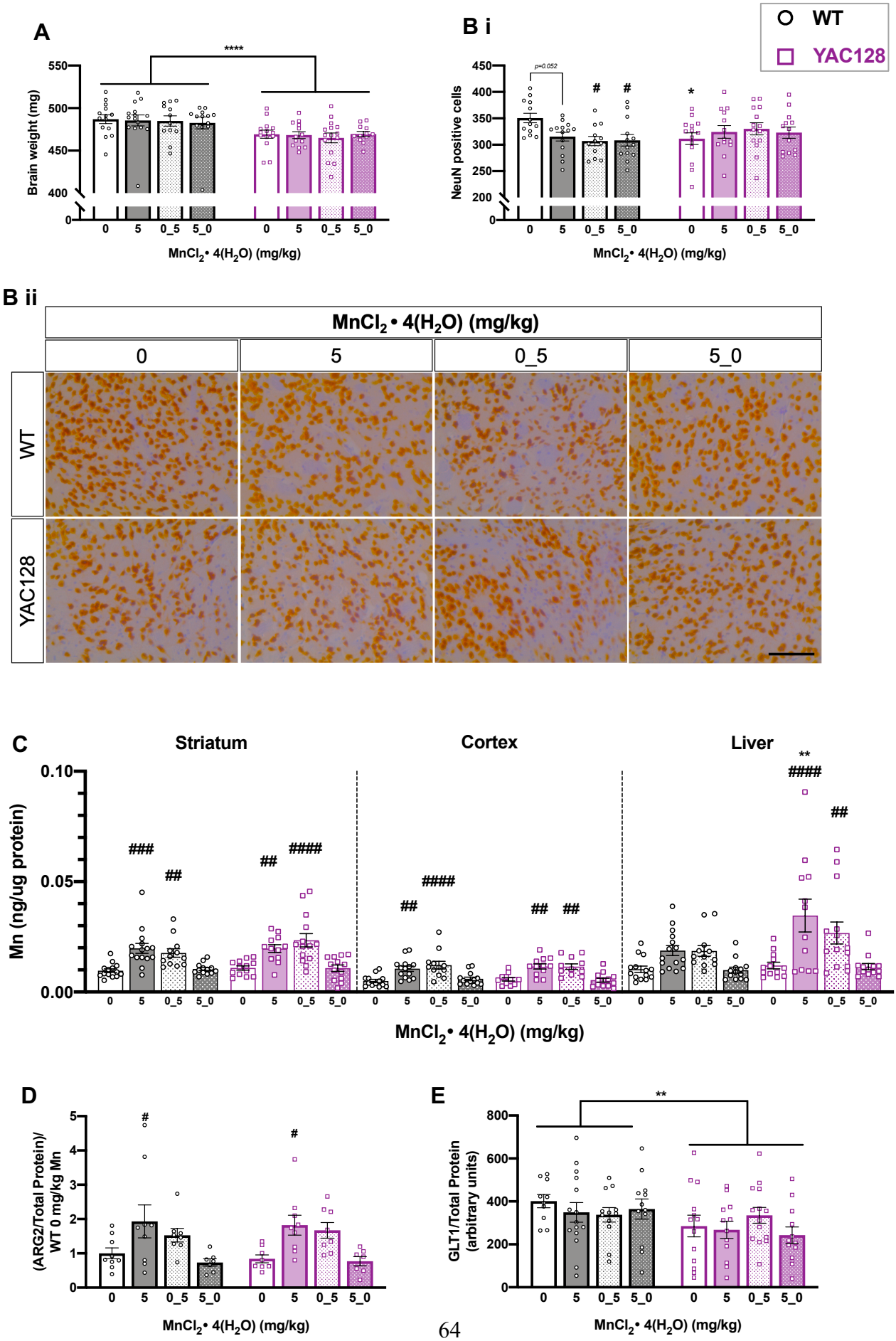
A
Brain weight (mg)
MnCl2• 4(H2O) (mg/kg)
B i
NeuN positive cells
WT
YAC128
B ii
MnCl2 • 4(H2O) (mg/kg)
WT
YAC128
C
Striatum
Cortex
Liver
Mn (ng/ug protein)
D
(ARG2/Total Protein)/ WT 0 mg/kg Mn
E
GLT1/Total Protein (arbitrary units)

Figure 3.6 Post-dissection outcomes for mice used in Study 2. **(A)** Total brain weights (mg). YAC128 mice weighed less than WT but there was no effect of Mn. **(B)** (i) YAC128 vehicle mice had a 10% decrease in NeuN positive cells compared to WT vehicle (*). Mn led to a significant decrease in NeuN positive cells in the "0_5" (p=0.015) and "5_0" groups (p=0.016) compared to WT vehicle (#), but NeuN positive cells in YAC128 mice were unaffected by Mn treatment. (ii) Representative NeuN positive cells at 40x magnification. Scale bar = 200 μm. **(C**) Mn levels in striatum (left), cortex (middle) and hepatic (right) tissue for all genotypes and exposure groups. There was a significant increase in Mn levels in all three tissue types following exposure. A # symbol indicates significant difference from vehicle (0) within that genotype. In liver, there was a significant main effect of genotype, but post-hoc Sidak's revealed that within Mn exposure groups, the only significant genotype difference was between YAC128 and WT that received the continuous 5 mg/kg Mn dose, with accumulation being greater in YAC128 mice compared to WT. **(D)** ARG2 protein expression by western blot in the striata of a subset of mice from Study 2. There was no significant effect of genotype, but Mn increased ARG2 expression. However, only the continuous 5 mg/kg Mn dose led to a significant increase in ARG2 compared to vehicle within each genotype. **(E)** GLT1 protein expression by western blot in mice from Study 2. There was no effect of Mn on GLT1 expression, but YAC128 mice had decreased expression compared to WT. For all, mean ± SEM plotted unless otherwise noted. Asterisks * indicate genotype effect, pound # indicates Mn effect within genotype. #/* $p < 0.05$, **, $p < 0.01$, *** $p < 0.001$, **** $p < 0.0001$

"5_0" groups, respectively) but there was no significant difference in NeuN positive cell counts between any Mn treatment groups in YAC128 (P> 0.05). Representative images are shown in **Fig. 3.6 B ii.**

3.4.5.2 Significant increases in brain and hepatic Mn levels were reversible

Brain Mn was increased by exposure similarly between the genotypes (**Fig. 3.6 C**). Mice that received Mn in the weeks immediately preceding sacrifice had significantly increased Mn in striatum (Genotype $F_{1, 98}$= 2.021, P=0.158, Treatment $F_{3, 98}$= 19.17, P<0.0001) and cortex (Genotype $F_{1, 92}$=0.032, P=0.856, Treatment $F_{3, 92}$= 19.51, P<0.0001). In brain, WT and YAC128 mice that started the study on Mn but then switched to vehicle at 31 weeks ("5_0") had Mn levels that matched vehicle-treated mice. This indicates that the increase, at least from exposure accumulating from 12-31 weeks of age, was reversible in brain tissue. In the liver, Mn accumulation differed by genotype (Genotype $F_{1, 98}$=8.004, P=0.0057, Treatment $F_{3, 98}$= 11.38, P<0.0001). Mn was significantly higher in YAC128 mice than WT receiving 5 mg/kg $MnCl_2 \cdot 4(H_2O)$ for the entirety of the study. Again, in both genotypes, hepatic Mn levels returned to normal (not significantly different from vehicle) in mice that switched from Mn to vehicle exposures at the 31-week mark.

3.4.5.3 Chronic Mn exposure changed striatal ARG2 protein expression but not GLT-1

Mn-dependent ARG2 was increased by Mn exposure in both genotypes but this was only significant following exposure throughout the entirety of the study (Genotype $F_{1, 57}$= 0.0146, P=0.904, Treatment $F_{3, 57}$= 8.433, P<0.0001) (**Fig. 3.6 D**). We also measured the Mn-responsive protein, GLT-1, and found no effect of Mn exposure but YAC128 mice had significantly lower overall GLT-1 expression in the striatum compared to WT (Genotype $F_{1, 92}$= 7.238, P=0.0085, Treatment $F_{3, 92}$= 0.437, P=0.727) (**Fig. 3.6 E**).

3.5 Discussion

We demonstrated that YAC128 mice respond differently to Mn exposure than WT mice across several behavioral tasks and molecular outcome measures. Following an acute exposure (three SC injections over one week) at 12-weeks of age, YAC128 mice were less sensitive to Mn-induced increases in striatal ARG2 protein. Increased ARG2 levels were comparable between genotypes at a high dose [50 mg/kg $MnCl_2 \cdot 4(H_2O)$], but significant increases from baseline were only seen at lower doses [20 mg/kg $MnCl_2 \cdot 4(H_2O)$] in WT mice (**Fig. 3.1 B**). The EC_{50} we approximated from this dose-response experiment was 2-fold greater (>20 mg/kg) in YAC128 compared to WT (10 mg/kg). We have previously reported impaired Mn uptake in YAC128 mice

following acute high-dose exposure (Pfalzer et al., 2020; Williams, Li, et al., 2010). The mechanism for this decreased uptake is unknown but it is important to note at 12 weeks of age YAC128 mice do not exhibit striatal cell loss and therefore is not due to fewer cells (Slow et al., 2003). Further, the decreased Mn uptake phenotype following the same acute exposure is no longer present in aged (32 weeks) YAC128 mice despite significantly blunted responses to Mn on the striatal metabolome (Pfalzer et al., 2020). A higher EC50 in YAC128 mice is therefore not due to simple defects in accumulation but rather Mn bioavailability (Bichell et al., 2017). The approximate EC_{50} values imputed from the acute exposure in Figure 1 informed the Mn dosing used in the chronic exposure for Study 1 (**Fig. 3.2 A**).

Because acute Mn exposures were successful in rescuing certain molecular HD phenotypes (Bichell et al., 2017; Bryan et al., 2020, 2019), we hypothesized that YAC128 mice exposed chronically to Mn would have attenuated behavioral phenotypes compared to vehicle treated YAC128 mice. Prior to Mn exposure (11 weeks of age), YAC128 mice exhibited motor coordination deficits on the accelerated rotarod but normal locomotor activity, strength, and anxiety levels. Our baseline behavioral findings are consistent with previous reports (Garcia-Miralles et al., 2017; Kordasiewicz et al., 2012) though some studies do not detect motor impairments until 4 months of age (Slow et al., 2003). In Study 1, we observed that chronic low dose Mn [5 mg/kg $MnCl_2 \cdot 4(H_2O)$] prevented motor coordination decline in YAC128 mice but higher doses did not provide the same protection. At 30 weeks of age, vehicle treated YAC128 mice declined to 57% of their baseline performance but low-dose Mn treated YAC128 mice maintained the same level of coordination from 11 to 30 weeks (**Fig. 3.2 I**). Importantly, this protective effect was observed at the low dose, which did not result in detection of a significant increase in brain or hepatic Mn levels after 20 weeks exposure (**Fig. 3.3 A**). This suggested that YAC128 mice could benefit from Mn at a dose that did not lead to significant, and potentially damaging, accumulation. There were no adverse behavioral effects on YAC128 mice from any of the three Mn doses in Study 1.

In Study 2, we exposed mice to only the lowest Mn dose [5 mg/kg $MnCl_2 \cdot 4(H_2O)$] from Study 1, or vehicle. We failed to detect the same protective effect of Mn against motor coordination decline on the rotarod in Study 2 (**Fig. 3.4 I**). Interestingly, WT mice declined to the same extent as YAC128 in Study 2. This was unexpected but may possibly be explained by differences in training between Study 1 and Study 2. Mice were re-trained on the rotarod (2 days training prior to testing on day 3) at each subsequent behavioral battery after 11 weeks in Study 1. These training days did not significantly change the group average rotarod performance and therefore were omitted in Study 2 to decrease the testing burden on the mice. In another study, YAC128 mice that were trained on the rotarod at 2 months and tested at 12 months were significantly impaired but still able to perform the task, but YAC128 mice that were not previously trained were unable to perform the rotarod at 12 months (J. M. Van Raamsdonk, 2005). Another study reported a defect in motor learning consolidation in YAC128 mice (Glangetas, Espinosa, & Bellone, 2020). It is possible that the combination of additional training

and Mn exposure was required to exert protective effects as seen in Study 1. Alternatively, there may have also been unintended and unknown Mn exposure based on differences in rodent housing. Mice in Study 1 were co-housed with mice in various Mn treatment groups, including the highest dose of 50 mg/kg $MnCl_2 \bullet 4(H_2O)$. Mn is excreted in the feces (P. Chen et al., 2018) and thus mice in Study 1 may have been exposed to an effectively larger dose than in Study 2 by inhalation of dust within the cage. The decreased Mn uptake phenotype in YAC128 mice is present following an acute exposure at 12 weeks (Bichell et al., 2017; Pfalzer et al., 2020) but this phenotype is not detectable in aged (42 weeks) female YAC128 mice (Bichell et al., 2017), nor do we report genotype differences in brain Mn accumulation in our current study. Therefore, it is possible that a "pre-loading" with higher doses of Mn could benefit YAC128 mice prior to the presentation of motor deficits. One research group found that pre-treatment with copper via either intraperitoneal injection or drinking water was neuroprotective against the excitotoxic damage observed in the quinolic acid rat model of HD (Martínez-Lazcano et al., 2014; Santamaría et al., 2003). These treatments took place prior to the excitotoxic event that models HD, and Mn pre-treatment that begins earlier may prove beneficial to HD models. Though no consistent protection against HD behavioral phenotypes was provided by Mn, the current study provides additional support for a gene by environment interaction between HD such that HD confers protection against Mn-induced behavioral changes. Further, while no therapeutic benefit of chronic Mn dosing is observed in the HD model, it remains unknown if the systemic subcutaneous Mn injections were able to impact brain Mn bioavailability. Thus, it remains untested if elevated bioavailable Mn in the brain could be therapeutic or protective in HD models.

We hypothesized that YAC128 mice would be resistant to Mn-induced impairments and thus have a greater lowest- or no-observed adverse effect level (LOAEL/NOAEL) for Mn compared to WT. In Study 1, WT mice exposed to the highest Mn dose [50 mg/kg $MnCl_2 \bullet 4(H_2O)$] exhibited behavioral changes by spending more time in the open zone of the EZM and were overall less active in the open field (**Fig. 3.2 L and 3.4 L**) but neither behavior was affected in YAC128 mice. Decreased locomotor activity in WT was an expected outcome of Mn-induced toxicity (Asser et al., 2019; Bouabid, Delaville, De Deurwaerdère, Lakhdar-Ghazal, & Benazzouz, 2014; Cordova et al., 2012; Vezér et al., 2005) though transient increases in locomotor activity have also been documented following Mn exposure (Avila-Costa et al., 2018; Nachtman, Tubben, & Commissaris, 1986). Reported effects of Mn on exploratory behavior or time spent in the open zone of the EZM are inconsistent (J. A. Moreno et al., 2009; Ye & Kim, 2015). In fact, we found the opposite effect on EZM behavior in Study 2, in which WT mice exposed to any Mn spent less time in the open zone of the EZM, indicative of an anxiety phenotype. Behavioral changes were again also not observed in the YAC128 mice, suggesting decreased sensitivity to these Mn-induced alterations.

Interestingly, we did not observe Mn-induced impairments on the rotarod in the current study, inconsistent with outcomes in other reported exposures. Young (8-10 weeks of age) WT C57/Bl6 received Mn via drinking

water for 6 weeks and using the same accelerating rotarod protocol as our study, deficits were detected in Mn-exposed WT at 14-16 weeks of age, but only in males. The same group of mice took longer to traverse the balance beam in another motor coordination task (Freeman et al., 2020). After 5 weeks of Mn exposure via drinking water, total brain Mn levels were approximately 2-fold greater than non-exposed mice (which is comparable to our striatal Mn increase in Study 2). A 14.7% reduction in rotarod performance was detected but this was only significant when comparing Mn- and vehicle-exposed mice in a model of hereditary hemochromatosis, not wild-type (Alsulimani, Ye, & Kim, 2015). *Slc39a14*$^{-/-}$ mice accumulate Mn in all extra-hepatic tissues and also exhibit significant motor coordination impairments on the rotarod (Jenkitkasemwong et al., 2018). In rats, just 5 days of 20 mg/kg intraperitoneal injections of $MnCl_2$ from postnatal days 8-12 severely affected rotarod performance. Due to the sensitive developmental period and increased sensitivity to Mn accumulation at this age, there was a nearly 10-fold increase in brain Mn that led to this effect (Cordova et al., 2012). We measured an approximately 3-fold increase in brain Mn in the high dose Mn group (50 mg/kg Mn) in Study 1 and approximately 2-fold increase in the treated mice in Study 2. Rats exposed to 0, 1 or 5 mg/kg $MnCl_2 \bullet 4(H_2O)$ via intraperitoneal injection 15 times over the course of 150 days exhibited significant rotarod impairments at the 5 mg/kg $MnCl_2 \bullet 4(H_2O)$ dose, but not the 1 mg/kg $MnCl_2 \bullet 4(H_2O)$. However, 5 mg/kg $MnCl_2 \bullet 4(H_2O)$ in rats is an effectively larger dose (~2 x) than in mice due to differences in metabolic rate (Nair & Jacob, 2016). Rodents in the aforementioned studies reporting effects were younger than in our study or required additional combined genetic factors to induce rotarod impairments following Mn exposure. Although rotarod performance was not significantly impaired, chronic Mn exposure resulted in significant (10-12%) loss of striatal NeuN positive cells. Others have reported cell loss in the globus pallidus (Tapin, Kennedy, Lambert, & Zayed, 2006), ventral tegmental area and substantia nigra pars compacta (Bouabid et al., 2014), but we focused on the striatum given its relevance to HD. YAC128 mice exhibited the expected 10% decrease in striatal NeuN positive cells (Slow et al., 2003) but were resistant to Mn-induced cell loss. This suggests that despite concurrent HD-related neurodegenerative processes in the striatum, the HD genotype protected the striatal neurons from chronic Mn induced cell loss. This argues in favor of a hypothesis that the mechanism of striatal cell death in HD is distinct from the neurotoxic mechanisms of Mn-induced cytotoxicity in the striatum.

The current study was unique in terms of exposure length and route – to our knowledge it is the longest reported Mn exposure by subcutaneous injection, which bypasses the gut and first-pass hepatic metabolism (P. Chen et al., 2018; Davis, Zech, & Greger, 1993). Other studies of appreciable length have employed different exposure routes, such as diet, drinking water, and inhalation (Avila-Costa et al., 2011; K M Erikson et al., 2004; Komura & Sakamoto, 1992; Morganti, Lown, Stineman, D'Agostino, & Massaro, 1985) or include case-studies of exposure via total parenteral nutrition (Khan et al., 2020). Exposure route, length, and chemical species are all critical determinants of toxicity outcomes. A comprehensive review (Gwiazda, Lucchini, & Smith, 2007) outlines

and discusses the consistency of behavioral and neurochemical outcome measures in both rodent and non-human primate studies in relation to chronic exposures in humans. They report widespread differences among studies, but one common theme was detrimental effects on the GABAergic system (increased GABA activity) at lower doses and negative effects on the dopaminergic system at higher doses. Our study is also unique in its randomized crossover design, with some animals receiving Mn in the earlier part of the study but not in the weeks immediately preceding sacrifice. We found that tissue Mn levels in those mice returned to levels that matched untreated mice, suggesting that if excess Mn exposure is terminated then levels can decrease to normal. However, significant behavioral impairments likely extend beyond normalized tissue levels of Mn, evidenced by mice receiving any Mn showing subtle deficits in the current study and by significant striatal cell loss in all Mn treated WT mice. A 1999 cross-sectional study examined the reversibility of neurobehavioral markers of chronic (8 year) excess Mn inhalation exposure in battery plant factory workers following mitigation of exposure and found that impairments were mostly irreversible (H. A. Roels, Ortega Eslava, Ceulemans, Robert, & Lison, 1999).

This study contributes to our knowledge of Mn toxicity and homeostasis by providing additional evidence of an HD-Mn interaction, such that YAC128 mice are less sensitive to Mn exposure than WT. Additional studies that examine Mn exposure in YAC128 mice via other routes and developmental periods can further elucidate mechanisms of this protection and indicate whether Mn treatment may offer therapeutic or protective effects in HD models.

Chapter 4

Excess Dietary Manganese Differentially Regulates Behavior in YAC128 Mice

4.1 Abstract

Deficient or excess dietary manganese (Mn) can negatively affect neurologic function, with ingestion of very high amounts of Mn resulting in motor and cognitive function impairments. Previous studies have shown that YAC128 HD model mice are resistant to Mn toxicity following acute and chronic subcutaneous injection exposures. The current study examined the HD-Mn interaction in response to excess dietary Mn. Young (3-week) and aged (12-month) WT and YAC128 mice of both sexes were placed on experimental diet containing either 70 ppm (control) or 2400 ppm Mn (high) for 8 weeks followed by a battery of behavioral tasks. In young females, we observed a significant genotype by diet interaction. Within this age and sex group, high Mn diet induced hyperactivity in WT mice across two independent behavioral tasks and HD-related hyperactivity in YAC128 mice on control diet was not detected in YAC128 mice on high Mn diet, potentially rescuing the early-HD phenotype. Changes in the expression of dopaminergic synthesis proteins (tyrosine hydroxylase; TH) were consistent with the behavioral data in young females such that elevated TH in YAC128 on control diet was decreased by high Mn diet. A potential rescue effect was also observed in young males; decreased TH expression measured in YAC128 control diet mice was elevated by high Mn diet despite no detected changes in young male behavior. Aged YAC128 mice showed the expected disease-relevant behavioral impairments but we observed no significant behavioral effects of Mn diet in either genotype of the aged group. TH expression in aged mice, which was lower in YAC128, was unaffected by Mn. These studies provide support for a significant role of both age and sex in the HD-Mn interaction following dietary Mn exposure, highlighting the importance of early intervention to maximize therapeutic effects in HD.

4.2 Introduction

Manganese (Mn) homeostasis is influenced by exposure route, sex, age, and disease as outlined in **Chapter 1**, section 1.4. **Chapters 2** and **3** examined the interaction between Huntington's Disease (HD) and Mn by acute and chronic subcutaneous injection. Here, in **Chapter 4**, we investigated how wild-type (WT) and YAC128 mice were affected by excess dietary Mn using young and aged animal groups of both sexes.

Sufficient Mn for optimal health is acquired via the diet and deficiency is rare under nonexperimental conditions (Horning et al., 2015; Martins et al., 2020). However, low Mn intake has been associated with

depressive phenotypes in adults (Nakamura et al., 2019) and children with low blood Mn concentrations were reported to perform poorly on the Stroop test of cognitive inhibition (Bhang et al., 2013). Experimental cases of Mn deficiency mimic certain HD-phenotypes including decreased arginase activity, impaired glucose uptake and insulin signaling, and increased oxidative stress ((Clegg et al., 1998; Keen et al., 1999; Zidenberg-Cherr, Keen, Casey, et al., 1985) (for more detail see **Chapter 1**, section 1.7). In mice fed a Mn-deficient diet (<0.01 ppm Mn) for two weeks, Mn concentration was significantly decreased ~13-14% in cortex and cerebellum (striatal data were not reported) and 137 genes were differentially expressed in cerebellum in response to the Mn-deficient diet (Seo, Choi, Aring, Paschall, & Iwase, 2020). Significant decreases in basal brain Mn are not detected in YAC128 HD model mice, but these mice do exhibit decreased Mn bioavailability and consequentially decreased activity of Mn-dependent enzymes such as arginase 2 (ARG2) (Bichell et al., 2017).

Although Mn is essential, overexposure to this micronutrient is detrimental. Toxicity is more commonly observed following inhalation exposures because Mn absorption is tightly regulated at the level of the gastrointestinal tract, but toxic oral exposures can occur (P. Chen et al., 2018). Excessive Mn consumption via food sources is unlikely to cause acutely toxic effects, but high dietary intake can result in long term accumulation and increased Mn load. Vegetarians typically consume more Mn than omnivores given that vegetables, grains, and legumes are Mn-rich food sources. Hair Mn concentrations were significantly higher in a group of vegetarian women compared to age-matched omnivores (Gibson, Anderson, & Sabry, 1983). These women did not experience adverse effects, but the results from this study show that variable dietary Mn intake influences total body Mn accumulation. Ingestion of very high amounts of Mn can significantly increase brain Mn and effect neurological outcomes. Toxic effects have not been reported from solely food-based exposures, but one case study reported a woman that displayed characteristic signs of Manganism (a Parkinsonian-like condition) following years of vitamin and mineral supplementation (Schuh, 2016). More typically, oral consumption of excessive Mn occurs from drinking contaminated water sources (Frisbie et al., 2002), or in the case of infants, drinking soy-based formula (Frisbie et al., 2019). A growing body of research has implicated high Mn exposure in early life in the development of attention-deficit/hyperactivity disorder (ADHD) (Schullehner et al., 2020).

In the present study, we explored the HD-Mn interaction in response to excess dietary Mn. We hypothesized that high Mn dietary intervention would yield toxic behavioral effects in young and aged wild-type (WT) mice, and YAC128 mice would be protected from these toxic effects at both ages. Further, we hypothesized that high Mn diet would prevent the manifestation of HD behavioral phenotypes in young YAC128 mice, but phenotypes already present in aged YAC128 mice would be too strongly established to undergo a rescue.

4.3 Methods

4.3.1 Animals

Animal husbandry and genotyping has been previously described in **Chapter 2**. Importantly, the current study used YAC128 mice backcrossed onto the C57BL/6J background (YAC128-C57) and their wild-type (WT) littermates. HD phenotypes are penetrant on the C57BL/6J background but are not as severe as in the original YAC128 FVB/NJ strain (Jeremy M. Van Raamsdonk, Metzler, et al., 2007). Mice were weaned at 21 days and housed in groups of 3-5 of a single sex in a temperature- and humidity-controlled housing room on a 12:12 light:dark cycle with food and water available *ad libitum.* Approximately equal numbers of male and female mice were used in each genotype-diet group. All protocols were approved by the Vanderbilt University Institutional Animal Care and Use Committee under protocol numbers M1600073 and M1900090. All experiments were conducted in accordance with the NIH Guide for the Care and Use of Laboratory Animals.

4.3.2 Manganese diets

Standard lab chow (LabDiet 5L0D, TX) containing approximately 70 ppm Mn (variable based on batch) was available *ad libitum* prior to dietary intervention. For dietary intervention mice were put on specially formulated diets (Research Diets, Inc.) that contained 70 ppm (control) or 2400 ppm Mn (high). Other micro- and macronutrient content was consistent between the two diets. The high Mn diet was chosen based previous reports that this Mn content significantly increased brain Mn after 30 days (Jenkitkasemwong et al., 2018). Diet was randomly assigned to a cage prior to any behavioral testing.

4.3.3 Study design

Mice in the young experimental group were put on experimental diet at weaning (3 weeks of age) and performed a behavioral battery test at 11 weeks of age prior to sacrifice and dissection at 12 weeks of age (**Fig. 4.1 A**). Mice in the aged experimental group were weaned at 3 weeks of age and remained in the housing room on regular chow until a pre-intervention behavioral battery at approximately 11.5 months of age. Aged mice were placed on experimental diet at 12 months of age, and 8 weeks later at approximately 14 months of age underwent a post-diet behavioral battery prior to sacrifice and dissection at approximately 14.5 months of age (**Fig. 4.2 A**).

4.3.4 Behavioral testing

4.3.4.1 Elevated zero maze (EZM). A standard white elevated zero maze was used as described in **Chapter 3**. Time spent in the open zone (s) and total distance travelled over 5 minutes was recorded automatically.

4.3.4.2 Locomotor activity, inverted screen, and grip strength. These tasks were performed as previously described in **Chapter 3**. Total time in locomotor activity chambers was 30 minutes.

4.3.4.3 Rotarod. Rotarod was performed as described in **Chapter 3**, except that ramp speed increased over 4 minutes (total test time 5 min, max speed for final minute) in the protocol used for young mice in the current study. Ramp speed increased to max speed over 5 minutes for aged mice.

4.3.4.4 Y-maze alternation. A closed, rounded top Y-maze made of clear acrylic tubing with arms 32-cm long was used to assess short-term spatial memory. Spontaneous alternation was measured in a single 6-minute trial. Mice explored freely as an experimenter blind to genotype and diet scored arm entries from an adjacent room via live video recording taken overhead the maze. Arm entries were only counted if the entire body of the mouse (all four paws and half of tail) entered the arm. Alternation was defined as consecutive entry into three different arms (e.g., ABC but not ABA). Percent alternation was calculated as [alternations/(total arm entries-2)] x 100.

4.3.4.5 Nest building. Mice were individually housed overnight (transferred from group housing just prior to start of dark cycle) in clean cages with standard bedding and a cotton nestlet (5 g; Ancare, NY). The following morning, un-shredded nestlet material was weighed and an experimenter blind to genotype and diet scored the nest quality on a scale between 0 – 5, adapted to include half-point increments (5 is the highest quality) (Deacon, 2006).

4.3.4.6 Food consumption. During the nest building task when mice were single housed, food was pre-weighed (approximately 5-10 g) prior to placing the mouse in the cage. The following morning, the remaining food was weighed to calculate food consumed overnight.

4.3.4.7 Test order. For young mice: Day 1: EZM, Day 2: Locomotor activity, grip strength, Days 3-5: Rotarod. For aged mice, the same behavioral battery was performed pre- and post-diet intervention: Day 1: EZM

and inverted screen, Day 2: Locomotor activity, grip strength, Days 3-5: Rotarod, Day 8: Y-maze alternation, Day 10: Nest building and food consumption.

4.3.5 Tissue collection

Mice were anesthetized using isoflurane prior to cervical dislocation and decapitation. The brain was removed, weighed, and striatum from both hemispheres collected by microdissection. Tissue was snap frozen on dry ice and stored at -80°C until used for biochemical analyses.

4.3.6 Mn levels

Mn concentration was measured by inductively coupled plasma mass spectrometry (ICP-MS) from a protein lysate (described below) using the methods previously described in **Chapters 2** and **3** (Pfalzer et al., 2020). Briefly, 50 uL protein lysate was digested at a 1:1 dilution in ultrapure nitric acid (70%) for 48 hours at 50 °C (water bath); 100 uL of digested tissue was further diluted to 2% nitric acid with DI water and Mn analyzed.

4.3.7 Western blotting

Protein lysates were prepared by homogenizing frozen tissue by hand with a plastic pestle in 200 uL Pierce RIPA lysis buffer (Thermo Scientific, cat # 89900) with protein and phosphatase inhibitors [cOmplete EDTA-free protease inhibitor cocktail (Roche, 04693132001), 1:100 phosphatase inhibitor cocktail 3 (MilliporeSigma, cat.no. P0044), and 1 mM sodium orthovanadate per 10 ml of RIPA buffer (Thermo Fisher Scientific, cat # 89900)]. Protein lysate was collected following centrifugation at 12,000 g for 5 min. Protein concentration was measured using standard bicinchoninic acid (BCA) assay protocol (Pierce BCA Protein Assay Kit, Thermo Scientific). Samples were denatured with NuPage LDS sample buffer (Thermo Scientific, cat # NP0007) and reducing agent (Thermo Scientific, cat # NP0009) and boiled at 95 °C for 3 minutes prior to loading on Bolt™ 4-12% Bis-Tris Plus gels (Thermo Scientific, cat # NW04120BOX). Protein was transferred to nitrocellulose membranes using the iBlot2™ system (Thermo Scientific, cat # IB23001). Gels were rehydrated overnight in DI water and stained with Coomassie blue (Bio-Rad, cat # 161-0786) for total protein used as loading control. Three sets of gels were run because of overlapping molecular weights and protein loading requirements. For pTH Ser31 and TH (anti-rabbit, Cell Signaling Technologies, cat # 3370 and 2792) 20 ug protein was loaded per well. For pERK1/2 and ERK1/2 (P-p44/42 MAPK and p44/42 MAPK, anti-rabbit, Cell Signaling Technologies, cat # 4370 and 9102) 40 ug protein was loaded. For DAT (anti-rat, Millipore Sigma, cat # MAB369) and SLC30A10

(anti-rabbit, Abcam, cat # ab229954; aged mice only) 20 ug protein was loaded per well. Following transfer, membranes were blocked for 30 min with 5% nonfat milk in tris-buffered saline with 0.1% Tween-20 (TBST) and then 30 min in 5% bovine albumin serum (BSA) in TBST. Blots were incubated in primary antibody (1:1,000 in 5% BSA in TBST) overnight at 4 °C followed by appropriate secondary antibody incubation (1:5,000 in 5% nonfat milk) for 2 hours. Protein bands were visualized using chemiluminescence (Western Lighting Plus ECL, Perkin Elmer, cat # 103E001EA). Phospho-proteins were probed first, and membranes stripped (Restore Stripping Buffer, Thermo Fisher Scientific, cat # 21059) before probing the total protein (TH and ERK1/2). For young mice, males and females were run on separate blots with 2-3 samples from each genotype-diet group per gel. Sexes were combined on gels for aged mice. Protein bands were quantified using ImageJ (imagej.nih.gov). Each protein band was normalized to its own total protein (Coomassie blue stained gel) as a loading control, and then to average WT control diet for that blot.

4.3.8 Statistics

Data are reported as mean ± S.E.M. unless otherwise noted. Data analyses were completed in SPSS 26.0 or GraphPad Prism 8. In young mice, we anticipated sex differences based on known sex differences observed in dietary Mn metabolism (Felber et al., 2019; Finley et al., 1994) thus females and males were analyzed separately for all behavioral tests and molecular outcomes. In aged mice, all analyses were first run with sex as a fixed variable, but no significant differences were detected and thus all data were collapsed, and sexes combined for analysis (except for body weight data). For all dependent variables in young mice two-way ANOVA (2 genotype x 2 diet) was conducted with appropriate post-hoc tests. For aged mice, two-way repeated-measures (RM)-ANOVA (RM of diet intervention/age x 2 genotype x 2 diet) was conducted for behavioral measurements and two-way ANOVA (2 genotype x 2 diet) for molecular data. Outliers were removed if they reflected experimental software error (e.g., beam tracking error in activity chambers) or if outside of 95% confidence interval (± 2 standard deviations).

4.4 Results

4.4.1 Body weight and anxiety were unaffected by high Mn diet in young mice

Mice were placed on experimental diets upon weaning (**Fig. 4.1 A**). Mice on high Mn diet were similar weight compared to mice on control diet, suggesting that there were no overtly aversive reactions to the diet nor a propensity to eat more or less of the assigned diet. We confirmed the expected sex and genotype differences, in

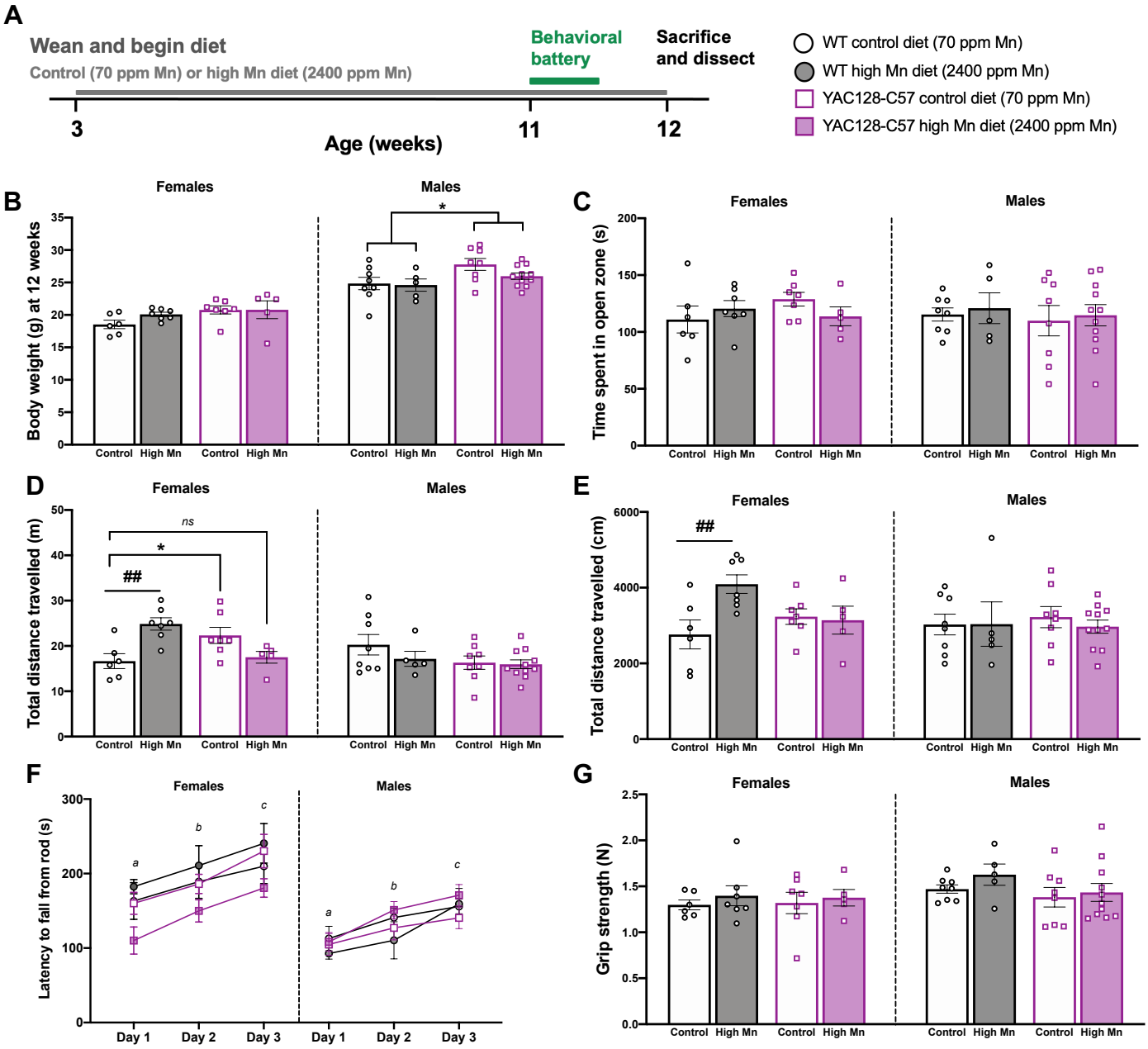
A
Wean and begin diet
Control (70 ppm Mn) or high Mn diet (2400 ppm Mn)
Behavioral battery
Sacrifice and dissect
3
11
12
Age (weeks)
WT control diet (70 ppm Mn)
WT high Mn diet (2400 ppm Mn)
YAC128-C57 control diet (70 ppm Mn)
YAC128-C57 high Mn diet (2400 ppm Mn)
B
Females
Males
Body weight (g) at 12 weeks
C
Time spent in open zone (s)
D
Total distance travelled (m)
ns
E
Total distance travelled (cm)
F
Latency to fall from rod (s)
Day 1
Day 2
Day 3
G
Grip strength (N)
Control
High Mn

Figure 4.1 **(A)** Experimental timeline. Mice were weaned at 3 weeks and put on either control or high Mn diet for the remainder of the study. After 8 weeks on diet, a behavioral battery was performed at 11 weeks of age and mice were sacrificed and dissected at 12 weeks of age. **(B)** The diet did not alter weight gain in any group, but males weighed more than females and YAC128 mice weighed more than WT. **(C)** There was no anxiety phenotype detected in any group based on time spent in the open zone of the EZM. **(D)** In females, the high Mn diet induced hyperactivity measured by distance travelled during the EZM. YAC128 control diet females were hyperactive, and this was normalized by the high Mn diet. **(E)** WT females on high Mn diet were hyperactive as measured by total distance travelled over 30 min in the open field. **(F)** There were no impairments in motor coordination as measured by latency to fall from the rotarod. Motor learning was intact; overall performance improved over each training day. Days that do not share a superscript letter are significantly different from each other within each sex. Females overall stayed on the rod longer than males. **(G)** Grip strength was similar among all genotype and diet groups. For all, mean ± SEM plotted unless otherwise noted. Asterisks * indicate genotype effect, pound # indicates Mn effect within genotype. */# $p < 0.05$, ## $p < 0.01$

which males weighed more than females and YAC128 mice weighed more than WT (Genotype $F_{1, 49}$= 10.18, P=0.002, Diet $F_{1, 49}$=0.041, P=0.841, Sex $F_{1, 49}$=102.07, P<0.0001) (**Fig. 4.1 B**). To ensure behavioral differences detected were not due to underlying anxiety phenotypes, mice were first tested on the elevated zero maze (EZM). We confirmed in both males and females that all genotype and diet groups spent comparable time (s) in the open zone (all Ps > 0.05) (**Fig. 4.1 C**).

4.4.2 Mn increased locomotor activity in young WT female mice

Despite similar time spent in the open zone of the EZM, the distance travelled (m) during this task varied among groups in females only (Genotype $F_{1, 21}$= 0.280, P=0.602, Diet $F_{1, 21}$= 1.134, P=0.299, Interaction $F_{1, 21}$=16.82, P<0.0001). WT mice on high Mn diet were hyperactive compared to WT mice on control diet (P=0.0024). Within the control diet, YAC128 mice were hyperactive compared to WT (P=0.034) but activity in YAC128 mice on high Mn diet was not different from WT control diet levels (**Fig. 4.1 D**). There were no effects of Mn nor genotype in young male mice on distance travelled in the EZM (all Ps > 0.05). The hyperactive phenotype in young WT females on high Mn diet was replicated in a second independent measure of locomotor activity (30 min open field) (Genotype $F_{1, 21}$= 0.280, P=0.602, Diet $F_{1, 21}$= 1.134, P=0.299, Interaction $F_{1, 21}$=16.82, P<0.0001) but there were no differences between other groups (all Ps > 0.05) (**Fig. 4.1 E**).

Motor coordination and motor learning were assessed on the accelerated rotarod. We did not detect a significant motor coordination impairment in YAC128 mice at this age nor did high Mn alter rotarod performance (all Ps > 0.05) (**Fig. 4.1 F**). Motor learning was intact in all groups based on improvement across training days (female training day $F_{2, 42}$= 25.032, P < 0.0001, male training day $F_{2, 56}$= 27.237, P < 0.0001). Grip strength, an important control measure, was similar among all groups and did not impact performance on any behavioral task (**Fig. 4.1 G**).

4.4.3 High Mn diet did not affect weight gain nor food consumption in aged mice

Similar to the young cohort, body weight was measured weekly to monitor the health of the animals following a diet change at 12 months of age after completion of the pre-diet behavioral battery (**Fig. 4.2 A**). Overall mice gained weight as they aged, with females gaining more than males and YAC128 mice gaining more than WT (Age $F_{1, 44}$= 85.583, P < 0.0001, Age*Genotype $F_{1, 44}$= 14.583, P=0.029, Age*Sex $F_{1, 44}$=8.506, P=0.006). Diet had no effect on weight (Age*Diet $F_{1, 44}$<0.001, P=0.999). Males (40.17 g ± 4.38) and females (38.49 g ± 6.55) did not differ by weight at 14 months of age (Sex $F_{1, 44}$=2.00, P=0.164). YAC128 mice were expected to weigh more than WT, and this was confirmed (Genotype $F_{1, 44}$=12.631, P=0.001) (**Fig. 4.2 B**).

Overnight food consumption was measured (**Fig. 4.2 C**) when mice were singly housed for one night during a nest building task (Fig. 4.2 K). Regular chow was provided pre-dietary intervention and the appropriate Mn diet was provided post-dietary intervention. Overall, mice consumed less food overnight following diet change, but this is likely a product of age and not the diet change. Importantly, there were no significant differences between Mn diet groups nor genotype, therefore within a diet group each genotype was exposed to approximately the same level of Mn and the high Mn food was not aversive (Genotype $F_{1, 48}$= 0.185, P=0.669, Diet $F_{1, 48}$=0.022, P=0.883, Diet Change/Age $F_{1, 48}$=40.41 P<0.0001).

4.4.4 Exploratory behavior decreased over time in aged mice independent of diet

Time spent in the open zone of the EZM, a proxy for anxiety, was measured prior to diet intervention and after 8 weeks on experimental diet. Time spent in the open zone was comparable among all groups at 12 months of age prior to the diet change, confirming absence of an anxiety phenotype that would confound results from other behavioral assays. However, upon repeat testing at 14 months of age, post-diet intervention, the average time spent in the open zone of the EZM decreased for all groups (Genotype $F_{1, 48}$= 2.437, P=0.125, Diet $F_{1, 48}$=0.042, P=0.839, Age $F_{1, 48}$=19.614, P<0.0001) (**Fig. 4.2 D**). Given that this was no longer a novel environment, this decreased exploratory behavior in the open zone upon repeat testing is to be expected and does not suggest increased anxiety.

4.4.5 Hypoactivity and motor coordination deficits in YAC128 worsened with age

Distance travelled in the EZM decreased with age and repeat exposure to the apparatus. However, the extent that locomotor activity decreased in the EZM was dependent on genotype and Mn diet (Age $F_{1, 48}$=44.686, P<0.0001, 3-way interaction $F_{1, 48}$=5.307, P=0.026). YAC128 mice were hypoactive in this task overall (Genotype $F_{1, 48}$= 10.668, P=0.002) and post-hoc analyses revealed that YAC128 control diet mice were the only group for which the total distance travelled in the EZM significantly decreased with age (P=0.0023) (**Fig. 4.2 E**). In a second independent locomotor activity task (30 min open field chambers), total activity decreased in all groups as mice aged and likely also as a result to repeated exposure to the test chamber (Age $F_{1, 48}$=123.071, P<0.0001) (**Fig. 4.2 F**). YAC128 mice were hypoactive compared to WT littermates and Mn diet did not affect total activity in either genotype (Genotype $F_{1, 48}$= 12.363, P=0.002, Diet $F_{1, 48}$=1.066, P=0.307). YAC128 mice exhibited significant motor coordination deficits on the accelerated rotarod, as expected (Genotype $F_{1, 48}$= 29.722, P<0.0001, Age $F_{1, 48}$= 10.538, P=0.002) (**Fig. 4.2 G**). Performance declined with age, but post-hoc analyses show that this motor coordination decline was only significant in YAC128 mice (P=0.0355).

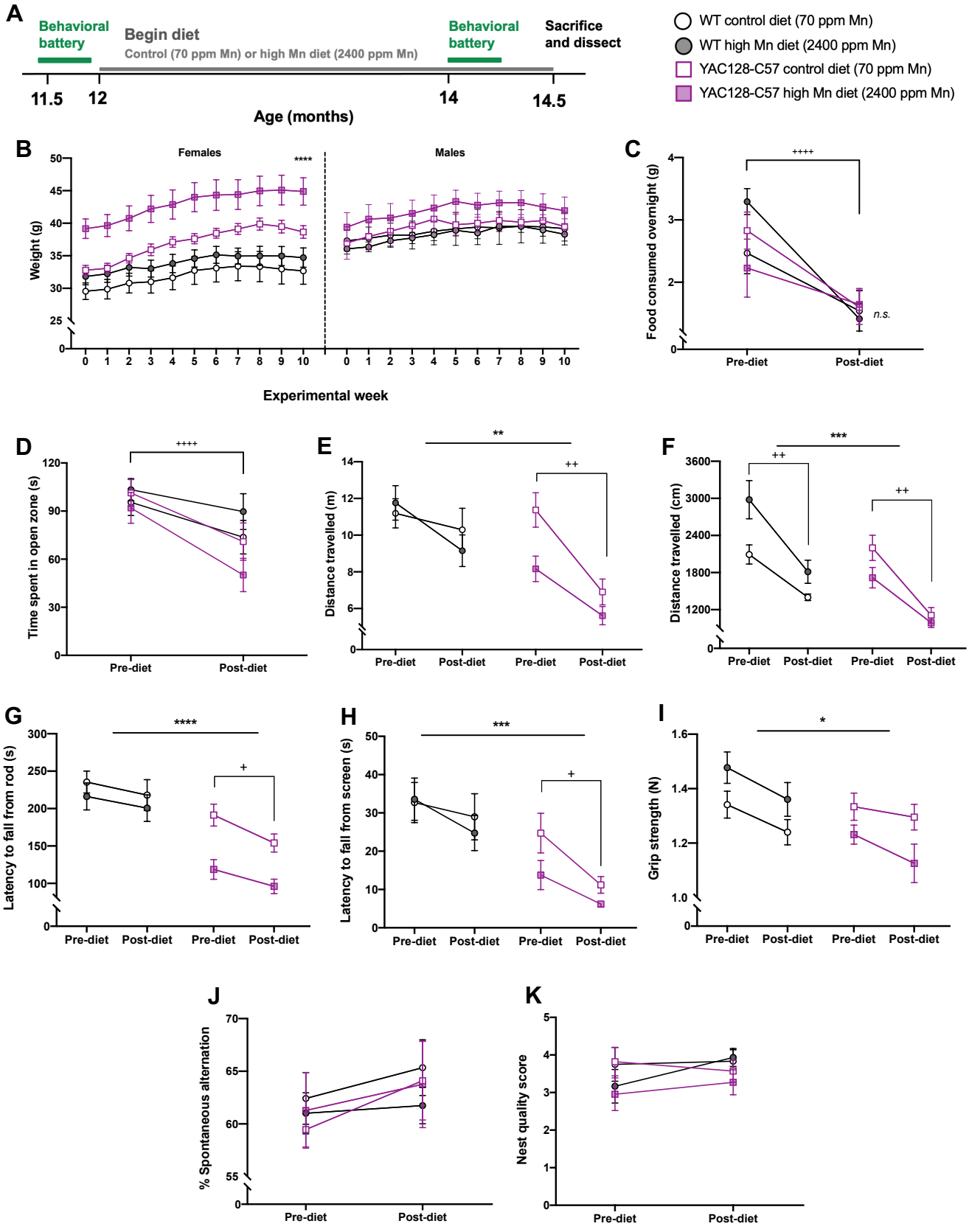
A
Behavioral battery
Begin diet
Control (70 ppm Mn) or high Mn diet (2400 ppm Mn)
Behavioral battery
Sacrifice and dissect
11.5
12
14
14.5
Age (months)
WT control diet (70 ppm Mn)
WT high Mn diet (2400 ppm Mn)
YAC128-C57 control diet (70 ppm Mn)
YAC128-C57 high Mn diet (2400 ppm Mn)
B
Females
Males
****
Weight (g)
Experimental week
C
++++
Food consumed overnight (g)
n.s.
Pre-diet
Post-diet
D
++++
Time spent in open zone (s)
Pre-diet
Post-diet
E
**
++
Distance travelled (m)
Pre-diet
Post-diet
Pre-diet
Post-diet
F
***
++
++
Distance travelled (cm)
Pre-diet
Post-diet
Pre-diet
Post-diet
G
****
+
Latency to fall from rod (s)
Pre-diet
Post-diet
Pre-diet
Post-diet
H
***
+
Latency to fall from screen (s)
Pre-diet
Post-diet
Pre-diet
Post-diet
I
*
Grip strength (N)
Pre-diet
Post-diet
Pre-diet
Post-diet
J
% Spontaneous alternation
Pre-diet
Post-diet
K
Nest quality score
Pre-diet
Post-diet

Figure 4.2 **(A)** Experimental timeline. Mice performed a behavioral battery pre-diet intervention at 11.5 months of age. Diet was changed at 12 months of age from regular chow to one of the two new diet conditions (control or high Mn). The behavioral battery was repeated after 8 weeks on diet, approximately 14 months of age. Mice were sacrificed and dissected following completion of the 2-week behavioral battery at approximately 14.5 months of age. **(B)** Body weight was not affected by diet. Females gained more weight than males so that weight was not significantly different by sex at 14 months of age. YAC128 mice were heavier (**** indicates main effect) and gained more weight over time than WT. **(C)** Food consumption per mouse was not affected by Mn diet nor genotype but did decrease with age. **(D)** Time spent in the open zone of the EZM. There were no anxiety differences between genotypes or Mn diet groups based on time spent in the open zone of the EZM. However, as mice aged and repeated this task post-diet change, they tended to spend less time exploring the open zone. **(E)** Distance travelled during the EZM task. YAC128 mice were hypoactive compared to WT and total distance travelled in YAC128 control diet mice decreased with age. **(F)** Total distance travelled during 30 min in the open field. YAC128 mice were significantly less active compared to WT. Total activity decreased with age in both genotypes independent of diet. **(G)** Motor coordination was significantly impaired in YAC128 mice based on latency to fall from the accelerated rotarod. As mice aged, performance declined in YAC128 mice. Average performance on day 3 pre- and post-diet is shown. **(H)** Strength, measured by average latency to fall from the inverted screen, was lower in YAC128 mice and declined with age. **(I)** Grip strength was lower in YAC128 mice compared to WT (*) with no effects of diet. **(J)** Percent spontaneous alternation in the Y-maze task of spatial memory was similar among all groups and did not change with age. **(K)** Nest quality score was consistent as mice aged and was not significantly different between genotype or diet groups.

For all, mean ± SEM plotted unless otherwise noted. Asterisks * indicate genotype effect, plus + indicates age effect. *p <0.05, **p<0.01, ***p<0.001, ****p<0.0001

4.4.6 Strength declined with age but was unaffected by diet

Latency to fall from the inverted screen, a measure of overall limb strength, also decreased with age for all genotype and diet groups. YAC128 mice fell from screen sooner than WT but there were no differences between diet groups (Genotype $F_{1, 48}$= 13.779, P=0.001, Age $F_{1, 48}$= 16.540, P <0.0001) (**Fig. 4.2 H**). Similarly, grip strength was weaker in YAC128 mice compared to WT, with no effects of diet and decreased with age among all groups (Genotype $F_{1, 48}$= 5.189, P=0.027, Age $F_{1, 48}$= 11.514, P=0.001) (**Fig. 4.2 I**).

4.4.7 Hippocampal-dependent behavioral tasks were unaffected by age, genotype, and diet

Two hippocampal-dependent behavioral tasks were also performed. Mn exposure has been linked to spatial memory deficits in rodents (Lu et al., 2014) and humans (Bauer et al., 2017). We did not detect differences between YAC128 and WT mice nor the diet groups in the percent spontaneous alternations made in the Y-maze, a hippocampal-dependent measure of spatial working memory. This task was also unaffected by age (all Ps> 0.05) (**Fig. 4.2 J**). Nest building is also shown to be hippocampal-dependent and reflects the personified behavior of overall well-being and ability to take care of oneself as well as some degree of executive function (C. L. C. Neely, Pedemonte, Boggs, & Flinn, 2019). This task was similarly unaffected by genotype and diet and the quality of nests were consistent as mice aged (all Ps > 0.05) (**Fig. 4.2 K**).

4.4.8 High Mn diet impacted brain weight and striatal Mn concentration in young mice

Total brain weight was measured immediately following dissection. Young males and females were analyzed separately based on sex differences in behavior. Brains of female mice of both genotypes on high Mn diet weighed less than brains from females on control diet (Genotype $F_{1, 21}$= 7.55, P=0.0121) at this age but no differences were observed in male mice (**Fig. 4.3 A**). Striatal Mn was significantly increased in females (Diet $F_{1, 27}$= 4.455, P=0.0442, Genotype $F_{1, 27}$= 2.073, P=0.1615) and males (Diet $F_{1, 27}$= 4.75, P=0.0308, Genotype $F_{1, 27}$= 0.837, P=0.368) with no differences between genotypes (**Fig. 4.3 B**).

4.4.9 Abnormal tyrosine hydroxylase (TH) expression in young YAC128 mice was normalized by high Mn diet

To further probe the molecular mechanisms underlying the changes in locomotor activity in young female mice we examined expression differences in dopaminergic (DAergic) pathway proteins in the striatum. TH expression was differentially dependent on both genotype and Mn diet in females (Interaction $F_{1, 22}$= 2.012, P=0.0078) and males (Interaction $F_{1, 25}$= 5.139, P=0.0323). TH expression was decreased in YAC128 high Mn

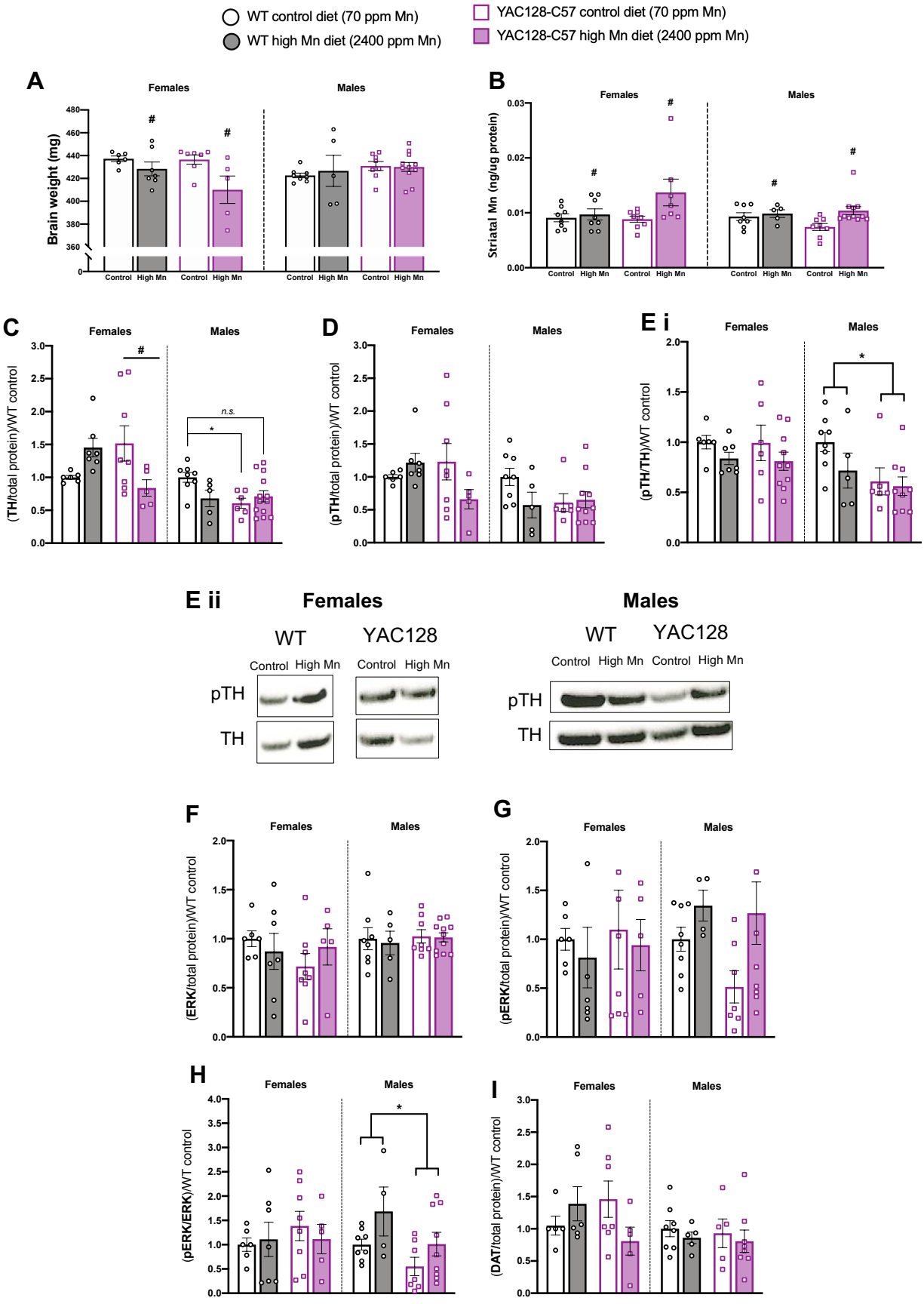
WT control diet (70 ppm Mn)
WT high Mn diet (2400 ppm Mn)
YAC128-C57 control diet (70 ppm Mn)
YAC128-C57 high Mn diet (2400 ppm Mn)
A
Females
Males
Brain weight (mg)
Control
High Mn
B
Striatal Mn (ng/ug protein)
C
(TH/total protein)/WT control
n.s.
D
(pTH/total protein)/WT control
E i
(pTH/TH)/WT control
E ii
WT
YAC128
pTH
TH
F
(ERK/total protein)/WT control
G
(pERK/total protein)/WT control
H
(pERK/ERK)/WT control
I
(DAT/total protein)/WT control

Figure 4.3 Post-dissection outcomes from young mice. **(A)** Brain weight was significantly lower in females on high Mn diet compared to control diet with no effect of genotype. No differences in brain weight were observed in males. # indicates a main effect. **(B)** Striatal Mn concentration significantly increased in males and females on high Mn diet with no differences between genotypes. # indicates a main effect. **(C)** Tyrosine hydroxylase (TH) was increased in YAC128 females but returned to normal levels on high Mn diet (n.s. from WT control diet). TH expression was significantly lower in YAC128 control diet males, but YAC128 males on high Mn diet had TH levels that were not significantly different from WT control diet. **(D)** Phosphorylated TH (pTH Ser 31) expression followed a similar pattern as total TH but did not reach statistical significance. **(E)** (i) No effect of genotype nor diet on pTH/TH ratio in females. YAC128 males had overall decreased pTH/TH ratio compared to WT regardless of diet. (ii) Representative blot images for changes pTH and TH in females (left) and males (right). For all western blots in young mice, sexes were run on separate blots and therefore cannot be directly compared to each other. **(F)** No changes in total ERK. **(G)** In males, there was a main effect of high Mn diet on phosphorylated ERK (pERK). **(H)** In males pERK/ERK ratio was increased in high Mn diet groups (main effect) and YAC128 mice had lower pERK/ERK compared to WT (main effect). **(I)** DAT expression was not significantly different.

For all, mean ± SEM plotted unless otherwise noted. Asterisks * indicate genotype effect, pound # indicates a Mn effect.

diet females compared to the elevated levels observed in control diet YAC128 females (P=0.0449). Importantly the TH levels in female YAC128 high Mn diet were normalized to levels that matched female WT control diet mice (P=0.99). In males, TH expression was lower in YAC128 control diet mice compared to WT (P=0.0231) but was increased to normal levels in YAC128 mice on high Mn diet (P=0.323 compared to WT control) (**Fig. 4.3 C**). Expression of phosphorylated TH (pTH Ser31), the active form of this enzyme (Dunkley, Bobrovskaya, Graham, Von Nagy-Felsobuki, & Dickson, 2004), was probed. The results in females followed the same pattern as total TH expression but did not reach statistical significance (Interaction $F_{1, 22}$= 3.846, P=0.0627) and no changes were detected in males (Interaction $F_{1, 25}$= 2.588, P=0.1202) (**Fig. 4.3 D**). Thus, when examining pTH/TH there were no effects of genotype or diet in females (all Ps > 0.05) but in males, YAC128 mice had decreased expression compared to WT with no effect of diet (Genotype $F_{1, 25}$= 5.237, P=0.0312) (**Fig. 4.3 E**). Representative blots are shown in **Fig. 4.3 E ii.**

ERK1/2 is responsible for phosphorylating TH ser31 (Dunkley et al., 2004) and thus we measured total expression of this protein as well as its phosphorylated (active) form. There were no differences in total ERK expression based on genotype or diet in either sex (all Ps > 0.05) (**Fig. 4.3 F**). In males, pERK expression was increased overall in high Mn diet mice (**Fig. 4.3 G**). The pERK/ERK ratio was not different between genotype and diet groups in females (all Ps > 0.05) but there was a main effect of genotype and diet in males (Genotype $F_{1, 24}$= 5.046, P=0.0342, Diet $F_{1, 24}$= 5.259, P=0.0309), however, within each genotype the diet effect was not statistically significant. Overall high Mn diet increased pERK/ERK ratio and YAC128 mice had decreased pERK/ERK in males (**Fig. 4.3 H**).

The expression pattern of DAT, the dopamine (DA) reuptake transporter, observed in females among genotype and diet groups mimicked the pattern of TH expression, but was not significant (Interaction $F_{1, 19}$= 3.847, P=0.0647) and there were no significant differences in DAT expression between groups in males (**Fig. 4.3 I**).

4.4.10 Brain weight and striatal Mn were differentially altered by high Mn diet in aged WT and YAC128 mice

Total brain weight was lower in aged YAC128 mice compared to WT (Genotype $F_{1,46}$= 8.954, P=0.0044) and high Mn decreased total brain weight (Diet $F_{1,46}$= 20.88, P <0.0001). However, post-hoc analyses revealed the main effect of diet was driven by the lower brain weights in YAC128 high Mn diet mice (P=0.0209) (**Fig. 4.4 A**). Males and females were combined based on comparable body weight and no differences in behavior outcomes at this age. Striatal Mn increased in WT mice on high Mn diet (P=0.0017) but not YAC128 (Diet $F_{1, 45}$= 7.032, P=0.0110, Interaction $F_{1, 45}$= 5.576, P=0.0226) (**Fig. 4.4 B**).

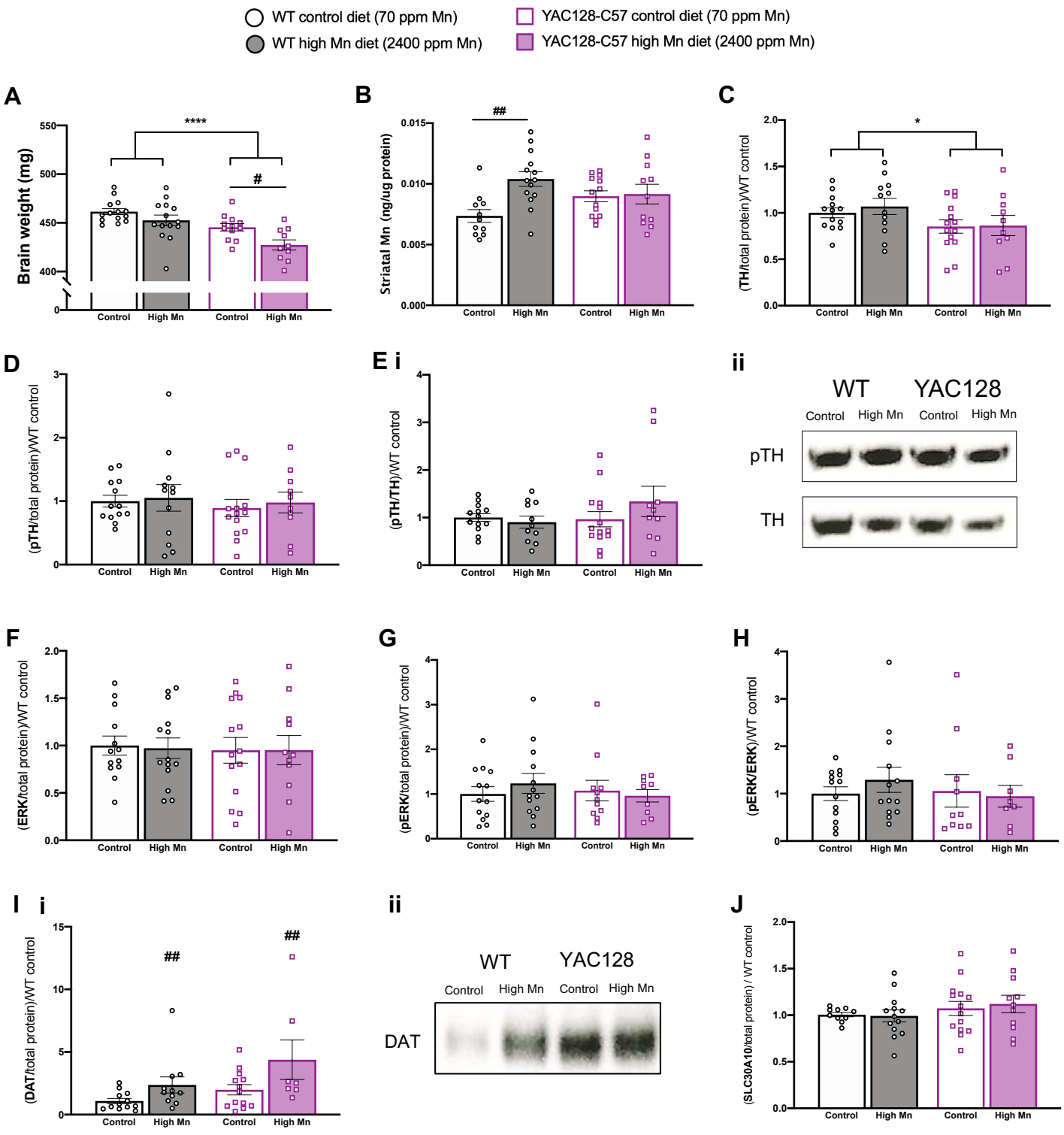
WT control diet (70 ppm Mn)
WT high Mn diet (2400 ppm Mn)
YAC128-C57 control diet (70 ppm Mn)
YAC128-C57 high Mn diet (2400 ppm Mn)
A
Brain weight (mg)
****
#
B
Striatal Mn (ng/ug protein)
##
C
(TH/total protein)/WT control
*
D
(pTH/total protein)/WT control
E i
(pTH/TH)/WT control
ii
WT
YAC128
Control
High Mn
pTH
TH
F
(ERK/total protein)/WT control
G
(pERK/total protein)/WT control
H
(pERK/ERK)/WT control
I i
(DAT/total protein)/WT control
##
ii
DAT
J
(SLC30A10/total protein) / WT control
Control
High Mn

Figure 4.4 Post-dissection outcomes from aged mice. **(A)** Brain weight was significantly lower in YAC128 mice compared to WT and decreased in mice on high Mn diet mice compared to those on control diet. Males and females combined due to lack of behavior and body weight differences. **(B)** Striatal Mn concentration was significantly increased in WT mice but not YAC128. **(C)** TH expression was lower in YAC128 compared to WT with no effect of diet. **(D)** There were no differences in pTH Ser 31 nor **(E)** (i) the pTH/TH ratio among genotype and diet groups. (ii) Representative blots for pTH and TH. **(F)** Total ERK, **(G)** pERK expression and **(H)** pERK/ERK ratio were not different between genotype nor diet groups. **(I)** (i) DAT expression was increased in groups on high Mn diet. ## indicates a main effect. (ii) Representative blot image for DAT. **(J)** There were no differences in SLC30A10 expression.

For all, mean ± SEM plotted unless otherwise noted. Asterisks * indicate genotype effect, pound # indicates a Mn effect. *p<0.05, **p<0.01, ****p<0.0001

4.4.11 DAergic synthesis proteins were unaffected but DAT was increased by high Mn diet in aged mice

TH was decreased in YAC128 mice compared to WT at 14.5 months, but Mn diet did not affect TH expression at this age (Genotype $F_{1,45}$= 4.947, P=0.0312) (**Fig. 4.4 C**). Expression of pTH (**Fig. 4.4 D**) and the pTH/TH ratio (**Fig. 4.4 E**) were not significantly different in YAC128 mice compared to WT and there were no effects of Mn diet (all Ps > 0.05). There were no differences in upstream protein ERK in its total expression (**Fig. 4.4 F**), phosphorylated expression (**Fig. 4.4 G**) nor the pERK/ERK ratio (**Fig. 4.4 H**) between genotype and Mn diet groups (all Ps > 0.05).

DAT expression was increased by high Mn diet in both genotypes (Diet $F_{1,39}$= 7.389, P=0.0098) (**Fig. 4.4 I**). SLC30A10 expression did not differ between YAC128 and WT and was not affected by Mn diet (all Ps > 0.05) (**Fig. 4.4 J**).

4.5 Discussion

The present study demonstrated that age, sex, and HD collectively affect Mn homeostasis; each of these variables influenced changes in behavior and the DAergic system as a result of excessive dietary Mn intake. We hypothesized that in young mice, high Mn diet would cause adverse effects in WT and prevent HD-phenotypes in YAC128. Our results examining locomotor behavior in young females support this hypothesized interaction. High Mn diet induced hyperactivity in two independent behavioral tasks in young WT females but not males (**Fig. 4.1 D and 4.1 E**). Regulation of locomotor activity is dependent on basal ganglia structures including striatum (Ortiz-Pulido et al., 2017) and DA is an important modulator of activity. Intranasal DA administration in C57Bl/6J (the background used here) is known to increase distance travelled in the open field and increase exploratory behavior in the elevated plus maze, with greater effects at lower DA doses (Kholodar, Amikishieva, & Anisimov, 2013). DA concentrations in striatum were not measured in the current study, but changes in the DAergic system were investigated by western blot. We identified increased TH, the rate-limiting enzyme in DA synthesis, in young female WT mice on high Mn diet (**Fig. 4.3 E ii**). We did not observe increased pTH Ser 31, the active form of this enzyme, in these mice.

Although we report no changes in pTH or its upstream kinase ERK1/2, the hyperactive behavioral phenotype observed is consistent with behavioral outcomes in children exposed to Mn. Several studies have made associations between elevated peripheral Mn (blood and hair concentrations) and ADHD (Farias et al., 2010; Shih et al., 2018). However, null associations and even decreased hair Mn concentrations have also been reported in ADHD groups compared to neurotypical children (Soler-Blasco et al., 2020; Tinkov et al., 2020). Interestingly, when examining associations between Mn exposure and ADHD, effects are stronger in females than males,

consistent with our results in the current study (Broberg et al., 2019; Farias et al., 2010). Increased prenatal exposure to Mn was also associated with poorer working memory and visuospatial ability in young girls and not boys, which highlights an age-specific window for increased sensitivity to detrimental effects from Mn exposure (Bauer et al., 2017).

We predicted high Mn diet in young YAC128 mice would prevent HD-behavioral phenotypes. Compared to WT, young female YAC128 mice on control diet travelled more in the EZM suggesting hyperactivity or increased exploratory behavior (**Fig. 4.1 D**). Hyperactivity in YAC128 mice at 3 months of age has been previously reported (Slow et al., 2003). Additionally, risk-taking behavior is common in individuals with HD (McDonell et al., 2020) and although not significant, young female YAC128 mice in the current study spent more time in the open zone of the EZM (**Fig. 4.1 C**) in addition to the significant increase in distance travelled (**Fig. 4.1 D**). Consistent with our behavioral findings and reports from others (Schwab et al., 2015), TH expression was increased in the striatum of these young YAC128 mice (**Fig. 4.3 C**). Hyperactivity and elevated TH expression were normalized to WT levels by the high Mn diet, rescuing these HD-phenotypes. We sought to determine if high Mn diet could prevent motor coordination deficits in HD, but we did not detect an impairment in the control diet YAC128 mice at this age (11 weeks). We have previously reported significant motor coordination deficits in YAC128 mice at this age (**Chapter 3,** *sections 3.4.2.1* and *3.4.4.1*) but those studies were performed using YAC128 mice on the FVB/N background whereas the current study used C57Bl/6J-YAC128 mice. Phenotypic severity is greater in YAC128 mice on the FVB/N background compared to C57Bl/6J (Jeremy M. Van Raamsdonk, Metzler, et al., 2007). No HD-behavioral phenotypes were present in young males, but TH expression was decreased in young YAC128 males on control diet compared to WT (**Fig. 4.1 C**) and the high Mn diet rescued this phenotype in males. TH expression in YAC128 mice was differentially altered between sexes, but high Mn diet corrected the phenotype in both sexes.

Females are more efficient at absorbing Mn than males (Finley et al., 1994). Our behavioral findings in young mice further support this sex difference despite comparable increases in brain Mn between sexes (**Fig. 4.3 B**). The mechanism responsible for the male-female difference in sensitivity to Mn toxicity is currently unknown. A recent study examining polymorphisms in the Mn transporters SLC30A10 and SLC39A8 suggests females are "genetically less efficient at regulating Mn" and polymorphisms in homeostatic proteins may underly this increased susceptibility to adverse outcomes following exposure (Broberg et al., 2019). Gut microbe differences between males and females may also explain these sex differences. In C57Bl/6J mice, Mn exposure in drinking water (100 ppm for 13 weeks) was shown to differentially alter the gut microbiome and the gut-brain axis in a sex-specific manner with greater effects in females. A bi-directional relationship between Mn and gut microbiota was proposed such that Mn effects the microbiome composition, but the microbiota influence the sex sensitivity to Mn toxicity (Chi et al., 2017).

In aged mice, there were no significant sex differences in our behavioral measurements in relation to Mn diet or genotype. Further, we did not observe detrimental behavioral outcomes following high Mn diet in the aged mice despite a significant increase in striatal Mn in WT (**Fig. 4.4 B**). Striatal Mn was not increased by high Mn diet in YAC128 mice. We have previously reported a Mn accumulation defect in HD cells (K. K. Kumar et al., 2015) and in YAC128 mice after acute subcutaneous injection (Pfalzer et al., 2020) (see also Chapter 2, *section 2.5.1*), but this is the first report of a striatal Mn uptake deficit in YAC128 mice fed a high Mn diet.

The lack of adverse behavioral outcomes following high Mn diet in the aged mice was somewhat surprising, especially given the significant increase in striatal Mn. Further, striatal DAT expression was the only molecular outcome examined in the current study that was affected by high Mn diet in aged mice. DAT expression was increased in both WT and YAC128 mice fed high Mn diet (**Fig. 4.4 I**). Inhalation of $MnSO_4$ increased DAT in non-human primates and was hypothesized to be a compensatory upregulation due to the ability for Mn to block DAT (M. K. Chen et al., 2006). DAT can also transport Mn into the cell, therefore increased DAT in response to Mn exposure can exacerbate toxicity (Keith M. Erikson, John, Jones, & Aschner, 2005). Interestingly, one study investigating associations between Mn and ADHD found that blood Mn was higher in ADHD children compared to neurotypical children and that elevated blood Mn was significantly decreased in children following methylphenidate (DAT and norepinephrine transporter inhibitor) treatment (Farias et al., 2010).

Consistent with our original hypothesis, HD phenotypes were not ameliorated in aged YAC128 mice fed a high Mn diet. The corrective effect observed in young YAC128 females on high Mn diet suggests early intervention is crucial and is influenced by sex. Future studies are needed investigating the HD-Mn interaction at earlier developmental timepoints. The current study contributes to the growing body of research examining Mn homeostasis across age, sex and disease states. The data suggest there may be a more subtle or transient change, such as dynamic changes in DA signaling, that underlie the mechanism of the Mn-HD interaction. This question is addressed in **Chapter 5.**

Chapter 5

Manganese Differentially Regulates Dopaminergic Dynamics and Striatal Glutamate Concentration in YAC128 mice

5.1 Abstract

Manganese (Mn) impacts several neurotransmitter systems which may contribute to the neurotoxicity of excessive Mn exposures. Genetic factors, including the autosomal dominant mutation that causes Huntington's Disease (HD), influence vulnerability to Mn toxicity. To better understand the differential effects of Mn in wild-type (WT) versus YAC128 HD model mice, we examined impacts of acute Mn exposure on dopamine (DA) dynamics and concentrations of biogenic amines and glutamate. Eight-month-old WT and YAC128 mice received three subcutaneous injections of 50 mg/kg $MnCl_2 \bullet 4(H_2O)$ or saline over one week followed by fast-scan cyclic voltammetry (FSCV) *ex vivo* recordings in nucleus accumbens or mass spectrometry of neurotransmitter concentrations. In WT mice, Mn exposure led to faster DA clearance that resembled saline treated YAC128 mice. Mn treatment increased DA release only in YAC128 mice, possibly indirectly correcting the faster DA clearance observed in saline treated YAC128 mice. Total striatal tissue DA concentration was decreased by Mn in WT but not YAC128 mice. Glutamate was lower in YAC128 vehicle mice compared to WT vehicle and was increased by Mn only in YAC128 to similar levels as WT vehicle. Serotonin (5-HT) was decreased by Mn in both genotypes and there were no significant changes in norepinephrine (NE). These studies support a role for Mn exposure in stabilizing dopaminergic dysfunction and abnormal glutamate concentrations in HD.

5.2 Introduction

Several neuronal and glial processes are disrupted following excess manganese (Mn) exposure but the specific mechanisms underlying Mn neurotoxicity are not well understood. Increased production of reactive oxygen and nitrogen species has been implicated in Mn toxicity (Martinez-Finley, Gavin, Aschner, & Gunter, 2013; M. D. Neely, Davison, Aschner, & Bowman, 2017). Mitochondrial dysfunction has also been described, but reports as to whether this induces or is a consequence of Mn toxicity are inconsistent (Fernandes et al., 2017; Warren et al., 2020). Elevated neuroinflammation due to microglial release of proinflammatory cytokines is also hypothesized to play a role in Mn toxicity (Kirkley, Popichak, Afzali, Legare, & Tjalkens, 2017). Mn-induced cellular apoptosis driven by each of these affected pathways – increased oxidative stress (Kitazawa, Wagner, Kirby, Anantharam, & Kanthasamy, 2002), mitochondrial dysfunction (Yang et al., 2019) and neuroinflammation

(Wang et al., 2017) – have been reported. Beyond cell death, Mn impacts neurological function by altering several neurotransmitter systems (Balachandran et al., 2020).

Mn is capable of affecting nearly every major small molecule neurotransmitter system through oxidative stress pathways, changes in transporter expression, or enzymatic activity (Balachandran et al., 2020). Tissue concentrations of glutamate and gamma-aminobutyric acid (GABA) have been changed by Mn exposure. Mn concentration (low versus high exposures) influenced whether these changes were observed as an increase or decrease in the two amino acid neurotransmitters (Keith M. Erikson & Aschner, 2003). Both acute (two days) and chronic (up to 60 days) Mn exposure decreased acetylcholinesterase (AChE) activity in rats (Yousefi Babadi, Sadeghi, Shirani, Malekirad, & Rezaei, 2014). Excess Mn exposure during the early postnatal period in rats also altered signaling of several biogenic amines in adulthood (dopamine (DA), norepinephrine (NE), serotonin (5-HT) (Lasley et al., 2020)). The glutamatergic, GABAergic and dopaminergic (DAergic) systems have been at the forefront of Mn neurotoxicity research given the selective accumulation of Mn in basal ganglia structures and the movement disorders that occur following excess exposure (Fitsanakis, Au, Erikson, & Aschner, 2006; Robison, Sullivan, Cannon, & Pushkar, 2015).

Both DAergic and glutamatergic signaling are disrupted in the inherited progressive neurodegenerative disorder Huntington's Disease (HD) (André, Cepeda, & Levine, 2010; Joshi et al., 2009). Animal and cell models of HD are resistant to Mn toxicity and display blunted responses to both acute and chronic Mn exposures (Pfalzer et al., 2020; Williams, Li, et al., 2010). The molecular mechanisms responsible for this neuroprotective effect against Mn toxicity are unclear but may involve differences in DA and glutamate neurotransmission present in HD. Additionally, Mn may offer therapeutic effects for the disruptions in these two neurotransmitter systems in HD. We previously demonstrated that abnormal expression of DAergic proteins (tyrosine hydroxylase) and an associated HD phenotype (hyperactivity) in young female YAC128 mice were corrected by high Mn diet (**Chapter 4,** *section 4.4.9*, p. 83).

In the present study, we sought to further examine the HD-Mn interaction by probing *ex vivo* DAergic dynamics and striatal tissue neurotransmitter metabolism following acute (1-week) *in vivo* Mn exposure. We maintained our longstanding hypothesis that Mn would induce detrimental effects in WT but not YAC128, and HD-relevant phenotypes would be rescued by Mn exposure.

5.3 Methods

5.3.1 Animals

Animal husbandry and genotyping has been previously described in **Chapter 2**. The current study used YAC128 mice backcrossed onto the C57BL/6J background (YAC128-C57) and their wild-type (WT) littermates as in **Chapter 4.** Mice were weaned at 21 days and housed in groups of 3-5 of a single sex in a temperature- and

humidity-controlled housing room on a 12:12 light:dark cycle with food and water available *ad libitum.* Approximately equal numbers of male and female mice were used in each genotype-diet group. All protocols were approved by the Vanderbilt University Institutional Animal Care and Use Committee under protocol numbers M1600073 and M1900090. All experiments were conducted in accordance with the NIH Guide for the Care and Use of Laboratory Animals.

5.3.2 Manganese exposure

Manganese chloride tetrahydrate ($MnCl_2 \cdot 4(H_2O)$, Fisher Scientific) was made up in DI water as a 1% stock solution, filtered through a 0.2 μm membrane, and administered as 50 mg/kg body weight. Saline (0.9%) was used as vehicle. Treatment was administered at a volume of 5 mL/kg injected subcutaneously in the left or right (alternating) inguinal area using an insulin syringe (27 G, ½ inch). A 50 mg/kg $MnCl_2 \cdot 4(H_2O)$ corresponds to a dose of 13.8 mg/kg Mn^{2+}.

Mice were exposed acutely (1-week exposure) at 8-9 months of age using a previously adapted exposure paradigm (Dodd et al., 2005) (also employed in **Chapter 2**). Mice were injected on days 1, 4, and 7 prior to sacrifice and FSCV (**Fig. 5.1 A**) or dissection (**Fig. 5.2 A**) on day 8 (24 hours after the final injection). Data in Figures 1 and 2 come from different animals.

5.3.3 Fast-scan cyclic voltammetry (FSCV)

FSCV was performed as previously described (Consoli, Brady, Bowman, Calipari, & Harrison, 2020). Briefly, mice were sacrificed by decapitation without anesthesia. The whole brain was removed and placed into cold-oxygenated artificial cerebral spinal fluid (aCSF) with 126 mM NaCl, 2.5 mM KCl, 1.2 mM NaH_2PO_4, 2.4 mM $CaCl_2$, 1.2 mM $MgCl_2$, 25 mM $NaHCO_3$, 0.4 mM ascorbate, and 11 mM glucose with pH adjusted to 7.4. Using a vibratome, 300 μM thick coronal sections were taken and allowed to equilibrate for 30 min at room temperature (22 ºC) in a holding chamber containing oxygenated aCSF. Sections were moved to a testing chamber containing aCSF at 32 ºC. Extracellular DA was measured in the core of the nucleus accumbens using a cylindrical carbon fiber microelectrode and a bipolar stimulating electrode (**Fig. 5.1 A**). Voltammetry data were collected and modeled using Demon Voltammetry and Analysis Software.

5.3.4 Neurotransmitter and metabolite measurements

Mice were briefly anesthetized with isoflurane before cervical dislocation and decapitation. The brain was removed, sliced coronally on a 1-mm mouse brain matrix, a small tissue punch containing dorsal striatum was removed, flash frozen on dry ice and stored at -80 ºC until all samples were collected. Glutamate, biogenic amines and major metabolites were measured by mass spectrometry by the Vanderbilt University Neurochemistry Core.

5.3.5 Statistics

Data are reported as mean ± S.E.M. Data analyses were completed in GraphPad Prism 8. Neurotransmitter and metabolite concentrations (**Fig. 5.2**) were first run with sex as a fixed variable. There were no differences according to sex, and thus all data were collapsed and analyzed together. FSCV data were not sufficiently powered to include sex as a variable (n=3-4 mice per group). For all dependent variables, two-way univariate ANOVA (2 genotype x 2 treatments) was conducted with appropriate post-hoc follow up tests. Outliers were removed if outside of 95% confidence interval.

5.4 Results

5.4.1 Mn differentially affected DA clearance and release in WT and YAC128 mice

Ex vivo FSCV was used to measure DA clearance and release in WT and YAC128 mice acutely exposed (3 injections over 1 week) to 50 mg/kg $MnCl_2 \cdot 4(H_2O)$, a dose known to significantly increase striatal Mn concentrations as shown in **Chapter 2** (Fig. 2.1 A) (Dodd et al., 2005; Pfalzer et al., 2020), or vehicle. DA release is measured by peak current (nA) (**Fig. 5.1 B**). Mn did not change DA release in WT Mn-exposed mice (Interaction $F_{1,86}$=12.07, P<0.0001, P=0.812 post-hoc Sidak's) but significantly increased DA release in YAC128 (post-hoc Sidak's P<0.0001) (Genotype $F_{1,86}$=27.09, P<0.0001, Treatment $F_{1,86}$=18.56, P<0.0001). Decay time is indicated by Tau (s). Shorter decay time indicates more rapid clearance of extracellular DA. Decay time was significantly shorter in WT Mn-exposed mice compared to WT vehicle (Interaction $F_{1,84}$=30.23, P<0.0001, post-hoc Sidak's P<0.0001) (**Fig. 5.1 C**). Thus, Mn exposure effectively decreased the amount of available DA in the synapse of WT mice because DA release was not altered but clearance was increased.

DA was more rapidly cleared in YAC128 mice compared to WT (Genotype $F_{1,84}$=48.54, P<0.0001) (**Fig. 5.1 C**). Mn exposure did not alter DA clearance in YAC128 mice, but because DA release was increased by Mn exposure (**Fig. 5.1 B**), the net effect is a potential indirect correction of the observed increase in clearance, therefore stabilizing the availability of DA in the synapse.

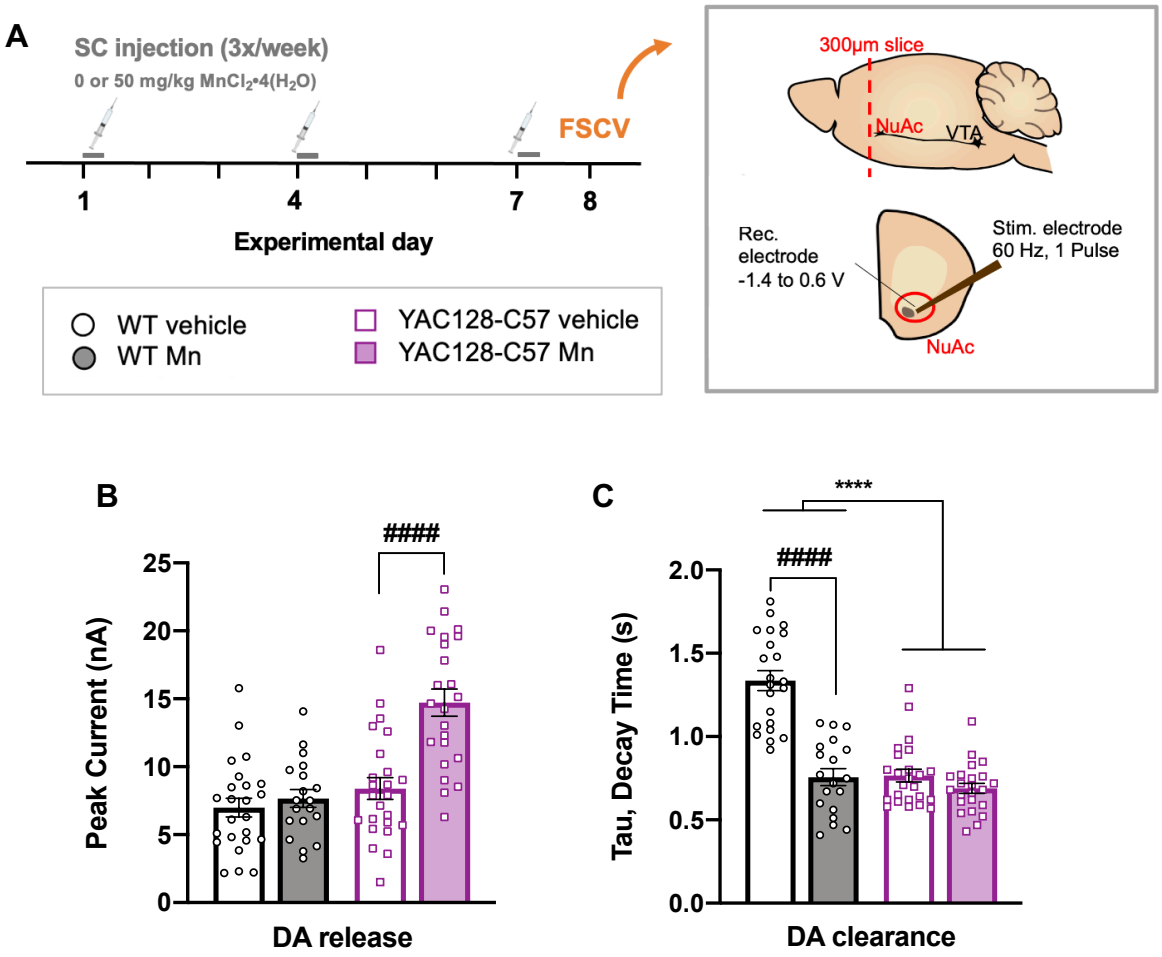

Figure 5.1 **(A)** Experimental timeline. Male and female mice (8-9 months of age) were injected with either vehicle or 50 mg/kg $MnCl_2 \cdot 4(H_2O)$ and fast-scan cyclic voltammetry (FSCV) was performed approximately 24 hours after the final injection. Inset image adapted from Consoli *et al*., 2020. NuAc, nucleus accumbens; VTA, ventral tegmental area. **(B)** Mn did not change DA release in WT but significantly increased DA release in YAC128, indicated by #### by post-hoc multiple comparisons. **(C)** DA clearance as indicated by decay time. Mn increased the rate of DA clearance (decreased tau) in WT mice. Clearance was significantly more rapid in YAC128 mice compared to WT with no effect of Mn. Asterisks **** indicate a main effect of genotype, pound #### indicates a Mn treatment effect within WT by post-hoc Sidak's multiple comparisons. Mean ± SEM plotted. Asterisks * indicate genotype effect, pound # indicates Mn effect within genotype. n=3-4 mice per group. ****p<0.0001, ####p<0.0001

5.4.2 Striatal DA metabolism was differentially altered by Mn in WT and YAC128 mice

DA and its three major metabolites, 3-methoxytyramine (3-MT), homovanillic acid (HVA), and 3,4-dihydroxyphenylacetic acid (DOPAC) were measured from dorsal striatal tissue from WT and YAC128 mice acutely (1-week) exposed to Mn or vehicle (**Fig. 5.2 A**). DA tissue concentrations were significantly decreased by Mn (Genotype $F_{1,26}$=0.5410, P=0.4686, Treatment $F_{1,26}$=4.786, P=0.0379, Interaction $F_{1,26}$=3.312, P=0.0885) (**Fig. 5.2 B i**). The main effect of treatment on DA concentration appears to be driven by the response observed in WT and not YAC128 mice but the interaction did not reach statistical significance. Tissue concentrations of 3-MT were significantly decreased in WT Mn-exposed mice compared to vehicle (P=0.0044) but not in YAC128 mice (Genotype $F_{1,26}$=2.531, P=0.1237, Treatment $F_{1,26}$=5.148, P=0.0318, Interaction $F_{1,26}$=7.654, P=0.0103) (**Fig. 5.2 B ii**). HVA was increased in YAC128 mice with no effect of Mn exposure in either genotype (Genotype $F_{1,27}$=5.558, P=0.0259, Treatment $F_{1,27}$=0.2285, P=0.6365, Interaction $F_{1,27}$=0.8685, P=0.3596) (**Fig. 5.2 B iii**). DOPAC concentration was not significantly affected by either genotype or Mn exposure (Genotype $F_{1,27}$=0.3854, P=0.5399, Treatment $F_{1,27}$=1.300, P=0.2643, Interaction $F_{1,27}$=0.8383, P=0.3680) (**Fig. 5.2 B iv**).

5.4.3 Mn decreased 5-HT and 5-HIAA but did not change norepinephrine (NE) concentration in striatum

Mn exposure decreased striatal tissue concentration of 5-HT regardless of genotype (Genotype $F_{1,28}$=2.401, P=0.1324, Treatment $F_{1,28}$=6.101, P=0.0199, Interaction $F_{1,28}$=0.0450, P=0.8335) (**Fig. 5.2 C i**). Major metabolite 5-HIAA was increased overall in YAC128 compared to WT, but Mn exposure decreased 5-HIAA concentrations in both genotypes (Genotype $F_{1,28}$=7.004, P=0.0132, Treatment $F_{1,28}$=6.741, P=0.0148, Interaction $F_{1,27}$=0.2127, P=0.6482) (**Fig. 5.2 C ii**). There were no significant differences in norepinephrine (NE) concentration (Genotype $F_{1,26}$=0.0043, P=0.9479, Treatment $F_{1,26}$=0.2567, P=0.6167, Interaction $F_{1,26}$=1.944, P=0.1751) (**Fig. 5.2 D**).

5.4.4 Decreased striatal glutamate concentration was corrected in Mn-exposed YAC128 mice

Tissue glutamate concentration was significantly lower in YAC128 vehicle mice compared to WT vehicle (P=0.0249). Glutamate was increased in Mn-exposed YAC128 mice compared to YAC128 vehicle (P=0.032) and not significantly different from WT vehicle (P=0.996) (Genotype $F_{1,31}$=1.361, P=0.2523, Treatment $F_{1,31}$=0.7788, P=0.3843, Interaction $F_{1,31}$=07.489, P=0.0102) (**Fig. 5.2 E**).

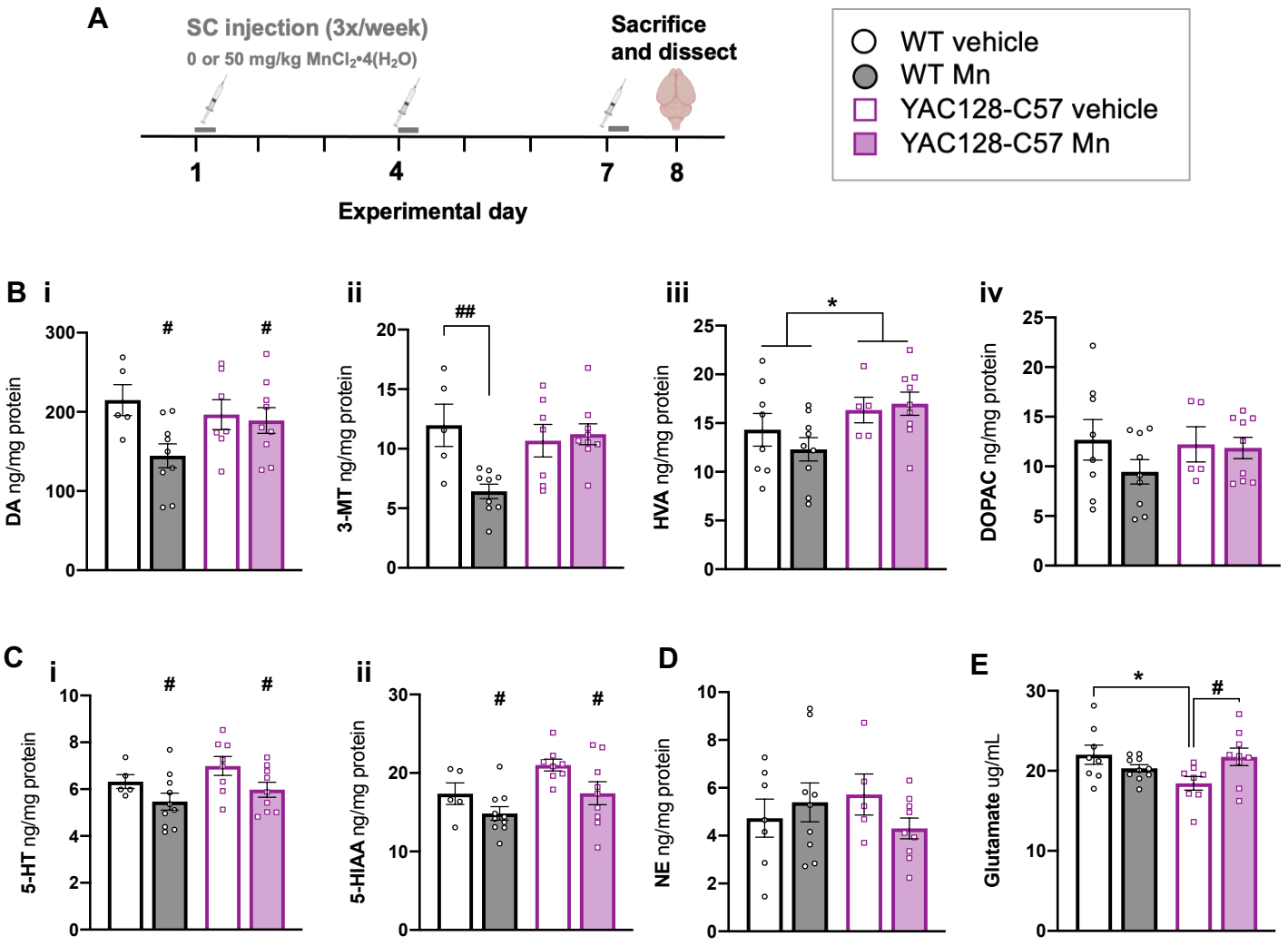

Figure 5.2 **(A)** Experimental timeline. Male and female mice (8-9 months of age) were injected with either vehicle or 50 mg/kg $MnCl_2 \cdot 4(H_2O)$ and euthanized 24 hours following the final injection. Neurotransmitter and metabolite measurements are from dorsal striatum. **(B)** Mn exposure decreased (i) DA, # indicates a main effect. Mn exposure decreased (ii) 3-MT in WT only, # indicates post-hoc Sidak's. (iii) HVA was increased in YAC128 mice (main effect) and there were no significant differences in (iv) DOPAC. **(C)** (i) 5-HT and its metabolite (ii) 5-HIAA were decreased in both genotypes by Mn exposure. Pound # indicates main effect. **(D)** NE levels were not significantly different. **(E)** Glutamate was significantly lower in YAC128 vehicle mice compared to WT vehicle. Mn exposure increased glutamate in YAC128 to levels not significantly different from WT vehicle (* and # by post-hoc Sidak's). For all, mean ± SEM plotted. Asterisks * indicate genotype effect, pound # indicates Mn effect. n=5-10 mice per group. */#p<0.05, ##p<0.01

5.5 Discussion

These experiments illustrate that in striatal tissue, the differential response to Mn in WT and YAC128 mice is clearly observed in DAergic and glutamatergic neurotransmitter systems. YAC128 vehicle mice in the current study exhibited increased DA clearance from the synapse (**Fig. 5.1 C**) but similar DA release compared to WT vehicle (**Fig. 5.1 B**), effectively decreasing the available DA in the synapse. Total DA tissue concentration was not significantly altered but major metabolite HVA was significantly increased in YAC128 mice regardless of Mn treatment (**Fig. 5.2 B**) suggesting increased DAergic activity. In a group of HD patients, plasma HVA levels were not altered in pre-symptomatic individuals with the genetic mutation for HD, but were significantly elevated in symptomatic individuals and were correlated with disease severity (Markianos, Panas, Kalfakis, & Vassilopoulos, 2009). Plasma HVA levels differed dependent on disease stage. In fact, many of the perturbations in the DAergic system in HD exhibit a biphasic pattern of dysfunction (Koch & Raymond, 2019). In pre-symptomatic and early-stage HD, DA levels are increased and contribute to presence of characteristic choreatic movements. Tyrosine hydroxylase (TH) levels and enzymatic activity are increased in early HD and perhaps as a compensatory mechanism, D1 and D2 receptors are reduced in early HD. In late-stage HD, the opposite trends are observed such that DA levels are decreased, TH levels and activity are reduced, but D1 and D2 receptor levels remain decreased (Koch & Raymond, 2019). Our YAC128 FSCV experimental results are consistent with symptomatic HD, given the decreased availability of DA in the synapse despite no changes in total DA concentration. This is to be expected based on the age of these animals (8-9 months) (Jeremy M. Van Raamsdonk, Metzler, et al., 2007). Mn treatment increased DA release in YAC128 mice, potentially stabilizing the available DA in the synapse given that clearance was unaffected in YAC128 mice (**Fig. 5.1 B and 5.1 C**). However, Mn treatment did not change concentration of DA or its metabolites in YAC128 mice (**Fig. 5.2 B**).

In WT, Mn decreased the availability of DA in the synapse by increasing DA clearance but not affecting DA release (**Fig. 5.1 C and 5.1 B**). Total DA concentration and metabolite 3-MT were significantly lower in WT Mn-exposed mice than in WT vehicle. Reports on Mn-induced DA changes are inconclusive. A microdialysis study in rats found decreased DA release in the striatum after intrastriatal administration of $MnCl_2$ (Vidal et al., 2005). The functional outcome (less DA in the synapse) is consistent with more rapid clearance detected in our Mn-treated WT mice. Another study employing the same acute Mn exposure paradigm used here observed no effect of Mn on DA clearance but instead found that Mn decreased DA release (Khalid, Aoun, & Mathews, 2011). DA can also be directly oxidized by Mn (Florence & Stauber, 1989). However, Mn can also increase spontaneous firing of DA neurons (M. Lin et al., 2019) and increase the binding of striatal vesicular monoamine transporter 2 (VMAT2) (Nguyen et al., 2003) thus potentially increasing DA in the synapse. Importantly, Mn altered DA clearance and tissue DA concentration and 3-MT concentration in WT but not YAC128 mice.

We did not detect any significant changes in NE dependent on either genotype or Mn treatment (**Fig. 5.2 D**). Developmental exposure to Mn in rats differentially alters NE and associated transporters (Anderson et al., 2010) and changes can persist into adulthood (Lasley et al., 2020). It is possible we did not observe these effects on NE because the Mn exposure occurred well into adulthood and was an acute exposure. Mn decreased 5-HT and its major metabolite 5-HIAA in both WT and YAC128 mice (**Fig. 5.2 C**). Interestingly, this was the only neurotransmitter measured that Mn affected similarly in both genotypes. Chronic Mn exposure (8-12 weeks) studies also report decreased 5-HT in the striatum of WT mice (Nielsen, Larsen, Ladefoged, & Lam, 2017). In post-mortem HD brains and the CAG140 knock-in mouse model of HD, increased serotonin transporter levels have been identified suggesting a role for serotonin in the pathology of HD (He et al., 2019). YAC128 mice had significantly increased striatal 5-HIAA (**Fig. 5.2 C ii**) and the observed Mn-induced decrease may serve a therapeutic role.

Glutamate concentration was differentially altered by Mn between YAC128 and WT mice (**Fig. 5.2 E**). In WT mice, striatal glutamate was lower in Mn-exposed mice, but the effect was not significant. While not significant, these findings are consistent with decreased striatal glutamate following sub-chronic Mn exposure in rats (Nielsen et al., 2017). It has been proposed that at higher Mn doses glutamate concentrations are increased (Keith M. Erikson & Aschner, 2003). This may be related to decreased expression of glutamate transporters GLT-1 and GLAST (E. Lee, Karki, Johnson, Hong, & Aschner, 2017). In YAC128 mice, glutamate concentration was lower in vehicle treated mice compared to WT vehicle. Biphasic changes in glutamate have been reported in HD, similar to DA, such that increased glutamate is observed in early-stage and decreased glutamate is characteristic of late-stage HD. In YAC128 mice, Mn treatment increased glutamate concentration to a level that was not significantly different from WT vehicle.

Our results show Mn affected the DA, 5-HT and glutamate neurotransmitter systems. Mn altered 5-HT and its metabolite 5-HIAA similarly in both WT and YAC128 mice. However, DAergic and glutamatergic systems were differentially altered by Mn in YAC128 and WT mice. Aberrant DAergic dynamics were potentially corrected in YAC128 by Mn exposure but YAC128 mice did not exhibit the decreases in DA and its metabolites that occurred in WT. Additionally, opposite effects on glutamate concentration were identified between genotypes in response to Mn. Taken together, these findings suggest the differential status of the DA and glutamate systems in YAC128 may contribute to the decreased sensitivity to Mn toxicity and that any therapeutic effects of Mn in HD may act on these systems.

Chapter 6

Conclusions and Future Directions

6.1 Conclusions

Manganese (Mn) is an essential micronutrient required for diverse biological processes, with detrimental effects occurring in both states of deficiency and excess (Horning et al., 2015). Since the first report of Mn-induced neurological impairments in 1837, understanding both the underlying mechanisms and modifying factors of Mn neurotoxicity have been at the forefront of Mn research (Blanc, 2018). Published in 2010, the Bowman lab identified a disease-toxicant interaction between Huntington's Disease (HD) and Mn whereby mutant *Huntingtin (Htt)* conferred a selective resistance to Mn toxicity (Williams, Li, et al., 2010). Research in our lab has since focused on elucidating mechanisms of this neuroprotective effect against Mn toxicity and simultaneously investigating the potential for Mn to rescue several HD phenotypes. HD is a progressive neurodegenerative disease with no cure and current treatment focuses on alleviating symptoms without any influence on disease progression (Yero & Rey, 2008). Thus, identifying treatments with any degree of disease-modifying effects is critical. The overarching hypothesis throughout each of the studies previously described was that YAC128 mice would be protected against Mn-induced toxicity, and HD-related phenotypes would be rescued by this treatment. I was especially interested in the effects Mn exposure would have on behavioral outcomes in YAC128 mice given the translational impact this could have for individuals with HD. Considering all of my results, I conclude that under the experimental paradigms utilized Mn did not appear to offer any therapeutic potential as a treatment for HD. Nevertheless, these findings contribute to the larger body of research on Mn neurobiology.

The preceding experimental chapters convey data that support two remarkably consistent themes in support of the HD-Mn interaction.

1) YAC128 mice exposed to Mn were generally less responsive to Mn-induced changes and in *some* cases experienced mild rescue of HD-phenotypes.
2) Outcomes measured in wild-type (WT) mice exposed to Mn frequently resembled those of vehicle-treated YAC128 mice.

These themes emerged across several ages (3 to 14 months) and disease stages (pre-manifest and manifest), in both sexes, in mice of two different genetic backgrounds (FVB/N and C57Bl/6J) and following Mn exposure via two distinct routes of administration (dietary ingestion and subcutaneous injection). We observed these themes in

behavioral tasks, differential expression of genes, alterations in the metabolome, as well as by changes in protein expression, immunohistochemistry, and neurochemistry. A summary and discussion of key findings in support of these two themes is outlined below.

The underlying mechanisms of Mn neurotoxicity remain unknown but there is substantial evidence that HD confers resistance to this toxicity and HD cell and animal models exhibit decreased responsiveness to Mn (Tidball et al., 2014; Williams, Kwakye, et al., 2010; Williams, Li, et al., 2010). At pre-manifest stages (12 weeks old) YAC128 mice accumulate less striatal Mn than WT following acute subcutaneous Mn exposure (Bichell et al., 2017; Williams, Li, et al., 2010) (**Fig. 2.1 A**) and aged YAC128 mice on high Mn diet exhibit reduced striatal Mn uptake (**Fig. 4.4 B**). However, the differential response to Mn goes beyond a simple difference in uptake. Following chronic subcutaneous injection of several different Mn doses, brain Mn levels are increased to comparable levels in both genotypes (**Figs. 2.3 A**, **2.4 A**, **3.3 A**, and **3.6 C**) and after 8 weeks on high Mn diet, striatal Mn levels are increased similarly between genotypes in young mice (**Fig. 4.3 B**). Even with equivalent increases in striatal Mn, we observed differential responses in the metabolome, protein expression, neuronal counts, neurotransmitter metabolites, and behavior in YAC128 compared to WT.

In **Chapter 2**, we reported that following an acute Mn exposure paradigm there were significantly more differentially expressed genes in WT than in YAC128 mice. Only 50% of the differentially expressed genes were altered in both genotypes, with the remainder of differentially expressed genes unique to each genotype (**Fig. 2.1 D**). Interestingly, the transcriptome is differentially altered by physiological versus toxic levels of Mn (Fernandes et al., 2019) and we did observe reduced uptake in YAC128 mice at this age following this exposure. However, after the same acute exposure at a later disease stage/older age, as well as a chronic exposure, we report similar increases in striatal Mn and significant differences in differentially altered striatal metabolites in YAC128 mice compared to WT (**Figs. 2.3 D** and **2.4 D**). Additionally, the Mn exporter SLC30A10 was significantly upregulated in WT within 24 hours following a single exposure to Mn but not in YAC128 (**Fig. 2.2 B**). In addition to blunted responses in YAC128 mice, Mn exposure caused changes in WT that were characteristic of YAC128 untreated mice. For example, a single Mn injection decreased *Bdnf* gene expression and GLT-1 protein in WT mice, resembling the HD phenotype (Massaro et al., 2018; Stansfield et al., 2014) (Chapter 3, *section 3.4.5.3*).

In **Chapter 3**, subtle behavioral impairments were induced by chronic Mn exposure in WT and not YAC128 mice. Locomotor activity (**Fig. 3.2 L**) and exploratory behavior were decreased in WT chronic Mn-exposed mice (**Fig. 3.5 D**) but not YAC128 mice. Striatal NeuN positive cells were also decreased by chronic Mn exposure in WT mice but not YAC128, which already exhibited a decrease in striatal NeuN cells as a result of HD pathology **(Fig. 3.6 B**). Both hypoactivity and striatal neuron loss are late-stage HD phenotypes. These outcomes were induced by Mn in WT though not worsened in YAC128, suggesting independent mechanisms and altered pathways for these two Mn- and HD-induced impairments.

In **Chapter 4**, young YAC128 were hyperactive compared to WT. This phenotype has been previously reported by others (Jeremy M. Van Raamsdonk, Metzler, et al., 2007). However, young female YAC128 mice on high Mn diet did not display this hyperactive phenotype and were not significantly different from WT control (**Fig. 4.1 D**) suggesting attenuation of this early-HD phenotype. Conversely, young WT females on high Mn diet were hyperactive compared to WT controls, resembling the early-HD phenotype. Following the same pattern, elevated tyrosine hydroxylase (TH) in the young YAC128 females on control diet was not observed in young YAC128 females on high Mn diet and young female WT mice on high Mn diet showed increased TH compared to WT control diet (**Fig. 4.3 C**).

Finally in **Chapter 5**, Mn increased dopamine (DA) clearance but did not change DA release in WT and thus effectively decreased the available DA in the synapse of WT mice exposed to Mn, resembling the late-stage HD phenotype. However, DA release was increased in YAC128 mice following acute Mn exposure potentially indirectly correcting the observed increase in DA clearance in YAC128 vehicle mice, thereby stabilizing the availability of DA in the synapse (**Fig. 5.1**). Striatal glutamate concentration was decreased in vehicle YAC128 mice but was similar to WT levels in YAC128 Mn-exposed mice (**Fig. 5.2 E**).

The differential response to Mn exposures despite similar increases in brain Mn suggest a possible Mn handling impairment in YAC128 mice, perhaps manifested as altered cellular localization or compartmentalization of Mn. In several instances, YAC128 mice were less responsive to Mn compared to WT, but there were subtle examples of attenuated HD phenotypes. Interestingly, Mn exposure frequently led to HD-like phenotypes in WT.

6.2 Future Directions

While the studies described here contribute to our knowledge of an HD-Mn interaction, there is certainly more to investigate. Elucidating the mechanisms of the reduced Mn uptake phenotype (under certain but not all Mn exposure conditions) in HD should be a priority. However, this depends on independent advancements in both the Mn biology field and in the understanding of HD pathophysiology.

Specifically relevant to the work presented here, further studies on the role of DA in the HD-Mn interaction should be pursued. The few mild phenotypes ameliorated by Mn exposure in YAC128 mice were related to the DA system, and this is one hypothesized target of Mn toxicity as well as a primary neurotransmitter system affected in HD (Nyarko-Danquah et al., 2020; Schwab et al., 2015). Mn itself can enter a cell via the dopamine transporter (DAT) and toxic accumulation of striatal Mn is dependent on DAT (Keith M. Erikson et al., 2005). Alterations in the DA system in HD may underlie aspects of the HD-Mn interaction and should be further examined.

In **Chapter 4**, high Mn diet introduced at weaning induced hyperactivity by 12 weeks in female WT mice, but attenuated hyperactivity normally observed in female YAC128 mice on control diet. The high Mn diet was hypothesized to prevent or delay the rotarod deficit in YAC128 mice, but we were unable to determine this because the YAC128 control diet mice had not yet manifested a detectible motor impairment phenotype. Targeting earlier disease stages is critical as it is unknown if we were unable to rescue effects in older mice due to the severity of phenotypes or due to a critical window for Mn biology. Mn is crucial for development and deficiency during this period may contribute to HD phenotypes later in life. Additionally, younger individuals accumulate Mn more readily (J. A. Moreno et al., 2009), and HD models could take advantage of this. Whether the Mn uptake impairment is present in YAC128 mice before 12 weeks of age is currently unknown. Further investigation of early Mn intervention in YAC128 mice should take precedence in future HD-Mn interaction studies.

Interestingly, the attenuated hyperactivity in YAC128 mice on high Mn diet was present only in females (**Chapter 4**). As previously mentioned there are sex differences in Mn homeostasis, with females absorbing Mn more efficiently and showing increased sensitivity to Mn toxicity (Finley et al., 1994; Oulhote et al., 2014). One study concluded females are "genetically less efficient at regulating Mn" (Broberg et al., 2019). Interestingly, HD affects males and females at a similar rate, with comparable disease burden and age of onset, but once symptomatic females have been shown to progress more rapidly (Zielonka & Stawinska-Witoszynska, 2020). Similarly, phenotypes have been more severe in female HD mouse models in our studies (Pfalzer et al., 2019). There are also notable sex differences in DA metabolism in the striatum (putamen), with females exhibiting a higher DA turnover rate (indicated by lower DA and increased DOPAC) with no sex-specific differences in norepinephrine or serotonin metabolism (Konradi et al., 1992).

Taking these connections into consideration, future studies should examine sex-specific effects in the DA system following early-life (pre-natal and early post-natal) Mn exposure in WT and YAC128 mice. Whether a therapeutic effect of Mn in HD would be revealed in these future studies is unknown, but the results would certainly add to our understanding of Mn neurobiology. The impact of both Mn deficiency and toxicity on neurobiological processes and behavior are profound and worthy of continuing investigation.

References

A. Jablonski, F. Salvat, C. J. Powell, A. Y. L. (2016). *NIST Electron Elastic-Scattering Cross-Section Database Version 4.0, NIST Standard Reference Database Number 64*.

Alsulimani, H. H., Ye, Q., & Kim, J. (2015). Effect of Hfe deficiency on memory capacity and motor coordination after manganese exposure by drinking water in mice. *Toxicological Research*, *31*(4), 347–354. https://doi.org/10.5487/TR.2015.31.4.347

Anderson, J. G., Fordahl, S. C., Cooney, P. T., Weaver, T. L., Colyer, C. L., & Erikson, K. M. (2010). Extracellular Norepinephrine, Norepinephrine Receptor and Transporter Protein and mRNA Levels Are Differentially Altered in the Developing Rat Brain Due to Dietary Iron Deficiency and Manganese Exposure. *Brain Res*, *1281*, 1–14. https://doi.org/10.1016/j.brainres.2009.05.050.Extracellular

André, V. M., Cepeda, C., & Levine, M. S. (2010). Dopamine and glutamate in huntington's disease: A balancing act. *CNS Neuroscience and Therapeutics*, *16*(3), 163–178. https://doi.org/10.1111/j.1755-5949.2010.00134.x

Andrew, S. E., Goldberg, Y. P., Kremer, B., Telenius, H., Theilmann, J., Adam, S., … Hayden, M. R. (1993). The relationship between trinucleotide (CAG) repeat length and clinical features of Huntington's disease. *Nature Genetics*, *3*, 73–96. https://doi.org/10.1038/ng0293-165

Arning, L., & Epplen, J. T. (2012). Genetic modifiers of Huntington's disease: beyond CAG. *Future Neurology*, *7*(1), 93–109. https://doi.org/10.2217/fnl.11.65

Arning, L., Saft, C., Wieczorek, S., Andrich, J., Kraus, P. H., & Epplen, J. T. (2005). NR2A and NR2B receptor gene variations modify age at onset in Huntington disease. *Human Genetics*, *6*, 25–28. https://doi.org/10.1007/s00439-007-0393-4

Aronin, N., Chase, K., Young, C., Sapp, E., Schwarz, C., Matta, N., … Beal, M. F. (1995). CAG expansion affects the expression of mutant Huntingtin in the Huntington's disease brain. *Neuron*, *15*(5), 1193–1201. https://doi.org/10.1016/0896-6273(95)90106-X

Arrasate, M., & Finkbeiner, S. (2012). Protein aggregates in Huntington's disease. *Experimental Neurology*, *238*(1), 1–11. https://doi.org/10.1016/j.expneurol.2011.12.013

Arteaga-Bracho, E. E., Gulinello, M., Winchester, M. L., Pichamoorthy, N., Petronglo, J. R., Zambrano, A. D., … Molero, A. E. (2016). Postnatal and adult consequences of loss of huntingtin during development: Implications for Huntington's disease. *Neurobiology of Disease*, *96*, 144–155. https://doi.org/10.1016/j.nbd.2016.09.006

Aschner, J. L., & Aschner, M. (2005). Nutritional aspects of manganese homeostasis. *Molecular Aspects of Medicine*, *26*(4-5 SPEC. ISS.), 353–362. https://doi.org/10.1016/j.mam.2005.07.003

Aschner, M. (1999). Manganese Homeostasis in the CNS. *Environmental Research*, *80*(2), 105–109. https://doi.org/10.1006/ENRS.1998.3918

Asser, A., Kõks, S., Soomets, U., Terasmaa, A., Sauk, M., Eltermaa, M., … Taba, P. (2019). Acute effects of methcathinone and manganese in mice: A dose response study. *Heliyon*, *5*(9), e02475. https://doi.org/10.1016/j.heliyon.2019.e02475

ATSDR. (2012). Toxicological Profile for Manganese. *U.S. Department of Health and Human Services*. https://doi.org/10.1201/9781420061888_ch4

Avila-Costa, M. R., Gutierrez-Valdez, A. L., Anaya-Martínez, V., Ordoñez-Librado, J. L., Sanchez-Betancourt, J., Montiel-Flores, E., … Rodríguez-Lara, V. (2018). Manganese Inhalation Induces Dopaminergic Cell Loss: Relevance to Parkinson's Disease. *Dopamine - Health and Disease*. https://doi.org/10.5772/intechopen.79473

Avila-Costa, M. R., Ordoñez-Librado, J. L., Anaya-Martínez, V., Gutierrez-Valdez, A. L., Colín-Barenque, L., & Montiel-Flores, E. (2011). Manganese inhalation as a Parkinson disease model. *Parkinson's Disease*, *2011*, 1–14. https://doi.org/10.4061/2011/612989

Aydemir, T. B., Thorn, T. L., Ruggiero, C. H., Pompilus, M., Febo, M., & Cousins, R. J. (2020). Intestine-specific deletion of metal transporter Zip14 (Slc39a14) causes brain manganese overload and locomotor

defects of manganism. *American Journal of Physiology - Gastrointestinal and Liver Physiology*, *318*(4), G673–G681. https://doi.org/10.1152/ajpgi.00301.2019

Balachandran, R. C., Mukhopadhyay, S., McBride, D., Veevers, J., Harrison, F. E., Aschner, M., … Bowman, A. B. (2020). Brain manganese and the balance between essential roles and neurotoxicity. *Journal of Biological Chemistry*, *295*(19), 6312–6329. https://doi.org/10.1074/jbc.REV119.009453

Bano, D., Zanetti, F., Mende, Y., & Nicotera, P. (2011). Neurodegenerative processes in Huntington's disease. *Cell Death and Disease*, *2*(11), 1–7. https://doi.org/10.1038/cddis.2011.112

Bao, J., Sharp, a H., Wagster, M. V, Becher, M., Schilling, G., Ross, C. a, … Dawson, T. M. (1996). Expansion of polyglutamine repeat in huntingtin leads to abnormal protein interactions involving calmodulin. *Proceedings of the National Academy of Sciences of the United States of America*, *93*(10), 5037–5042. https://doi.org/10.1073/pnas.93.10.5037

Bates, G. P., Dorsey, R., Gusella, J. F., Hayden, M. R., Kay, C., Leavitt, B. R., … Tabrizi, S. J. (2015). Huntington disease. *Nature Reviews Disease Primers*, *1*(April), 1–21. https://doi.org/10.1038/nrdp.2015.5

Bauer, J. A., Claus Henn, B., Austin, C., Zoni, S., Fedrighi, C., Cagna, G., … Arora, M. (2017). Manganese in teeth and neurobehavior: Sex-specific windows of susceptibility. *Environment International*, *108*, 299–308. https://doi.org/https://doi.org/10.1016/j.envint.2017.08.013

Behrens, P. F., Franz, P., Woodman, B., Lindenberg, K. S., & Landwehrmeyer, G. B. (2002). Impaired glutamate transport and glutamate-glutamine cycling: downstream effects of the Huntington mutation. *Brain*, *125*, 1908–1922. https://doi.org/10.1093/brain/awf180

Benn, C. L., Sun, T., Sadri-Vakili, G., McFarland, K. N., DiRocco, D. P., Yohrling, G. J., … Cha, J.-H. J. (2008). Huntingtin Modulates Transcription, Occupies Gene Promoters In Vivo, and Binds Directly to DNA in a Polyglutamine-Dependent Manner. *Journal of Neuroscience*, *28*(42), 10720–10733. https://doi.org/10.1523/JNEUROSCI.2126-08.2008

Berggren, K. L., Chen, J., Fox, J. H. J., Miller, J., Dodds, L., Dugas, B., … Fox, J. H. J. (2015). Neonatal iron supplementation potentiates oxidative stress, energetic dysfunction and neurodegeneration in the R6/2 mouse model of Huntington's disease. *Redox Biology*, *4*, 363–374. https://doi.org/10.1016/j.redox.2015.02.002

Berggren, K. L., Lu, Z., Fox, J. A., Dudenhoeffer, M., & Agrawal, S. (2016). Neonatal Iron Supplementation Induces Striatal Atrophy in Female YAC128 Huntington's Disease Mice. *Journal of Huntington's Disease*, *5*, 53–63. https://doi.org/10.3233/JHD-150182

Bhang, S. Y., Cho, S. C., Kim, J. W., Hong, Y. C., Shin, M. S., Yoo, H. J., … Kim, B. N. (2013). Relationship between blood manganese levels and children's attention, cognition, behavior, and academic performance-A nationwide cross-sectional study. *Environmental Research*, *126*, 9–16. https://doi.org/10.1016/j.envres.2013.05.006

Bichell, T. J. V., Wegrzynowicz, M., Tipps, K. G., Bradley, E. M., Uhouse, M. A., Bryan, M., … Bowman, A. B. (2017). Reduced bioavailable manganese causes striatal urea cycle pathology in Huntington's disease mouse model. *Biochimica et Biophysica Acta - Molecular Basis of Disease*. https://doi.org/10.1016/j.bbadis.2017.02.013

Blanc, P. D. (2018). The early history of manganese and the recognition of its neurotoxicity, 1837-1936. *Neurotoxicology*, *64*, 5–11. https://doi.org/10.1016/j.neuro.2017.04.006

Bosomworth, H. J., Thornton, J. K., Coneyworth, L. J., Ford, D., & Valentine, R. A. (2012). Efflux function, tissue-specific expression and intracellular trafficking of the Zn transporter ZnT10 indicate roles in adult Zn homeostasis. *Metallomics*, *4*(8), 771–779. https://doi.org/10.1039/c2mt20088k

Bouabid, S., Delaville, C., De Deurwaerdère, P., Lakhdar-Ghazal, N., & Benazzouz, A. (2014). Manganese-induced atypical parkinsonism is associated with altered basal ganglia activity and changes in tissue levels of monoamines in the rat. *PLoS ONE*, *9*(6). https://doi.org/10.1371/journal.pone.0098952

Bowman, A. B., Kwakye, G. F., Herrero Hernández, E., & Aschner, M. (2011). Role of manganese in neurodegenerative diseases. *Journal of Trace Elements in Medicine and Biology*, *25*(4), 191–203. https://doi.org/10.1016/j.jtemb.2011.08.144

Broberg, K., Taj, T., Guazzetti, S., Peli, M., Cagna, G., Pineda, D., … Wahlberg, K. (2019). Manganese

transporter genetics and sex modify the association between environmental manganese exposure and neurobehavioral outcomes in children. *Environment International*, *130*(March), 104908. https://doi.org/10.1016/j.envint.2019.104908

Brock, A. M. Y. A., Chapman, S. A., & Ãœlman, E. A. (1994). Dietary Manganese Deficiency Decreases Rat Hepatic Arginase Activity. *J. Nutr.*, (124), 340–344.

Brown, K. A., Didion, S. P., Andresen, J. J., & Faraci, F. M. (2007). Effect of aging, MnSOD deficiency, and genetic background on endothelial function: Evidence for MnSOD haploinsufficiency. *Arteriosclerosis, Thrombosis, and Vascular Biology*, *27*(9), 1941–1946. https://doi.org/10.1161/ATVBAHA.107.146852

Bryan, M. R., & Bowman, A. B. (2017). Manganese and the Insulin-IGF Signaling Network in Huntington's Disease and Other Neurodegenerative Disorders. *Advances in Neurobiology*, *18*, 113–142. https://doi.org/10.1007/978-3-319-60189-2_6

Bryan, M. R., Nordham, K. D., Rose, D. I. R., O'Brien, M. T., Joshi, P., Foshage, A. M., … Bowman, A. B. (2020). Manganese Acts upon Insulin/IGF Receptors to Phosphorylate AKT and Increase Glucose Uptake in Huntington's Disease Cells. *Molecular Neurobiology*, *57*(3), 1570–1593. https://doi.org/10.1007/s12035-019-01824-1

Bryan, M. R., O'brien, M. T., Nordham, K. D., Rose, D. I. R., Foshage, A. M., Joshi, P., … Bowman, A. B. (2019). Acute manganese treatment restores defective autophagic cargo loading in Huntington's disease cell lines. *Human Molecular Genetics*, *28*(22), 3825–3841. https://doi.org/10.1093/hmg/ddz209

Bryan, M. R., Uhouse, M. A., Nordham, K. D., Joshi, P., Rose, D. I. R., O'Brien, M. T., … Bowman, A. B. (2018). Phosphatidylinositol 3 kinase (PI3K) modulates manganese homeostasis and manganese-induced cell signaling in a murine striatal cell line. *NeuroToxicology*, *64*, 185–194. https://doi.org/https://doi.org/10.1016/j.neuro.2017.07.026

Butterworth, J. (1986). Changes in Nine Enzyme Markers for Neurons, Glia, and Endothelial Cells in Agonal State and Huntington's Disease Caudate Nucleus. *Journal of Neurochemistry*, *47*(2), 583–587. https://doi.org/10.1111/j.1471-4159.1986.tb04539.x

Carl, G. F., Keen, C. L., Gallagher, B. ., Clegg, M. S., Littleton, W. H., Flannery, D. B., & Hurley, L. S. (1986). Association of low blood manganese concentrations with epilepsy. *Neurology*, *36*, 1584–1587.

Carmona, A., Zogzas, C. E., Roudeau, S., Porcaro, F., Garrevoet, J., Spiers, K. M., … Ortega, R. (2019). SLC30A10 Mutation Involved in Parkinsonism Results in Manganese Accumulation within Nanovesicles of the Golgi Apparatus. *ACS Chemical Neuroscience*, *10*(1), 599–609. https://doi.org/10.1021/acschemneuro.8b00451

Carroll, J. B., Deik, A., Fossale, E., Weston, R. M., Guide, J. R., Arjomand, J., … MacDonald, M. E. (2015). HdhQ111 Mice Exhibit Tissue Specific Metabolite Profiles that Include Striatal Lipid Accumulation. *PLOS ONE*, *10*(8), e0134465. Retrieved from https://doi.org/10.1371/journal.pone.0134465

Carter, C. J. (1982). Glutamine synthetase activity in Huntington's Disease. *Life Sciences*, *31*, 1151–1159.

Carter, C. J. (1983). Glutamine synthetase and fructose-1, 6-diphosphatase activity in the putamen of control and Huntington's disease brain post mortem. *Life Sciences*, *32*, 1949–1955.

Cattaneo, E., Zuccato, C., & Tartari, M. (2005). Normal huntingtin function: An alternative approach to Huntington's disease. *Nature Reviews Neuroscience*, *6*(12), 919–930. https://doi.org/10.1038/nrn1806

Cersosimo, M. G., & Koller, W. C. (2006). The diagnosis of manganese-induced parkinsonism. *Neurotoxicology*, *27*(3), 340–346. https://doi.org/10.1016/j.neuro.2005.10.006

Chang, Y., Lee, J.-J., Seo, J.-H., Song, H.-J., Kim, J.-H., Bae, S.-J., … Kim, Y. (2010). Altered working memory process in the manganese-exposed brain. *NeuroImage*, *53*(4), 1279–1285. https://doi.org/10.1016/j.neuroimage.2010.07.001

Chaves, G., Özel, R. E., Rao, N. V., Hadiprodjo, H., Costa, Y. Da, Tokuno, Z., & Pourmand, N. (2017). Metabolic and transcriptomic analysis of Huntington's disease model reveal changes in intracellular glucose levels and related genes. *Heliyon*, *3*(8), 1–28. https://doi.org/10.1016/j.heliyon.2017.e00381

Chen, M. K., Lee, J. S., McGlothan, J. L., Furukawa, E., Adams, R. J., Alexander, M., … Guilarte, T. R. (2006). Acute manganese administration alters dopamine transporter levels in the non-human primate striatum. *NeuroToxicology*, *27*(2), 229–236. https://doi.org/10.1016/j.neuro.2005.10.008

Chen, P., Bornhorst, J., & Aschner, M. (2018). Manganese metabolism in humans. *Frontiers in Bioscience*, *23*, 1655–1679. https://doi.org/10.2741/4665
Chen, P., Bowman, A. B., Mukhopadhyay, S., & Aschner, M. (2015). SLC30A10: A novel manganese transporter. *Worm*, *3*(3).
Chen, P., Parmalee, N., & Aschner, M. (2014). Genetic factors and manganese-induced neurotoxicity. *Frontiers in Genetics*, *5*, 265. https://doi.org/10.3389/fgene.2014.00265
Chi, L., Gao, B., Bian, X., Tu, P., Ru, H., & Lu, K. (2017). Manganese-induced sex-specific gut microbiome perturbations in C57BL/6 mice. *Toxicology and Applied Pharmacology*, *331*, 142–153. https://doi.org/10.1016/j.taap.2017.06.008
Chiang, M. C., Chen, H. M., Lee, Y. H., Chang, H. H., Wu, Y. C., Soong, B. W., … Chern, Y. (2007). Dysregulation of C/EBPα by mutant Huntingtin causes the urea cycle deficiency in Huntington's disease. *Human Molecular Genetics*, *16*(5), 483–498. https://doi.org/10.1093/hmg/ddl481
Chua, A. C., & Morgan, E. H. (1996). Effects of iron deficiency and iron overload on manganese uptake and deposition in the brain and other organs of the rat. *Biological Trace Element Research*, *55*(1–2), 39–54. https://doi.org/10.1007/BF02784167
Cicero, C. E., Mostile, G., Vasta, R., Rapisarda, V., Signorelli, S. S., Ferrante, M., … Nicoletti, A. (2017). Metals and neurodegenerative diseases. A systematic review. *Environmental Research*, *159*, 82–94. https://doi.org/10.1016/j.envres.2017.07.048
Cisbani, G., & Cicchetti, F. (2012). An in vitro perspective on the molecular mechanisms underlying mutant huntingtin protein toxicity. *Cell Death and Disease*. https://doi.org/10.1038/cddis.2012.121
Clabough, E. B. D. (2013). Huntington's disease: The past, present, and future search for disease modifiers. *Yale Journal of Biology and Medicine*, *86*(2), 217–233. https://doi.org/10.1093/hmg/11.8.905
Clegg, M., Donovan, S., Monaco, M., Baly, D., Ensunsa, J., & Keen, C. (1998). The influence of manganese deficiency on serum IGF-1 and IGF binding proteins in the male rat. *Proc Soc Exp Biol Med*, *219*, 41–47.
Colin, E., Régulier, E., Perrin, V., Dürr, A., Brice, A., Aebischer, P., … Saudou, F. (2005). Akt is altered in an animal model of Huntington's disease and in patients. *European Journal of Neuroscience*, *21*(6), 1478–1488. https://doi.org/10.1111/j.1460-9568.2005.03985.x
Colin, E., Zala, D., Liot, G., Rangone, H., Borrell-Pagès, M., Li, X. J., … Humbert, S. (2008). Huntingtin phosphorylation acts as a molecular switch for anterograde/retrograde transport in neurons. *EMBO Journal*, *27*(15), 2124–2134. https://doi.org/10.1038/emboj.2008.133
Consoli, D. C., Brady, L. J., Bowman, A. B., Calipari, E. S., & Harrison, F. E. (2020). Ascorbate deficiency decreases dopamine release in gulo–/– and APP/PSEN1 mice. *Journal of Neurochemistry*, (June), 1–10. https://doi.org/10.1111/jnc.15151
Cordova, F. M., Aguiar, A. S., Peres, T. V., Lopes, M. W., Gonçalves, F. M., Remor, A. P., … Leal, R. B. (2012). In vivo manganese exposure modulates Erk, Akt and Darpp-32 in the striatum of developing rats, and impairs their motor function. *PLoS ONE*, *7*(3). https://doi.org/10.1371/journal.pone.0033057
Crossgrove, J. S., Allen, D. D., Bukaveckas, B. L., Rhineheimer, S. S., & Yokel, R. A. (2003). Manganese distribution across the blood-brain barrier. Evidence for carrier-mediated influx of manganese citrate as well as manganese and manganese transferrin. *NeuroToxicology*, *24*(1), 3–13. https://doi.org/10.1016/S0161-813X(02)00089-X
Davis, C. D., Zech, L., & Greger, J. L. (1993). Manganese Metabolism in Rats: An Improved Methodology for Assessing Gut Endogenous Losses. *Proceedings of the Society for Experimental Biology and Medicine*, *202*(1), 103–108. https://doi.org/10.3181/00379727-202-43518
De Bie, R. M. A., Gladstone, R. M., Strafella, A. P., Ko, J. H., & Lang, A. E. (2007). Manganese-induced parkinsonism associated with methcathinone (Ephedrone) abuse. *Archives of Neurology*, *64*(6), 886–889. https://doi.org/10.1001/archneur.64.6.886
Deacon, R. M. J. (2006). Assessing nest building in mice. *Nature Protocols*, *1*(3), 1117–1119. https://doi.org/10.1038/nprot.2006.170
Dlamini, W. W., Nelson, G., Nielsen, S. S., & Racette, B. A. (2020). Manganese exposure, parkinsonian signs, and quality of life in South African mine workers. *American Journal of Industrial Medicine*, *63*(1), 36–43.

https://doi.org/10.1002/ajim.23060
Dobson, A. W., Erikson, K. M., & Aschner, M. (2014). Manganese neurotoxicity. *Handbook of Neurotoxicity*, *2*, 843–864. https://doi.org/10.1007/978-1-4614-5836-4_3
Dodd, C. A., Ward, D. L., & Klein, B. G. (2005). Basal ganglia accumulation and motor assessment following manganese chloride exposure in the C57BL/6 mouse. *International Journal of Toxicology*, *24*(6), 389–397. https://doi.org/10.1080/10915810500366500
Dorman, D C, Struve, M. F., James, R. A., McManus, B. E., Marshall, M. W., & Wong, B. A. (2001). Influence of dietary manganese on the pharmacokinetics of inhaled manganese sulfate in male CD rats. *Toxicological Sciences : An Official Journal of the Society of Toxicology*, *60*(2), 242–251. https://doi.org/10.1093/toxsci/60.2.242
Dorman, David C, Struve, M. F., & Wong, B. A. (2002). Brain manganese concentrations in rats following manganese tetroxide inhalation are unaffected by dietary manganese intake. *Neurotoxicology*, *23*(2), 185–195. https://doi.org/10.1016/s0161-813x(01)00075-4
Du Montcel, S. T., Durr, A., Bauer, P., Figueroa, K. P., Ichikawa, Y., Brussino, A., … Stevanin, G. (2014). Modulation of the age at onset in spinocerebellar ataxia by CAG tracts in various genes. *Brain*, *137*(9), 2444–2455. https://doi.org/10.1093/brain/awu174
Duan, W., Guo, Z., Jiang, H., Ware, M., Li, X.-J. J., & Mattson, M. P. (2003). Dietary restriction normalizes glucose metabolism and BDNF levels, slows disease progression, and increases survival in huntingtin mutant mice. *Proc Natl Acad Sci U S A*, *100*(5), 2911–2916. https://doi.org/10.1073/pnas.0536856100\r0536856100 [pii]
Duflou, H., Maenhaut, W., & De Reuck, J. (1989). Regional distribution of potassium, calcium, and six trace elements in normal human brain. *Neurochemical Research*, *14*(11), 1099–1112. https://doi.org/10.1007/BF00965616
Dunkley, P. R., Bobrovskaya, L., Graham, M. E., Von Nagy-Felsobuki, E. I., & Dickson, P. W. (2004). Tyrosine hydroxylase phosphorylation: Regulation and consequences. *Journal of Neurochemistry*, *91*(5), 1025–1043. https://doi.org/10.1111/j.1471-4159.2004.02797.x
Duyao, M., Ambrose, C., Myers, R., Novelletto, A., Persichetti, F., Frontali, M., … Macdonald, M. (1993). Trinucleotide repeat length instability and age of onset in Huntington's disease. *Nature Genetics*, *4*(4), 387–392. https://doi.org/10.1038/ng0893-387
Eisenberg, D., Gill, H. S., Pfluegl, G. M. U., & Rotstein, S. H. (2000). Structure–function relationships of glutamine synthetases. *Biochimica et Biophysica Acta (BBA) - Protein Structure and Molecular Enzymology*, *1477*(1–2), 122–145. https://doi.org/10.1016/S0167-4838(99)00270-8
Eltokhi, A., Kurpiers, B., & Pitzer, C. (2020). Behavioral tests assessing neuropsychiatric phenotypes in adolescent mice reveal strain- and sex-specific effects. *Scientific Reports*, *10*(1), 1–15. https://doi.org/10.1038/s41598-020-67758-0
Erikson, K M, Dorman, D. C., Lash, L. H., Dobson, A. W., & Aschner, M. (2004). Airborne manganese exposure differentially affects end points of oxidative stress in an age- and sex-dependent manner. *Biol Trace Elem Res*, *100*(1), 49–62. https://doi.org/10.1385/BTER:100:1:049
Erikson, Keith M., & Aschner, M. (2003). Manganese neurotoxicity and glutamate-GABA interaction. *Neurochemistry International*, *43*(4–5), 475–480. https://doi.org/10.1016/S0197-0186(03)00037-8
Erikson, Keith M., John, C. E., Jones, S. R., & Aschner, M. (2005). Manganese accumulation in striatum of mice exposed to toxic doses is dependent upon a functional dopamine transporter. *Environmental Toxicology and Pharmacology*, *20*(3), 390–394. https://doi.org/10.1016/j.etap.2005.03.009
Erikson, Keith M., Thompson, K., Aschner, J., & Aschner, M. (2007). Manganese neurotoxicity: A focus on the neonate. *Pharmacology and Therapeutics*. https://doi.org/10.1016/j.pharmthera.2006.09.002
Farias, A. C., Cunha, A., Benko, C. R., McCracken, J. T., Costa, M. T., Farias, L. G., & Cordeiro, M. L. (2010). Manganese in children with attention-deficit/hyperactivity disorder: Relationship with methylphenidate exposure. *Journal of Child and Adolescent Psychopharmacology*, *20*(2), 113–118. https://doi.org/10.1089/cap.2009.0073
Farrer, L. A. (1985). Diabetes mellitus in Huntington disease. *Clinical Genetics*, *27*(1), 62–67.

https://doi.org/10.1111/j.1399-0004.1985.tb00185.x
Felber, D. M., Wu, Y., & Zhao, N. (2019). Regulation of the metal transporters zip14 and znt10 by manganese intake in mice. *Nutrients*, *11*(9). https://doi.org/10.3390/nu11092099
Fernandes, J., Chandler, J. D., Lili, L. N., Uppal, K., Hu, X., Hao, L., … Jones, D. P. (2019). Transcriptome Analysis Reveals Distinct Responses to Physiologic versus Toxic Manganese Exposure in Human Neuroblastoma Cells. *Frontiers in Genetics*, *10*, 676. https://doi.org/10.3389/fgene.2019.00676
Fernandes, J., Hao, L., Bijli, K. M., Chandler, J. D., Orr, M., Hu, X., … Go, Y.-M. (2017). Manganese Stimulates Mitochondrial H2O2 Production in SH-SY5Y Human Neuroblastoma Cells Over Physiologic as well as Toxicologic Range. *Toxicol Sci*, *155*(1), 213–223. https://doi.org/10.1093/toxsci/kfw196
Fernandes, J., Uppal, K., Liu, K. H., Hu, X., Go, Y.-M., & Jones, D. (2018). 182 - Time-course metabolomic analysis of manganese toxicity reveals biomarkers of oxidative stress and amino acid metabolism as early cellular targets. *Free Radical Biology and Medicine*, *128*, S83. https://doi.org/https://doi.org/10.1016/j.freeradbiomed.2018.10.187
Finkbeiner, S. (2011). Huntington's disease. *Cold Spring Harbor Perspectives in Biology*, *3*(6), 1–24. https://doi.org/10.1101/cshperspect.a007476
Finley, J. W., Johnson, P. E., & Johnson, L. K. (1994). Sex affects manganese absorption and retention by humans from a diet adequate in manganese. *The American Journal of Clinical Nutrition*, *60*(6), 949–955. https://doi.org/10.1093/ajcn/60.6.949
Fitsanakis, V. A., Au, C., Erikson, K. M., & Aschner, M. (2006). The effects of manganese on glutamate, dopamine and γ-aminobutyric acid regulation. *Neurochemistry International*, *48*(6–7), 426–433. https://doi.org/10.1016/j.neuint.2005.10.012
Fitsanakis, V. A., Piccola, G., Dos Santos, A. P. M., Aschner, J. L., & Aschner, M. (2007). Putative proteins involved in manganese transport across the blood-brain barrier. *Human and Experimental Toxicology*, *26*(4), 295–302. https://doi.org/10.1177/0960327107070496
Florence, T. M., & Stauber, J. L. (1989). Manganese catalysis of dopamine oxidation. *Sci Total Environ*, *78*, 233–240. https://doi.org/10.1016/0048-9697(89)90036-3
Frank, S. (2014). Treatment of Huntington's Disease. *Neurotherapeutics*, *11*(1), 153–160. https://doi.org/10.1007/s13311-013-0244-z
Freeman, D. M., O'Neal, R., Zhang, Q., Bouwer, E. J., & Wang, Z. (2020). Manganese-induced Parkinsonism in mice is reduced using a novel contaminated water sediment exposure model. *Environmental Toxicology and Pharmacology*, *78*(June 2019), 103399. https://doi.org/10.1016/j.etap.2020.103399
Frisbie, S. H., Mitchell, E. J., Roudeau, S., Domart, F., Carmona, A., & Ortega, R. (2019). Manganese levels in infant formula and young child nutritional beverages in the United States and France: Comparison to breast milk and regulations. *PloS One*, *14*(11), e0223636. https://doi.org/10.1371/journal.pone.0223636
Frisbie, S. H., Ortega, R., Maynard, D. M., & Sarkar, B. (2002). The concentrations of arsenic and other toxic elements in Bangladesh's drinking water. *Environmental Health Perspectives*, *110*(11), 1147–1153. https://doi.org/10.1289/ehp.021101147
Ganini, D., Santos, J. H., Bonini, M. G., & Mason, R. P. (2018). Switch of Mitochondrial Superoxide Dismutase into a Prooxidant Peroxidase in Manganese-Deficient Cells and Mice. *Cell Chemical Biology*, *25*(4), 413-425.e6. https://doi.org/10.1016/j.chembiol.2018.01.007
Gao, B., Chi, L., Mahbub, R., Bian, X., Tu, P., Ru, H., & Lu, K. (2017). Multi-Omics Reveals that Lead Exposure Disturbs Gut Microbiome Development, Key Metabolites, and Metabolic Pathways. *Chemical Research in Toxicology*, *30*(4), 996–1005. https://doi.org/10.1021/acs.chemrestox.6b00401
Garcia-Miralles, M., Geva, M., Tan, J. Y., Yusof, N. A. B. M., Cha, Y., Kusko, R., … Pouladi, M. A. (2017). Early pridopidine treatment improves behavioral and transcriptional deficits in YAC128 Huntington disease mice. *JCI Insight*, *2*(23), 1–18. https://doi.org/10.1172/jci.insight.95665
Garcia, S. J., Gellein, K., Syversen, T., & Aschner, M. (2006). A manganese-enhanced diet alters brain metals and transporters in the developing rat. *Toxicological Sciences*, *92*(2), 516–525. https://doi.org/10.1093/toxsci/kfl017
Gauthier, L. R., Charrin, B. C., Borrell-Pagès, M., Dompierre, J. P., Rangone, H., Cordelières, F. P., … Saudou,

F. (2004). Huntingtin controls neurotrophic support and survival of neurons by enhancing BDNF vesicular transport along microtubules. *Cell*, *118*(1), 127–138. https://doi.org/10.1016/j.cell.2004.06.018
Gelman, A., Rawet-Slobodkin, M., & Elazar, Z. (2015). Huntingtin facilitates selective autophagy. *Nature Cell Biology*, *17*(3), 214–215. https://doi.org/10.1038/ncb3125
Gerke, T. L., Little, B. J., & Barry Maynard, J. (2016). Manganese deposition in drinking water distribution systems. *The Science of the Total Environment*, *541*, 184–193. https://doi.org/10.1016/j.scitotenv.2015.09.054
Gibson, R. S., Anderson, B. M., & Sabry, J. H. (1983). The trace metal status of a group of post-menopausal vegetarians. *Journal of the American Dietetic Association*, *82*(3), 246–250.
Gil-Mohapel, J. (2016). Are Antioxidants Good Therapeutic Candidates for Huntington's Disease? *International Journal of Medical and Biological Frontiers*, *22*(4).
Glangetas, C., Espinosa, P., & Bellone, C. (2020). Deficit in motor skill learning-dependent synaptic plasticity at motor cortex to Dorso Lateral Striatum synapses in a mouse model of Huntington's disease. *ENeuro*, *7*(2), 1–14. https://doi.org/10.1101/544718
Go, Y.-M., Sutliff, R. L., Chandler, J. D., Khalidur, R., Kang, B.-Y., Anania, F. A., … Jones, D. P. (2015). Low-Dose Cadmium Causes Metabolic and Genetic Dysregulation Associated With Fatty Liver Disease in Mice. *Toxicological Sciences*, *147*(2), 524–534. https://doi.org/10.1093/toxsci/kfv149
Gray, M. (2019). Astrocytes in Huntington's Disease. *Advances in Experimental Medicine and Biology*, *1175*, 355–381. https://doi.org/10.1007/978-981-13-9913-8_14
Guo, Q., Huang, B., Cheng, J., Seefelder, M., Engler, T., Pfeifer, G., … Kochanek, S. (2018). The cryo-electron microscopy structure of huntingtin. *Nature*, *555*(7694), 117–120. https://doi.org/10.1038/nature25502
Gusella, J. F., & Macdonald, M. E. (2009). *Huntington ' s disease : the case for genetic modifiers*. 1–6.
Gwiazda, R., Lucchini, R., & Smith, D. (2007). Adequacy and consistency of animal studies to evaluate the neurotoxicity of chronic low-level manganese exposure in humans. *Journal of Toxicology and Environmental Health - Part A: Current Issues*, *70*(7), 594–605. https://doi.org/10.1080/10937400600882897
Handley, R. R., Reid, S. J., Brauning, R., Maclean, P., Mears, E. R., Fourie, I., … Snell, R. G. (2017). Brain urea increase is an early Huntington's disease pathogenic event observed in a prodromal transgenic sheep model and HD cases. *Proceedings of the National Academy of Sciences*, *114*(52), E11293–E11302. https://doi.org/10.1073/pnas.1711243115
Hanker, G. O. S., & Onnewald, U. R. S. (2005). *In Vitro Uptake of Glutamate in GLAST- and GLT-1-Transfected Mutant CHO-K1 Cells Is Inhibited by the Ethylmercury-Containing Preservative Thimerosal*. *105*, 221–230.
He, Y., Suofu, Y., Yablonska, S., Wang, X., Larkin, T. M., Kim, J., … Friedlander, R. M. (2019). Increased Serotonin Transporter Expression in Huntington's Disease Patients Is Not Consistently Replicated in Murine Models. *Journal of Huntington's Disease*, *8*(4), 449–457. https://doi.org/10.3233/JHD-180318
Henn, B. C., Ettinger, A. S., Schwartz, J., Tellez-Rojo, M. M., Lamadrid-Figueroa, H., Hernández-Avila, M., … Wright, R. O. (2011). Early Postnatal Blood Manganese Levels and Children's Neurodevelopment. *Epidemiology*, *21*(4), 433–439.
Henriksson, J., & Tjälve, H. (2000). Manganese Taken Up into the CNS via the Olfactory Pathway in Rats Affects Astrocytes. *Toxicological Sciences*, *55*(2), 392–398. https://doi.org/10.1093/toxsci/55.2.392
Hine, C. H., & Pasi, A. (1975). Manganese Intoxication. *The Western Journal of Medicine*, *123*, 101–107. https://doi.org/10.1177/003591574904200209
Hiney, J. K., Srivastava, V. K., & Dees, W. Les. (2011). Manganese induces IGF-1 and cyclooxygenase-2 gene expressions in the basal hypothalamus during prepubertal female development. *Toxicological Sciences*, *121*(2), 389–396. https://doi.org/10.1093/toxsci/kfr057
Holley, A. K., Bakthavatchalu, V., Velez-Roman, J. M., & St. Clair, D. K. (2011). Manganese superoxide dismutase: Guardian of the powerhouse. *International Journal of Molecular Sciences*, *12*(10), 7114–7162. https://doi.org/10.3390/ijms12107114
Horning, K. J., Caito, S. W., Tipps, K. G., Bowman, A. B., & Aschner, M. (2015). Manganese Is Essential for

Neuronal Health. *Annual Review of Nutrition*, *35*(1), 71–108. https://doi.org/10.1146/annurev-nutr-071714-034419

Humbert, S., Bryson, E. A., Cordelières, F. P., Connors, N. C., Datta, S. R., Finkbeiner, S., … Saudou, F. (2002). The IGF-1/Akt pathway is neuroprotective in Huntington's disease and involves huntingtin phosphorylation by Akt. *Developmental Cell*, *2*(6), 831–837. https://doi.org/10.1016/S1534-5807(02)00188-0

Hutchens, S., Liu, C., Jursa, T., Shawlot, W., Chaffee, B. K., Yin, W., … Mukhopadhyay, S. (2017). Deficiency in the manganese efflux transporter SLC30A10 induces severe hypothyroidism in mice. *Journal of Biological Chemistry*, *292*(23), 9760–9773. https://doi.org/10.1074/jbc.M117.783605

Ikeda, S., Yamaguchi, Y., Sera, Y., Ohshiro, H., Uchino, S., Yamashita, Y., & Ogawa, M. (2000). Manganese Deposition in the Globus Pallidus in Patients with Biliary Atresia. *Transplantation*, *69*(11). Retrieved from https://journals.lww.com/transplantjournal/Fulltext/2000/06150/MANGANESE_DEPOSITION_IN_THE_GLOBUS_PALLIDUS_IN.21.aspx

Jenkitkasemwong, S., Akinyode, A., Paulus, E., Weiskirchen, R., Hojyo, S., Fukada, T., … Knutson, M. D. (2018). SLC39A14 deficiency alters manganese homeostasis and excretion resulting in brain manganese accumulation and motor deficits in mice. *Proceedings of the National Academy of Sciences*, *115*(20), E4730. https://doi.org/10.1073/pnas.1806613115

Jiang, Y., & Zheng, W. (2005). Cardiovascular toxicities upon manganese exposure. *Cardiovascular Toxicology*, *5*(4), 345–354. https://doi.org/10.1385/ct:5:4:345

Joshi, P. R., Wu, N. P., André, V. M., Cummings, D. M., Cepeda, C., Joyce, J. A., … Bamford, N. S. (2009). Age-dependent alterations of corticostriatal activity in the YAC128 mouse model of huntington disease. *Journal of Neuroscience*, *29*(8), 2414–2427. https://doi.org/10.1523/JNEUROSCI.5687-08.2009

Kanyo, Z. F., Scolnick, L. R., Ash, D. E., & Christianson, D. W. (1996). Structure of a unique binuclear manganese cluster in arginase. *Nature*, *383*, 554–557.

Karki, P., Smith, K., Johnson, J., Aschner, M., & Lee, E. (2015). Role of transcription factor yin yang 1 in manganese-induced reduction of astrocytic glutamate transporters: Putative mechanism for manganese-induced neurotoxicity. *Neurochemistry International*, *88*, 53–59. https://doi.org/10.1016/j.neuint.2014.08.002

Karki, P., Webb, A., Smith, K., Johnson, J., Lee, K., Son, D.-S., … Lee, E. (2014). Yin Yang 1 is a Repressor of Glutamate Transporter EAAT2 and it Mediates Manganese-induced Decrease of EAAT2 Expression in Astrocytes. *Molecular and Cellular Biology*, MCB.01176-13. https://doi.org/10.1128/MCB.01176-13

Kasarskis, E. J. (1984). Zinc metabolism in normal and zinc-deficient rat brain. *Experimental Neurology*, *85*(1), 114–127. https://doi.org/10.1016/0014-4886(84)90166-3

Keen, C., Ensunsa, J., Waston, M., Baly, D., Donovan, S., Monaco, M., & Clegg, M. (1999). Nutritional aspects of manganese from experimental studies. *NeuroToxicology*, *20*, 213–223.

Kendzia, B., Van Gelder, R., Schwank, T., Hagemann, C., Zschiesche, W., Behrens, T., … Pesch, B. (2017). Occupational Exposure to Inhalable Manganese at German Workplaces. *Annals of Work Exposures and Health*, *61*(9), 1108–1117. https://doi.org/10.1093/annweh/wxx080

Kern, C., Stanwood, G., & Smith, D. R. (2011). Pre-weaning manganese exposure causes hyperactivity, disinhibition, and spatial learning and memory deficits associated with altered dopamine receptor and transporter levels. *Control*, *64*(5), 363–378. https://doi.org/10.1002/syn.20736.Pre-weaning

Khakh, B. S., Beaumont, V., Cachope, R., Munoz-Sanjuan, I., Goldman, S. A., & Grantyn, R. (2017). Unravelling and Exploiting Astrocyte Dysfunction in Huntington's Disease. *Trends in Neurosciences*, *40*(7), 422–437. https://doi.org/10.1016/j.tins.2017.05.002

Khalid, M., Aoun, R. A., & Mathews, T. A. (2011). Altered striatal dopamine release following a sub-acute exposure to manganese. *Journal of Neuroscience Methods*, *202*(2), 182–191. https://doi.org/https://doi.org/10.1016/j.jneumeth.2011.06.019

Khan, A., Hingre, J., & Dhamoon, A. S. (2020). Manganese Neurotoxicity as a Complication of Chronic Total Parenteral Nutrition. *Case Reports in Neurological Medicine*, *2020*(March 2017), 1–6. https://doi.org/10.1155/2020/9484028

Kholodar, A. V., Amikishieva, A. V., & Anisimov, M. P. (2013). Effects of intranasal administration of dopamine on anxiety and locomotor activity in two mouse strains. *Neuroscience and Behavioral Physiology*, *43*(3), 409–415. https://doi.org/10.1007/s11055-013-9747-7

Kim, Y. (2018). μSex, pregnancy, and age-specific differences of blood manganese levels in relation to iron status; what does it mean? *Toxicology Reports*, *5*, 28–30. https://doi.org/10.1016/j.toxrep.2017.12.003

Kirkley, K. S., Popichak, K. A., Afzali, M. F., Legare, M. E., & Tjalkens, R. B. (2017). Microglia amplify inflammatory activation of astrocytes in manganese neurotoxicity. *Journal of Neuroinflammation*, *14*(1), 99. https://doi.org/10.1186/s12974-017-0871-0

Kitazawa, M., Wagner, J. R., Kirby, M. L., Anantharam, V., & Kanthasamy, A. G. (2002). Oxidative stress and mitochondrial-mediated apoptosis in dopaminergic cells exposed to methylcyclopentadienyl manganese tricarbonyl. *The Journal of Pharmacology and Experimental Therapeutics*, *302*(1), 26–35. https://doi.org/10.1124/jpet.302.1.26

Koch, E. T., & Raymond, L. A. (2019). Dysfunctional striatal dopamine signaling in Huntington's disease. *Journal of Neuroscience Research*, *97*(12), 1636–1654. https://doi.org/10.1002/jnr.24495

Komura, J., & Sakamoto, M. (1992). Effects of manganese forms on biogenic amines in the brain and behavioral alterations in the mouse: Long-term oral administration of several manganese compounds. *Environmental Research*, *57*(1), 34–44. https://doi.org/https://doi.org/10.1016/S0013-9351(05)80017-9

Konradi, C., Kornhuber, J., Sofic, E., Heckers, S., Riederer, P., & Beckmann, H. (1992). Variations of monoamines and their metabolites in the human brain putamen. *Brain Research*, *579*(2), 285–290. https://doi.org/10.1016/0006-8993(92)90062-e

Kordasiewicz, H. B., Stanek, L. M., Wancewicz, E. V., Mazur, C., McAlonis, M. M., Pytel, K. A., … Cleveland, D. W. (2012). Sustained Therapeutic Reversal of Huntington's Disease by Transient Repression of Huntingtin Synthesis. *Neuron*, *74*(6), 1031–1044. https://doi.org/10.1016/j.neuron.2012.05.009

Koyuncu, S., Fatima, A., Gutierrez-Garcia, R., & Vilchez, D. (2017). Proteostasis of huntingtin in health and disease. *International Journal of Molecular Sciences*, *18*(7), 11–13. https://doi.org/10.3390/ijms18071568

Kumar, A., & Ratan, R. R. (2016). Oxidative Stress and Huntington's Disease: The Good, The Bad, and The Ugly. *J Huntingtons Dis*, *5*(3), 217–237. https://doi.org/10.1021/jacs.5b07154.Total

Kumar, K. K., Goodwin, C. R., Uhouse, M. A., Bornhorst, J., Schwerdtle, T., Aschner, M., … Bowman, A. B. (2015). Untargeted metabolic profiling identifies interactions between Huntington's disease and neuronal manganese status. *Metallomics*, *7*(2), 363–370. https://doi.org/10.1039/c4mt00223g

Laprairie, R. B., Petr, G. T., Sun, Y., Fischer, K. D., Eileen, M., & Rosenberg, P. A. (2018). Huntington's disease pattern of transcriptional dysregulation in the absence of mutant huntingtin is produced by knockout of neuronal GLT-1. *Neurochemistry International*. https://doi.org/10.1016/j.neuint.2018.04.015

Larsen, N. A., Pakkenberg, H., Damsgaard, E., & Heydorn, K. (1979). Topographical distribution of arsenic, manganese, and selenium in the normal human brain. *Journal of the Neurological Sciences*, *42*(3), 407–416. https://doi.org/10.1016/0022-510x(79)90173-4

Lasley, S. M., Fornal, C. A., Mandal, S., Strupp, B. J., Beaudin, S. A., & Smith, D. R. (2020). Early Postnatal Manganese Exposure Reduces Rat Cortical and Striatal Biogenic Amine Activity in Adulthood. *Toxicological Sciences*, *173*(1), 144–155. https://doi.org/10.1093/toxsci/kfz208

Lee, E., Karki, P., Johnson, J. J., Hong, P., & Aschner, M. (2017). Manganese Control of Glutamate Transporters' Gene Expression. *Advances in Neurobiology*, *16*, 1–12. https://doi.org/10.1007/978-3-319-55769-4_1

Lee, J., Ramos, E., & Lee, J. (2012). CAG repeat expansion in Huntington's disease determines age of onset in a fully dominant version. *Neurology*, *78*, 690–695.

Lee, S. H., Jouihan, H. A., Cooksey, R. C., Jones, D., Kim, H. J., Winge, D. R., & McClain, D. A. (2013). Manganese supplementation protects against diet-induced diabetes in wild type mice by enhancing insulin secretion. *Endocrinology*, *154*(3), 1029–1038. https://doi.org/10.1210/en.2012-1445

Leoni, V., & Caccia, C. (2015). The impairment of cholesterol metabolism in Huntington disease. *Biochimica et Biophysica Acta - Molecular and Cell Biology of Lipids*, *1851*(8), 1095–1105. https://doi.org/10.1016/j.bbalip.2014.12.018

Leyva-Illades, D., Chen, P., Zogzas, C. E., Hutchens, S., Mercado, J. M., Swaim, C. D., … Mukhopadhyay, S. (2014). SLC30A10 is a cell surface-localized manganese efflux transporter, And parkinsonism-causing mutations block its intracellular trafficking and efflux activity. *Journal of Neuroscience*, *34*(42), 14079–14095. https://doi.org/10.1523/JNEUROSCI.2329-14.2014

Liang, G., Qin, H., Zhang, L., Ma, S., Huang, X., Lv, Y., … Zou, Y. (2015). Effects of chronic manganese exposure on the learning and memory of rats by observing the changes in the hippocampal cAMP signaling pathway. *Food and Chemical Toxicology : An International Journal Published for the British Industrial Biological Research Association*, *83*, 261–267. https://doi.org/10.1016/j.fct.2015.07.005

Liao, Y., Smyth, G. K., & Shi, W. (2014). featureCounts: an efficient general purpose program for assigning sequence reads to genomic features. *Bioinformatics (Oxford, England)*, *30*(7), 923–930. https://doi.org/10.1093/bioinformatics/btt656

Liévens, J. C., Woodman, B., Mahal, A., Spasic-Boscovic, O., Samuel, D., Kerkerian-Le Goff, L., & Bates, G. P. (2001). Impaired glutamate uptake in the R6 Huntington's disease transgenic mice. *Neurobiology of Disease*, *8*(5), 807–821. https://doi.org/10.1006/nbdi.2001.0430

Lin, M., Colon-Perez, L. M., Sambo, D. O., Miller, D. R., Lebowitz, J. J., Jimenez-Rondan, F., … Khoshbouei, H. (2019). Mechanism of manganese dysregulation of dopamine neuronal activity. *Journal of Neuroscience*, *40*(30), 5871–5891. https://doi.org/10.1101/792143

Lin, W., Vann, D. R., Doulias, P. T., Wang, T., Landesberg, G., Li, X., … Rader, D. J. (2017). Hepatic metal ion transporter ZIP8 regulates manganese homeostasis and manganese-dependent enzyme activity. *Journal of Clinical Investigation*, *127*(6), 2407–2417. https://doi.org/10.1172/JCI90896

Lopes, C., Ribeiro, M., Duarte, A. I., Humbert, S., Saudou, F., Pereira De Almeida, L., … Rego, A. C. (2014). IGF-1 intranasal administration rescues Huntington's disease phenotypes in YAC128 mice. *Molecular Neurobiology*, *49*(3), 1126–1142. https://doi.org/10.1007/s12035-013-8585-5

Love, M. I., Huber, W., & Anders, S. (2014). Moderated estimation of fold change and dispersion for RNA-seq data with DESeq2. *Genome Biology*, *15*(12), 550. https://doi.org/10.1186/s13059-014-0550-8

Lu, C. L., Tang, S., Meng, Z. J., He, Y. Y., Song, L. Y., Liu, Y. P., … Guo, S. C. (2014). Taurine improves the spatial learning and memory ability impaired by sub-chronic manganese exposure. *Journal of Biomedical Science*, *21*(1), 1–8. https://doi.org/10.1186/1423-0127-21-51

Lüesse, H. G., Schiefer, J., Spruenken, A., Puls, C., Block, F., & Kosinski, C. M. (2001). Evaluation of R6/2 HD transgenic mice for therapeutic studies in Huntington's disease: Behavioral testing and impact of diabetes mellitus. *Behavioural Brain Research*, *126*(1–2), 185–195. https://doi.org/10.1016/S0166-4328(01)00261-3

Luthi-Carter, R., & Cha, J. H. J. (2003). Transcriptional dysregulation in Huntington's disease. *Clinical Neuroscience Research*, *3*(3), 165–177. https://doi.org/10.1016/S1566-2772(03)00059-8

Madison, J. L., Wegrzynowicz, M., Aschner, M., & Bowman, A. B. (2012). Disease-toxicant interactions in manganese exposed Huntington disease mice: Early changes in striatal neuron morphology and dopamine metabolism. *PLoS ONE*. https://doi.org/10.1371/journal.pone.0031024

Malecki, E. A., Devenyi, A. G., Beard, J. L., & Connor, J. R. (1999). Existing and emerging mechanisms for transport of iron and manganese to the brain. *Journal of Neuroscience Research*, *56*(2), 113–122. https://doi.org/10.1002/(sici)1097-4547(19990415)56:2<113::aid-jnr1>3.0.co;2-k

Markianos, M., Panas, M., Kalfakis, N., & Vassilopoulos, D. (2009). Plasma homovanillic acid and prolactin in huntington's disease. *Neurochemical Research*, *34*(5), 917–922. https://doi.org/10.1007/s11064-008-9851-1

Martinez-Finley, E. J., Gavin, C. E., Aschner, M., & Gunter, T. E. (2013). Manganese neurotoxicity and the role of reactive oxygen species. *Free Radical Biology and Medicine*, *62*, 65–75. https://doi.org/https://doi.org/10.1016/j.freeradbiomed.2013.01.032

Martínez-Lazcano, J. C., Montes, S., Sánchez-Mendoza, M. A., Rodríguez-Páez, L., Pérez-Neri, I., Boll, M. C., … Pérez-Severiano, F. (2014). Sub-Chronic Copper Pretreatment Reduces Oxidative Damage in an Experimental Huntington's Disease Model. *Biological Trace Element Research*, *162*(1–3), 211–218. https://doi.org/10.1007/s12011-014-0127-0

Martins, A. C., Krum, B. N., Queirós, L., Tinkov, A. A., Skalny, A. V., Bowman, A. B., & Aschner, M. (2020). Manganese in the Diet: Bioaccessibility, Adequate Intake, and Neurotoxicological Effects. *Journal of Agricultural and Food Chemistry*, *68*(46), 12893–12903. https://doi.org/10.1021/acs.jafc.0c00641

Martins Jr., A. C., Morcillo, P., Ijomone, O. M., Venkataramani, V., Harrison, F. E., Lee, E., … Aschner, M. (2019). New insights on therole of manganese in Alzheimer 's Disease and Parkinson 's Disease. *International Journal of Environmental Research and Public Health*, *16*, 1–8.

Massaro, A. N., Wu, Y. W., Bammler, T. K., Comstock, B., Mathur, A., McKinstry, R. C., … Juul, S. (2018). Plasma Biomarkers of Brain Injury in Neonatal Hypoxic-Ischemic Encephalopathy. *The Journal of Pediatrics*, *194*, 67-75.e1. https://doi.org/10.1016/j.jpeds.2017.10.060

Mazziota, J. C., Phelps, M. E., Phal, J. J., Huang, S.-C., Baxter, L. R., Riege, W. H., … Markham, C. H. (1987). Reduced Cerebral Glucose Metabolism in Asymptomatic Subjects at Risk for Huntington's Disease. *The New England Journal of Medicine*, *316*(7), 357–362.

McDonell, K. E., Ciriegio, A. E., Pfalzer, A. C., Hale, L., Shiino, S., Riordan, H., … Claassen, D. O. (2020). Risk-Taking Behaviors in Huntington's Disease. *Journal of Huntington's Disease*, *9*(4), 359–369. https://doi.org/10.3233/JHD-200431

McDowell, L. (2017). *Mineral Nutrition History: The Early Years*.

Mercadante, C. J., Prajapati, M., Conboy, H. L., Dash, M. E., Herrera, C., Pettiglio, M. A., … Bartnikas, T. B. (2019). Manganese transporter Slc30a10 controls physiological manganese excretion and toxicity. *Journal of Clinical Investigation*, *129*(12), 5442–5461. https://doi.org/10.1172/JCI129710

Metzger, S., Saukko, M., Van Che, H., Tong, L., Puder, Y., Riess, O., & Nguyen, H. P. (2010). Age at onset in Huntington's disease is modified by the autophagy pathway: Implication of the V471A polymorphism in Atg7. *Human Genetics*, *128*(4), 453–459. https://doi.org/10.1007/s00439-010-0873-9

Mezzaroba, L., Alfieri, D. F., Colado Simão, A. N., & Vissoci Reiche, E. M. (2019). The role of zinc, copper, manganese and iron in neurodegenerative diseases. *NeuroToxicology*, *74*, 230–241. https://doi.org/10.1016/j.neuro.2019.07.007

Milatovic, D., Zaja-Milatovic, S., Gupta, R. C., Yu, Y., & Aschner, M. (2009). Oxidative damage and neurodegeneration in manganese-induced neurotoxicity. *Toxicology and Applied Pharmacology*, *292*(3), 342–351. https://doi.org/10.1002/ar.20849.3D

Mo, C., Hannan, A. J., & Renoir, T. (2015). Environmental factors as modulators of neurodegeneration: Insights from gene-environment interactions in Huntington's disease. *Neuroscience and Biobehavioral Reviews*, *52*, 178–192. https://doi.org/10.1016/j.neubiorev.2015.03.003

Moreno, C. L., Ehrlich, M. E., & Mobbs, C. V. (2016). Protection by dietary restriction in the YAC128 mouse model of Huntington's disease: Relation to genes regulating histone acetylation and HTT. *Neurobiology of Disease*, *85*, 25–34. https://doi.org/10.1016/j.nbd.2015.09.012

Moreno, J. A., Yeomans, E. C., Streifel, K. M., Brattin, B. L., Taylor, R. J., & Tjalkens, R. B. (2009). Age-dependent susceptibility to manganese-induced neurological dysfunction. *Toxicological Sciences*, *112*(2), 394–404. https://doi.org/10.1093/toxsci/kfp220

Morganti, J. B., Lown, B. A., Stineman, C. H., D'Agostino, R. B., & Massaro, E. J. (1985). Uptake, distribution and behavioral effects of inhalation exposure to manganese (MnO2) in the adult mouse. *Neurotoxicology*, *6*(1), 1–15.

Morris, S. M. (2002). Regulation Of Enzymes of the Urea Cycle and Arginine Metabolism. *Annual Review of Nutrition*, *22*(1), 87–105. https://doi.org/10.1146/annurev.nutr.22.110801.140547

Morris, S. M., Bhamidipati, D., & Kepka-Lenhart, D. (1997). Human type II arginase: Sequence analysis and tissue-specific expression. *Gene*, *193*(2), 157–161. https://doi.org/10.1016/S0378-1119(97)00099-1

Mukhopadhyay, S. (2018). Familial manganese-induced neurotoxicity due to mutations in SLC30A10 or SLC39A14. *NeuroToxicology*, *64*, 278–283. https://doi.org/10.1016/j.neuro.2017.07.030

Muller, M., & Leavitt, B. R. (2014). Iron dysregulation in Huntington's Disease. *Journal of Neurochemistry*, *130*, 328–350. https://doi.org/10.1111/jnc.12739

Nachtman, J. P., Tubben, R. E., & Commissaris, R. L. (1986). Behavioral effects of chronic manganese administration in rats: locomotor activity studies. *Neurobehavioral Toxicology and Teratology*, *8*(6), 711–

715.
Naia, L., Ferreira, I. L., Cunha-Oliveira, T., Duarte, A. I., Ribeiro, M., Rosenstock, T. R., … Rego, A. C. (2014). Activation of IGF-1 and Insulin Signaling Pathways Ameliorate Mitochondrial Function and Energy Metabolism in Huntington's Disease Human Lymphoblasts. *Molecular Neurobiology*, *51*(1), 331–348. https://doi.org/10.1007/s12035-014-8735-4
Naia, L., Ribeiro, M., Rodrigues, J., Duarte, A. I., Lopes, C., Rosenstock, T. R., … Rego, A. C. (2016). Insulin and IGF-1 regularize energy metabolites in neural cells expressing full-length mutant huntingtin. *Neuropeptides*, *58*, 73–81. https://doi.org/10.1016/j.npep.2016.01.009
Nair, A., & Jacob, S. (2016). A simple practice guide for dose conversion between animals and human. *Journal of Basic and Clinical Pharmacy*, *7*(2), 27. https://doi.org/10.4103/0976-0105.177703
Nakamura, M., Miura, A., Nagahata, T., Shibata, Y., Okada, E., & Ojima, T. (2019). Low zinc, copper, and manganese intake is associated with depression and anxiety symptoms in the Japanese working population: Findings from the eating habit and well-being study. *Nutrients*, *11*(4). https://doi.org/10.3390/nu11040847
Neely, C. L. C., Pedemonte, K. A., Boggs, K. N., & Flinn, J. M. (2019). Nest building behavior as an early indicator of behavioral deficits in mice. *Journal of Visualized Experiments*, *2019*(152), 1–8. https://doi.org/10.3791/60139
Neely, M. D., Davison, C. A., Aschner, M., & Bowman, A. B. (2017). Manganese and Rotenone-Induced Oxidative Stress Signatures Differ in iPSC-Derived Human Dopamine Neurons. *Toxicol Sci*, *159*(2), 366–379. https://doi.org/10.1093/toxsci/kfx145
Neth, K., Lucio, M., Walker, A., Zorn, J., Schmitt-Kopplin, P., & Michalke, B. (2015). Changes in Brain Metallome/Metabolome Pattern due to a Single i.v. Injection of Manganese in Rats. *PLOS ONE*, *10*(9), e0138270. Retrieved from https://doi.org/10.1371/journal.pone.0138270
Nguyen, H. O. X., Goracke-Postle, C. J., Kaminski, L. L., Overland, A. C., Morgan, A. D., & Fairbanks, C. A. (2003). Neuropharmacokinetic and Dynamic Studies of Agmatine (Decarboxylated Arginine). *Annals of the New York Academy of Sciences*, *1009*, 82–105. https://doi.org/10.1196/annals.1304.009
Nielsen, B. S., Larsen, E. H., Ladefoged, O., & Lam, H. R. (2017). Subchronic, Low-Level Intraperitoneal Injections of Manganese (IV) Oxide and Manganese (II) Chloride Affect Rat Brain Neurochemistry. *International Journal of Toxicology*, *36*(3), 239–251. https://doi.org/10.1177/1091581817704378
NM, L., J, M., M, S., A, J., E, S., K, L., … VS., K. (2008). Glucose Homeostasis in Huntington Disease. *Arch Neurol*, *65*(4), 476–480. https://doi.org/10.1001/archneur.65.4.476.
Nopoulos, P. C. (2016). Huntington disease: a single-gene degenerative disorder of the striatum. *Dialogues in Clinical Neuroscience*, *18*(1), 91. https://doi.org/PMCID: PMC4826775
Normandin, L., & Hazell, A. S. (2002). Manganese neurotoxicity: An update of pathophysiologic mechanisms. *Metabolic Brain Disease*, *17*(4), 375–387. https://doi.org/10.1023/A:1021970120965
Novak, M. J. U., & Tabrizi, S. J. (2011). Huntington's disease: Clinical presentation and treatment. In *International Review of Neurobiology* (Vol. 98). https://doi.org/10.1016/B978-0-12-381328-2.00013-4
Nyarko-Danquah, I., Pajarillo, E., Digman, A., Soliman, K. F. A., Aschner, M., & Lee, E. (2020). Manganese Accumulation in the Brain via Various Transporters and Its Neurotoxicity Mechanisms. *Molecules*, *25*(24), 1–21. https://doi.org/10.3390/molecules25245880
O'Neal, S. L., & Zheng, W. (2015). Manganese Toxicity Upon Overexposure: a Decade in Review. *Current Environmental Health Reports*, *2*(3), 315–328. https://doi.org/10.1007/s40572-015-0056-x
Ordway, J. M., Tallaksen-Greene, S., Gutekunst, C. A., Bernstein, E. M., Cearley, J. A., Wiener, H. W., … Detloff, P. J. (1997). Ectopically expressed CAG repeats cause intranuclear inclusions and a progressive late onset neurological phenotype in the mouse. *Cell*, *91*(6), 753–763. https://doi.org/10.1016/S0092-8674(00)80464-X
Ortiz-Pulido, R., Hernández-Briones, Z. S., Tamariz-Rodríguez, A., Hernández, M. E., Aranda-Abreu, G. E., Coria-Avila, G. A., … García, L. I. (2017). Effect of electrolytic lesion of the dorsomedial striatum on sexual behaviour and locomotor activity in rats. *Neurología (English Edition)*, *32*(5), 278–283. https://doi.org/10.1016/j.nrleng.2015.11.008
Oulhote, Y., Mergler, D., & Bouchard, M. F. (2014). Sex-and age-differences in blood manganese levels in the

U.S. general population: National health and nutrition examination survey 2011-2012. *Environmental Health: A Global Access Science Source*, *13*(1), 1–10. https://doi.org/10.1186/1476-069X-13-87

Pajarillo, E., Johnson, J. J., Kim, J., Karki, P., Son, D.-S., Aschner, M., & Lee, E. (2018). 17β-estradiol and tamoxifen protect mice from manganese-induced dopaminergic neurotoxicity. *Neurotoxicology*, *65*, 280–288. https://doi.org/10.1016/j.neuro.2017.11.008

Patassini, S., Begley, P., Reid, S. J., Xu, J., Church, S. J., Curtis, M., … Cooper, G. J. S. (2015). Identification of elevated urea as a severe, ubiquitous metabolic defect in the brain of patients with Huntington's disease. *Biochemical and Biophysical Research Communications*, *468*(1–2), 161–166. https://doi.org/10.1016/j.bbrc.2015.10.140

Patassini, S., Begley, P., Xu, J., Church, S. J., Reid, S. J., Kim, E. H., … Cooper, G. J. S. (2016). Metabolite mapping reveals severe widespread perturbation of multiple metabolic processes in Huntington's disease human brain. *Biochimica et Biophysica Acta - Molecular Basis of Disease*, *1862*(9), 1650–1662. https://doi.org/10.1016/j.bbadis.2016.06.002

Pfalzer, A. C., & Bowman, A. B. (2017). Relationships Between Essential Manganese Biology and Manganese Toxicity in Neurological Disease. *Current Environmental Health Reports*, *4*(2), 223–228. https://doi.org/10.1007/s40572-017-0136-1

Pfalzer, A. C., Wages, P. A., Porter, N. A., & Bowman, A. B. (2019). Striatal Cholesterol Precursors Are Altered with Age in Female Huntington's Disease Model Mice. *Journal of Huntington's Disease*, *8*, 161–169. https://doi.org/10.3233/JHD-180321

Pfalzer, A. C., Wilcox, J. M., Codreanu, S. G., Totten, M., Bichell, T. J. V., Halbesma, T., … Bowman, A. B. (2020). Huntington's disease genotype suppresses global manganese-responsive processes in pre-manifest and manifest YAC128 mice. *Metallomics*, *12*(7), 1118–1130. https://doi.org/10.1039/d0mt00081g

Potter, N. T., Spector, E. B., & Prior, T. W. (2004). Technical Standards and Guidelines for Huntington Disease Testing. *Genetics in Medicine*, *6*(1), 61–65. https://doi.org/10.1097/01.GIM.0000106165.74751.15

Pouladi, M. A., Xie, Y., Skotte, N. H., Ehrnhoefer, D. E., Graham, R. K., Kim, J. E., … Hayden, M. R. (2010). Full-length huntingtin levels modulate body weight by influencing insulin-like growth factor 1 expression. *Human Molecular Genetics*, *19*(8), 1528–1538. https://doi.org/10.1093/hmg/ddq026

Ramos, P., Santos, A., Pinto, N. R., Mendes, R., Magalhães, T., & Almeida, A. (2014). Anatomical Region Differences and Age-Related Changes in Copper, Zinc, and Manganese Levels in the Human Brain. *Biological Trace Element Research*, *161*(2), 190–201. https://doi.org/10.1007/s12011-014-0093-6

Reaney, S. H., Kwik-uribe, C. L., & Smith, D. R. (2002). Manganese Oxidation State and Its Implications for Toxicity. *Chem Res Toxicol*, *15*, 1119–1126.

Reddy, P. H. (2014). Increased mitochondrial fission and neuronal dysfunction in Huntington's disease: Implications for molecular inhibitors of excessive mitochondrial fission. *Drug Discovery Today*, *19*(7), 951–955. https://doi.org/10.1016/j.drudis.2014.03.020

Reddy, P. H., Mao, P., & Manczak, M. (2009). Mitochondrial structural and functional dynamics in Huntington's disease. *Brain Research Reviews*, *61*(1), 33–48. https://doi.org/10.1016/j.brainresrev.2009.04.001

Reyes, M. B., Martínez-Oyanedel, J., Navarrete, C., Mardones, E., Martínez, I., Salas, M., … Uribe, E. (2020). Insights into the MN2+ binding site in the agmatinase-like protein (ALP): A critical enzyme for the regulation of agmatine levels in mammals. *International Journal of Molecular Sciences*, *21*(11), 1–13. https://doi.org/10.3390/ijms21114132

Richter Schmitz, C. R., Eichwald, T., Branco Flores, M. V., Varela, K. G., Mantovani, A., Steffani, J. A., … Remor, A. P. (2019). Sex differences in subacute manganese intoxication: Oxidative parameters and metal deposition in peripheral organs of adult Wistar rats. *Regulatory Toxicology and Pharmacology*, *104*(September 2018), 98–107. https://doi.org/10.1016/j.yrtph.2019.03.005

Rigamonti, D., Bauer, J. H., De-Fraja, C., Conti, L., Sipione, S., Sciorati, C., … Cattaneo, E. (2000). Wild-type huntingtin protects from apoptosis upstream of caspase-3. *The Journal of Neuroscience : The Official Journal of the Society for Neuroscience*, *20*(10), 3705–3713. https://doi.org/20/10/3705 [pii]

Rikani, A. A., Choudhry, Z., Choudhry, A. M., Rizvi, N., Ikram, H., Mobassarah, N. J., & Tulli, S. (2014). The

mechanism of degeneration of striatal neuronal subtypes in Huntington disease. *Annals of Neurosciences*, *21*(3), 112–114. https://doi.org/10.5214/ans.0972.7531.210308

Robison, G., Sullivan, B., Cannon, J. R., & Pushkar, Y. (2015). Identification of dopaminergic neurons of the substantia nigra pars compacta as a target of manganese accumulation†‡. *Metallomics*, *7*(5), 748–755. https://doi.org/10.1039/c5mt00023h

Roels, H. A., Ortega Eslava, M. I., Ceulemans, E., Robert, A., & Lison, D. (1999). Prospective study on the reversibility of neurobehavioral effects in workers exposed to manganese dioxide. *Neurotoxicology*, *20*(2–3), 255–271.

Roels, H., Meiers, G., Delos, M., Ortega, I., Lauwerys, R., Buchet, J. P., & Lison, D. (1997). Influence of the route of administration and the chemical form (MnCl2, MnO2) on the absorption and cerebral distribution of manganese in rats. *Archives of Toxicology*, *71*(4), 223–230. https://doi.org/10.1007/s002040050380

Röllin, H., Mathee, A., Levin, J., Theodorou, P., & Wewers, F. (2005). Blood manganese concentrations among first-grade schoolchildren in two South African cities. *Environmental Research*, *97*(1), 93–99. https://doi.org/10.1016/j.envres.2004.05.003

Romero, N., Benítez, J., Garcia, D., González, A., Bennun, L., García-Robles, M. A., … Uribe, E. (2017). Mammalian agmatinases constitute unusual members in the family of Mn2 +-dependent ureahydrolases. *Journal of Inorganic Biochemistry*, *166*, 122–125. https://doi.org/10.1016/j.jinorgbio.2016.11.015

Rosas, H. D., Chen, Y. I., Doros, G., Salat, D. H., Chen, N. K., Kwong, K. K., … Hersch, S. M. (2012). Alterations in brain transition metals in Huntington disease: An evolving and intricate story. *Archives of Neurology*, *69*(7), 887–893. https://doi.org/10.1001/archneurol.2011.2945

Rose, C., Butterworth, R. F., Zayed, J., Normandin, L., Todd, K., Michalak, A., … Pomier-Layrargues, G. (1999). Manganese deposition in basal ganglia structures results from both portal-systemic shunting and liver dysfunction. *Gastroenterology*, *117*(3), 640–644. https://doi.org/10.1016/S0016-5085(99)70457-9

Sandstead, H. H. (1986). Nutrition and brain function: trace elements. *Nutrition Reviews*, *44*(5), 37–41.

Santamaría, A., Flores-Escartín, A., Martínez, J. C., Osorio, L., Galván-Arzate, S., Chaverrí, J. P., … Ríos, C. (2003). Copper blocks quinolinic acid neurotoxicity in rats: Contribution of antioxidant systems. *Free Radical Biology and Medicine*, *35*(4), 418–427. https://doi.org/10.1016/S0891-5849(03)00317-4

Santamaría, A., Pérez-Severiano, F., Rodríguez-Martínez, E., Maldonado, P. D., Pedraza-Chaverri, J., Ríos, C., … (Accepted. (2001). Comparative analysis of superoxide dismutase activity between acute pharmacological models and a transgenic mouse model of Huntington's disease. *Neurochemical Research*, *26*(4), 419–424. https://doi.org/10.1023/A:1010911417383

Saudou, F., & Humbert, S. (2016). The Biology of Huntingtin. *Neuron*, *89*(5), 910–926. https://doi.org/10.1016/j.neuron.2016.02.003

Schaefer, M. H., Wanker, E. E., & Andrade-Navarro, M. A. (2012). Evolution and function of CAG/polyglutamine repeats in protein-protein interaction networks. *Nucleic Acids Research*, *40*(10), 4273–4287. https://doi.org/10.1093/nar/gks011

Schaffar, G., Breuer, P., Boteva, R., Behrends, C., Tzvetkov, N., Strippel, N., … Hartl, F. U. (2004). Cellular toxicity of polyglutamine expansion proteins: Mechanism of transcription factor deactivation. *Molecular Cell*, *15*(1), 95–105. https://doi.org/10.1016/j.molcel.2004.06.029

Schneider, J. S., Williams, C., Ault, M., & Guilarte, T. R. (2015). Effects of chronic manganese exposure on attention and working memory in non-human primates. *Neurotoxicology*, *48*, 217–222. https://doi.org/10.1016/j.neuro.2015.04.004

Schuh, M. J. (2016). Possible Parkinson's Disease Induced by Chronic Manganese Supplement Ingestion. *Consult Pharm*, *31*(12), 698–703. https://doi.org/10.4140/TCP.n.2016.698

Schullehner, J., Thygesen, M., Kristiansen, S. M., Hansen, B., Pedersen, C. B., & Dalsgaard, S. (2020). Exposure to Manganese in Drinking Water during Childhood and Association with Attention-Deficit Hyperactivity Disorder: A Nationwide Cohort Study. *Environmental Health Perspectives*, *128*(9), 97004. https://doi.org/10.1289/EHP6391

Schulte, J., & Littleton, J. T. (2011). The biological function of the Huntingtin protein and its relevance to Huntington's Disease pathology. *Current Trends in Neurology*, *5*, 65–78. Retrieved from

http://www.pubmedcentral.nih.gov/articlerender.fcgi?artid=3237673&tool=pmcentrez&rendertype=abstract
Schwab, L. C., Garas, S. N., Drouin-Ouellet, J., Mason, S. L., Stott, S. R., & Barker, R. A. (2015). Dopamine and Huntington's disease. *Expert Review of Neurotherapeutics*, *15*(4), 445–458. https://doi.org/10.1586/14737175.2015.1025383
Scrutton, M. C., Utter, M. F., & Mildvan, A. S. (1966). Pyruvate Carboxylase: The Presence of Tightly Bound Manganese. *Journal of Biological Chemistry*, *241*(15), 3480–3487. https://doi.org/10.1016/s0021-9258(18)99858-3
Seo, Y. A., Choi, E. K., Aring, L., Paschall, M., & Iwase, S. (2020). Transcriptome Analysis of the Cerebellum of Mice Fed a Manganese-Deficient Diet. *Frontiers in Genetics*, *11*(December), 1–13. https://doi.org/10.3389/fgene.2020.558725
Shih, J.-H., Zeng, B.-Y., Lin, P.-Y., Chen, T.-Y., Chen, Y.-W., Wu, C.-K., … Wu, M.-K. (2018). Association between peripheral manganese levels and attention-deficit/hyperactivity disorder: a preliminary meta-analysis. *Neuropsychiatric Disease and Treatment*, *14*, 1831–1842. https://doi.org/10.2147/NDT.S165378
Sidoryk-Wegrzynowicz, M., Lee, E., & Aschner, M. (2012). Mechanism of Mn(II)-mediated dysregulation of glutamine–glutamate cycle: focus on glutamate turnover. *Journal of Neurochemistry*, *122*(4), 856–867. https://doi.org/https://doi.org/10.1111/j.1471-4159.2012.07835.x
Sikk, K., Haldre, S., Aquilonius, S. M., & Taba, P. (2011). Manganese-induced parkinsonism due to ephedrone abuse. *Parkinson's Disease*, *2011*. https://doi.org/10.4061/2011/865319
Simonin, C., Duru, C., Salleron, J., Hincker, P., Charles, P., Delval, A., … Speaking, F. (2013). Association between caffeine intake and age at onset in Huntington's disease. *Neurobiology of Disease*, *58*, 179–182. https://doi.org/10.1016/j.nbd.2013.05.013
Skene, D. J., Middleton, B., Fraser, C. K., Pennings, J. L. A., Kuchel, T. R., Rudiger, S. R., … Morton, A. J. (2017). Metabolic profiling of presymptomatic Huntington's disease sheep reveals novel biomarkers. *Scientific Reports*, *7*(January), 1–16. https://doi.org/10.1038/srep43030
Slow, E. J., van Raamsdonk, J., Rogers, D., Coleman, S. H., Graham, R. K., Deng, Y., … Hayden, M. R. (2003). Selective striatal neuronal loss in a YAC128 mouse model of Huntington disease. *Human Molecular Genetics*, *12*(13), 1555–1567. https://doi.org/10.1093/hmg/ddg169
Smart, J. L., & Dobbing, J. (1971). Vulnerability of the developing rat brain. VI. Relative effects of foetal and early postnatal undernutrition on reflex ontogeny and development of behaviour in the rat. *Brain Research*, *33*, 303–314.
Smith, C. A., O'Maille, G., Want, E. J., Qin, C., Trauger, S. A., Brandon, T. R., … Siuzdak, G. (2005). METLIN: a metabolite mass spectral database. *Therapeutic Drug Monitoring*, *27*(6), 747–751. https://doi.org/10.1097/01.ftd.0000179845.53213.39
Snell, R. G., MacMillan, J. C., Cheadle, J. P., Fenton, I., Lazarou, L. P., Davies, P., … Shaw, D. J. (1993). Relationship between trinucleotide repeat expansion and phenotypic variation in Huntington's disease. *Nature Genetics*, *4*, 393–397. https://doi.org/10.1038/ng0893-393
Soler-Blasco, R., Murcia, M., Lozano, M., González-Safont, L., Amorós, R., Ibarluzea, J., … Llop, S. (2020). Prenatal manganese exposure and neuropsychological development in early childhood in the INMA cohort. *International Journal of Hygiene and Environmental Health*, *224*, 113443. https://doi.org/10.1016/j.ijheh.2019.113443
Spahr, L., Butterworth, R. F., Fontaine, S., Bui, L., Therrien, G., Milette, P. C., … Pomier-Layrargues, G. (1996). Increased blood manganese in cirrhotic patients: Relationship to pallidal magnetic resonance signal hyperintensity and neurological symptoms. *Hepatology*, *24*(5), 1116–1120. https://doi.org/10.1053/jhep.1996.v24.pm0008903385
Spector, E. B., Jenkinson, C. P., Grigor, M. R., Kern, R. M., & Cederbaum, S. D. (1994). Subcellular location and differential antibody specificity of arginase in tissue culture and whole animals. *International Journal of Developmental Neuroscience*, *12*(4), 337–342. https://doi.org/10.1016/0736-5748(94)90083-3
Stansfield, K. H., Bichell, T. J., Bowman, A. B., & Guilarte, T. R. (2014). BDNF and Huntingtin protein modifications by manganese: Implications for striatal medium spiny neuron pathology in manganese

neurotoxicity. *Journal of Neurochemistry*, *131*(5), 655–666. https://doi.org/10.1111/jnc.12926
Stefanko, D. P., Shah, V. D., Yamasaki, W. K., Petzinger, G. M., & Jakowec, M. W. (2017). Treadmill exercise delays the onset of non-motor behaviors and striatal pathology in the CAG140knock-in mouse model of Huntington's disease. *Neurobiology of Disease*, *105*, 15–32. https://doi.org/10.1016/j.nbd.2017.05.004
Suárez, I., Bodega, G., & Fernández, B. (2002). Glutamine synthetase in brain: Effect of ammonia. *Neurochemistry International*, *41*(2–3), 123–142. https://doi.org/10.1016/S0197-0186(02)00033-5
Subasinghe, S., Greenbaum, A. L., & McLean, P. (1985). The insulin-mimetic action of Mn2+: Involvement of cyclic nucleotides and insulin in the regulation of hepatic hexokinase and glucokinase. *Biochemical Medicine*, *34*(1), 83–92.
Sunuwar, L., Frkatović, A., Sharapov, S., Wang, Q., Neu, H. M., Wu, X., … Melia, J. (2020). Pleiotropic ZIP8 A391T implicates abnormal manganese homeostasis in complex human disease. *JCI Insight*, *5*(20). https://doi.org/10.1172/jci.insight.140978
Tapin, D., Kennedy, G., Lambert, J., & Zayed, J. (2006). Bioaccumulation and locomotor effects of manganese sulfate in Sprague-Dawley rats following subchronic (90 days) inhalation exposure. *Toxicology and Applied Pharmacology*, *211*(2), 166–174. https://doi.org/10.1016/j.taap.2005.07.007
Taylor, C. A., Hutchens, S., Liu, C., Jursa, T., Shawlot, W., Aschner, M., … Mukhopadhyay, S. (2019). SLC30A10 transporter in the digestive system regulates brain manganese under basal conditions while brain SLC30A10 protects against neurotoxicity. *Journal of Biological Chemistry*, *294*(6), 1860–1876. https://doi.org/10.1074/jbc.RA118.005628
Tian, Y., Guo, S., Chen, C., Zhao, L., Li, Z., & Yan, Y. (2018). Gene sequence screening for manganese poisoning-susceptible genes and analysis of gene interaction effects. *Environmental Toxicology and Pharmacology*, *64*, 60–69. https://doi.org/10.1016/j.etap.2018.09.013
Tidball, A. M., Bryan, M. R., Uhouse, M. A., Kumar, K. K., Aboud, A. A., Feist, J. E., … Bowman, A. B. (2014). A novel manganese-dependent ATM-p53 signaling pathway is selectively impaired in patient-based neuroprogenitor and murine striatal models of Huntington's disease. *Human Molecular Genetics*, *24*(7), 1929–1944. https://doi.org/10.1093/hmg/ddu609
Tinkov, A. A., Mazaletskaya, A. L., Ajsuvakova, O. P., Bjørklund, G., Huang, P. T., Chernova, L. N., … Skalny, A. V. (2020). ICP-MS Assessment of Hair Essential Trace Elements and Minerals in Russian Preschool and Primary School Children with Attention-Deficit/Hyperactivity Disorder (ADHD). *Biological Trace Element Research*, *196*(2), 400–409. https://doi.org/10.1007/s12011-019-01947-5
Totzeck, F., Andrade-Navarro, M. A., & Mier, P. (2017). The protein structure context of polyQ regions. *PLoS ONE*, *12*(1), 2–11. https://doi.org/10.1371/journal.pone.0170801
Tran, T. T., Chowanadisai, W., Crinella, F. M., Chicz-DeMet, A., & Lönnerdal, B. (2002). Effect of high dietary manganese intake of neonatal rats on tissue mineral accumulation, striatal dopamine levels, and neurodevelopmental status. *NeuroToxicology*, *23*(4–5), 635–643. https://doi.org/10.1016/S0161-813X(02)00091-8
Trumbo, P., Yates, A. A., Schlicker, S., & Poos, M. (2001). Dietary Reference Intakes: Vitamin A, Vitamin K, Arsenic, Boron, Chromium, Copper, Iodine, Iron, Manganese, Molybdenum, Nickel, Silicon, Vanadium, and Zinc. *J Am Diet Assoc*, *101*(3), 294–301.
Trushina, E., Dyer, R. B., Ii, J. D. B., Eide, L., Tran, D. D., Vrieze, B. T., … Bender, A. (2004). Mutant Huntingtin Impairs Axonal Trafficking in Mammalian Neurons In Vivo and In Vitro. *Mol. Cell. Biol.*, *24*(18), 8195–8209. https://doi.org/10.1128/MCB.24.18.8195
Turner, P. V., Brabb, T., Pekow, C., & Vasbinder, M. A. (2011). Administration of substances to laboratory animals: Routes of administration and factors to consider. *Journal of the American Association for Laboratory Animal Science*, *50*(5), 600–613.
Tuschl, K., Meyer, E., Valdivia, L. E., Zhao, N., Dadswell, C., Abdul-Sada, A., … Wilson, S. W. (2016). Mutations in SLC39A14 disrupt manganese homeostasis and cause childhood-onset parkinsonism-dystonia. *Nature Communications*, *7*(May), 1–16. https://doi.org/10.1038/ncomms11601
Van Dellen, A., Blakemore, C., Deacon, R., York, D., & Hannan, A. J. (2000). Delaying the onset of Huntington's in mice. *Nature*, *404*(April), 721–722.

Van Dellen, A., & Hannan, A. J. (2004). Genetic and environmental factors in the pathogenesis of Huntington's disease. *Neurogenetics*, *5*(1), 9–17. https://doi.org/10.1007/s10048-003-0169-5
Van Raamsdonk, J. M. (2005). Cognitive Dysfunction Precedes Neuropathology and Motor Abnormalities in the YAC128 Mouse Model of Huntington's Disease. *Journal of Neuroscience*, *25*(16), 4169–4180. https://doi.org/10.1523/JNEUROSCI.0590-05.2005
Van Raamsdonk, Jeremy M., Metzler, M., Slow, E., Pearson, J., Schwab, C., Carroll, J., … Hayden, M. R. (2007). Phenotypic abnormalities in the YAC128 mouse model of Huntington disease are penetrant on multiple genetic backgrounds and modulated by strain. *Neurobiology of Disease*, *26*(1), 189–200. https://doi.org/10.1016/j.nbd.2006.12.010
Van Raamsdonk, Jeremy M., Warby, S. C., & Hayden, M. R. (2007). Selective degeneration in YAC mouse models of Huntington disease. *Brain Research Bulletin*, *72*(2-3 SPEC. ISS.), 124–131. https://doi.org/10.1016/j.brainresbull.2006.10.018
Vezér, T., Papp, A., Hoyk, Z., Varga, C., Náray, M., & Nagymajtényi, L. (2005). Behavioral and neurotoxicological effects of subchronic manganese exposure in rats. *Environmental Toxicology and Pharmacology*, *19*(3), 797–810. https://doi.org/https://doi.org/10.1016/j.etap.2004.12.046
Vidal, L., Alfonso, M., Campos, F., Faro, L. R. F., Cervantes, R. C., & Durán, R. (2005). Effects of manganese on extracellular levels of dopamine in rat striatum: An analysis in vivo by brain microdialysis. *Neurochemical Research*, *30*(9), 1147–1154. https://doi.org/10.1007/s11064-005-7775-6
Võikar, V., Kõks, S., Vasar, E., & Rauvala, H. (2001). Strain and gender differences in the behavior of mouse lines commonly used in transgenic studies. *Physiology and Behavior*, *72*(1–2), 271–281. https://doi.org/10.1016/S0031-9384(00)00405-4
Walker, F. O. (2007). Huntington's disease. *Lancet*, *369*(9557), 218–228. https://doi.org/10.1016/S0140-6736(07)60111-1
Wang, D., Zhang, J., Jiang, W., Cao, Z., Zhao, F., Cai, T., … Luo, W. (2017). The role of NLRP3-CASP1 in inflammasome-mediated neuroinflammation and autophagy dysfunction in manganese-induced, hippocampal-dependent impairment of learning and memory ability. *Autophagy*, *13*(5), 914–927. https://doi.org/10.1080/15548627.2017.1293766
Warren, E. B., Bryan, M. R., Morcillo, P., Hardeman, K. N., Aschner, M., & Bowman, A. B. (2020). Manganese-induced Mitochondrial Dysfunction Is Not Detectable at Exposures Below the Acute Cytotoxic Threshold in Neuronal Cell Types. *Toxicol Sci*, *176*(2), 446–459. https://doi.org/10.1093/toxsci/kfaa079
Wedler, F C, & Denman, R. B. (1984). Glutamine synthetase: the major Mn(II) enzyme in mammalian brain. *Current Topics in Cellular Regulation*, *24*, 153–169. https://doi.org/10.1016/b978-0-12-152824-9.50021-6
Wedler, Frederick C., Denman, R. B., & Roby, W. G. (1982). Glutamine Synthetase from Ovine Brain Is a Manganese(II) Enzyme. *Biochemistry*, *21*(25), 6389–6396. https://doi.org/10.1021/bi00268a011
Wexler, N. S. (2004). Venezuelan kindreds reveal that genetic and environmental factors modulate Huntington's disease age of onset. *Proceedings of the National Academy of Sciences of the United States of America*, *101*(10), 3498–3503. https://doi.org/10.1073/pnas.0308679101
Weydt, P., Soyal, S. M., Gellera, C., Didonato, S., Weidinger, C., Oberkofler, H., … Patsch, W. (2009). The gene coding for PGC-1α modifies age at onset in Huntington's Disease. *Molecular Neurodegeneration*, *4*(1), 2–7. https://doi.org/10.1186/1750-1326-4-3
Williams, B. B., Kwakye, G. F., Wegrzynowicz, M., Li, D., Aschner, M., Erikson, K. M., & Bowman, A. B. (2010). Altered manganese homeostasis and manganese toxicity in a huntington's disease striatal cell model are not explained by defects in the iron transport system. *Toxicological Sciences*. https://doi.org/10.1093/toxsci/kfq174
Williams, B. B., Li, D., Wegrzynowicz, M., Vadodaria, B. K., Anderson, J. G., Kwakye, G. F., … Bowman, A. B. (2010). Disease-toxicant screen reveals a neuroprotective interaction between Huntington's disease and manganese exposure. *Journal of Neurochemistry*, *112*(1), 227–237. https://doi.org/10.1111/j.1471-4159.2009.06445.x
Winslow, J. W. W., Limesand, K. H., & Zhao, N. (2020). The functions of ZIP8, ZIP14, and ZnT10 in the

regulation of systemic manganese homeostasis. *International Journal of Molecular Sciences*, *21*(9). https://doi.org/10.3390/ijms21093304

Wishart, D. S., Jewison, T., Guo, A. C., Wilson, M., Knox, C., Liu, Y., … Scalbert, A. (2013). HMDB 3.0--The Human Metabolome Database in 2013. *Nucleic Acids Research*, *41*(Database issue), D801-7. https://doi.org/10.1093/nar/gks1065

Wong, Y. C., & Holzbaur, E. L. F. (2014). The Regulation of Autophagosome Dynamics by Huntingtin and HAP1 Is Disrupted by Expression of Mutant Huntingtin, Leading to Defective Cargo Degradation. *Journal of Neuroscience*, *34*(4), 1293–1305. https://doi.org/10.1523/JNEUROSCI.1870-13.2014

Xie, Y., Hayden, M. R., & Xu, B. (2010). BDNF Overexpression in the Forebrain Rescues Huntington's Disease Phenotypes in YAC128 Mice. *Journal of Neuroscience*, *30*(44), 14708–14718. https://doi.org/10.1523/JNEUROSCI.1637-10.2010

Yamada, M., Ohno, S., Okayasu, I., Okeda, R., Hatakeyama, S., Watanabe, H., … Tsukagoshi, H. (1986). Chronic manganese poisoning: A neuropathological study with determination of manganese distribution in the brain. *Acta Neuropathologica*, *70*(3–4), 273–278. https://doi.org/10.1007/BF00686083

Yang, Y., Ma, S., Wei, F., Liang, G., Yang, X., Huang, Y., … Zou, Y. (2019). Pivotal role of cAMP-PKA-CREB signaling pathway in manganese-induced neurotoxicity in PC12 cells. *Environmental Toxicology*, *34*(9), 1052–1062. https://doi.org/10.1002/tox.22776

Ye, Q., & Kim, J. (2015). Effect of olfactory manganese exposure on anxiety-related behavior in a mouse model of iron overload hemochromatosis. *Environmental Toxicology and Pharmacology*, *40*(1), 333–341. https://doi.org/10.1016/j.etap.2015.06.016

Yero, T., & Rey, J. A. (2008). Tetrabenazine (Xenazine), An FDA-Approved Treatment Option For Huntington ' s Disease – Related Chorea. *P & T*, *33*(12), 690–694. Retrieved from http://www.ncbi.nlm.nih.gov/pubmed/19750050%5Cnhttp://www.pubmedcentral.nih.gov/articlerender.fcgi?artid=PMC2730806

Yokel, R. A. (2009). Manganese flux across the blood-brain barrier. *NeuroMolecular Medicine*, *11*(4), 297–310. https://doi.org/10.1007/s12017-009-8101-2

Yousefi Babadi, V., Sadeghi, L., Shirani, K., Malekirad, A. A., & Rezaei, M. (2014). The Toxic Effect of Manganese on the Acetylcholinesterase Activity in Rat Brains. *Journal of Toxicology*, *2014*, 946372. https://doi.org/10.1155/2014/946372

Yu, C., Li, C. H., Chen, S., Yoo, H., Qin, X., & Park, H. (2018). Decreased BDNF Release in Cortical Neurons of a Knock-in Mouse Model of Huntington's Disease. *Scientific Reports*, *8*(1), 16976. https://doi.org/10.1038/s41598-018-34883-w

Zeitlin, S., Liu, J. P., Chapman, D. L., Papaioannou, V. E., & Efstratiadis, a. (1995). Increased apoptosis and early embryonic lethality in mice nullizygous for the Huntington's disease gene homologue. *Nature Genetics*, *11*(2), 155–163. https://doi.org/10.1038/ng1095-155

Zheng, S., Clabough, E. B. D., Sarkar, S., Futter, M., Rubinsztein, D. C., & Zeitlin, S. O. (2010). Deletion of the huntingtin polyglutamine stretch enhances neuronal autophagy and longevity in mice. *PLoS Genetics*, *6*(2). https://doi.org/10.1371/journal.pgen.1000838

Zidenberg-Cherr, S., Keen, C. L., Casey, S. M., & Hurley, L. S. (1985). Developmental Changes Affected by Mn Deficiency. *Biol*, *7*, 209–222.

Zidenberg-Cherr, S., Keen, C. L., & Hurley, L. S. (1985). The effects of manganese deficiency during prenatal and postnatal development on mitochondrial structure and function in the rat. *Biological Trace Element Research*, *7*(1), 31–48. https://doi.org/10.1007/BF02916545

Zielonka, D., & Stawinska-Witoszynska, B. (2020). Gender Differences in Non-sex Linked Disorders: Insights From Huntington's Disease. *Frontiers in Neurology*, *11*, 571. https://doi.org/10.3389/fneur.2020.00571

Zou, J., Wang, Y. X., Dou, F. F., Lü, H. Z., Ma, Z. W., Lu, P. H., & Xu, X. M. (2010). Glutamine synthetase down-regulation reduces astrocyte protection against glutamate excitotoxicity to neurons. *Neurochemistry International*, *56*(4), 577–584. https://doi.org/10.1016/j.neuint.2009.12.021

Zuccato, C., Belyaev, N., Conforti, P., Ooi, L., Tartari, M., Papadimou, E., … Cattaneo, E. (2007). Widespread Disruption of Repressor Element-1 Silencing Transcription Factor/Neuron-Restrictive Silencer Factor

Occupancy at Its Target Genes in Huntington's Disease. *Journal of Neuroscience*, *27*(26), 6972–6983. https://doi.org/10.1523/JNEUROSCI.4278-06.2007

Zuccato, Chiara, Ciammola, A., Rigamonti, D., Leavitt, B. R., Goffredo, D., Conti, L., … Cattaneo, E. (2001). *Loss of Huntingtin-Mediated BDNF Gene Transcription in Huntington ' s Disease*. *293*(July), 493–498. https://doi.org/10.1126/science.1059581

Zuccato, Chiara, Tartari, M., Crotti, A., Goffredo, D., Valenza, M., Conti, L., … Cattaneo, E. (2003). Huntingtin interacts with REST/NRSF to modulate the transcription of NRSE-controlled neuronal genes. *Nature Genetics*, *35*(1), 76–83. https://doi.org/10.1038/ng1219